Development of composite beam theory and its application in composite and prestressed concrete structures

by

Fengtao Bai

A dissertation submitted to the Graduate Faculty of
Auburn University
in partial fulfillment of the
requirements for the Degree of
Doctor of Philosophy

Auburn, Alabama
May 7, 2016

Keywords: Composite theory, sandwich panel, transfer length, prestress losses, bond-slip, prestressed concrete

Approved by

James S. Davidson, Committee Chair, Professor of Civil Engineering
Robert W. Barnes, Associate Professor of Civil Engineering
Justin D. Marshall, Associate Professor of Civil Engineering
J. Michael Stallings, Professor of Civil Engineering

Abstract

For some complex structural engineering problems like behavior of sandwich structures and prestressed concrete structures, extensive experimental works and finite element analyses might not be able to help understand the mechanics completely rather than providing the numerical results of specific cases. On the other hand, conventional structural analysis approach like Euler-Bernoulli beam theory is inherently incapable of dealing with such composite behaviors due to the plane section assumption. For those complex problems in structural engineering, an appropriate and rigorous theory has been needed for a while but unfortunately absent.

This dissertation provides a new perspective, composite beam theory that defines the structures as interacting components. The structural mechanics and mathematical manipulation are the primary tools and the balance between accuracy and applicability is carefully maintained so that the conclusions arrived in this research can be readily applied to engineering practice.

This dissertation firstly derives the composite theory in a general form, and then applies the theory to various concrete structure analysis applications, including sandwich structures and prestressed concrete. Specifically, it provides a systematic analysis methodology for sandwich structures with symmetrical and unsymmetrical wythes (sandwich structures that have identical wythes and properties will be referred as symmetrical wythes sandwich structures since the

wythes are symmetrical about the neutral axis). Both longitudinal and transverse governing equations and closed form solutions are derived and studied. For prestressed concrete structures, the immediate prestress loss formulas in current design provisions and specifications are evaluated and improved, and a new type of loss due to slip is presented. The transfer length of prestressed concrete structures is redefined by investigating the mechanics and new methodologies to improve current transfer length prediction are presented. The validation against comprehensive test data demonstrates the success of the new approach, and comparisons with current formula suggest significant improvement.

Acknowledgements

This dissertation is dedicated to my family, especially my wife Wenxiu Liu who has been essential to any of my achievements, and my grandfather Chunxue Hao who encouraged me to pursue a doctoral degree when I was little.

I came to Auburn knowing little about lots of things but left with much more abundant knowledge in them. I am grateful for everything Auburn has to offer. I am especially grateful for the help, guidance and support from my advisor Dr. James Davidson, and this dissertation would not have be accomplished without his help. I would also like to thank China Scholarship Council for the continuous financial support that keeps me focused on my research; my Ph.D. committee members Dr. Robert Barnes, Dr. Justin Marshall, Dr. J. Michael Stallings and Dr. Jeffrey Suhling for their valuable suggestions and advices; and my fellow graduate students and scholar, Xin Sha, Hongyang Wu, Pengfei Chen, Yanchao Shi and Yalin Liu for the joy.

There are a lot of other people and things to thank and I would keep them in my heart for this moment.

Table of Contents

List of Figures

List of Tables

List of Abbreviations

PCI	Prestressed/Precast Concrete Institute
ACI	American Concrete Institute
AASHTO	American Association of State Highway Transportation Officials
LRFD	Load and Resistance Factor Design
ICSP	Insulated Concrete Sandwich Panel

List of Symbols

(In the order of appearance)

Chapter 3

σ_c = axial stress in concrete

$\sigma_{s,x}$ = concrete axial component of axial stress in strand

φ_{2c} = concrete axial component of the concrete beam displacement from its original centroid due to axial deformation

$\varphi_{2s,x}$ = concrete axial component of the tendon displacement from its original centroid due to axial deformation

E_c = moduli of elasticity of concrete

E_s = moduli of elasticity of prestressing strand

q_x = concrete axial component of shear force per unit length at the interface

N_c = resultant axial force in the concrete beam

A_c = area of the concrete beam

$\varphi_{2,x}$ = concrete axial component of slip (between concrete and tendon) due to axial deformation

$N_{s,x}$ = concrete axial component of resultant axial force in the strand

N = concrete axial component of axial force in both concrete bean and strand

K = shear stiffness of the concrete strand interface

$\varphi_x = \varphi_1 + \varphi_{2,x} + \varphi_{3,x}$ = concrete axial component of the total slip

$\varphi_1 = ey'$ = slip due to bending

$\varphi_{3,x} = \int(\varepsilon_{is} \cos\vartheta)dx$ = concrete axial component of the slip due to prestressed strands

e = the eccentricity function between the concrete beam centroid and the strand centroid.

y = deflection of concrete beam

ε_{is} = initial applied strain, before transfer, in the prestressing strand

$\chi_B^2 = K / \eta$

M_{ex} = External applied bending moment

M_c = internal bending moment of the concrete beam

I_c = Moment of Inertia for the concrete beam

$D_B = E_c I_c + e^2\eta$

$\alpha_B^2 = e^2\eta / D_B$

$\cos\vartheta = 1 / \sqrt{(1+(e')^2)}$

Chapter 4

q_w = external applied uniform pressure

b = width of wythes

$P_1 = 0.5q_w blE_1I_1 / (E_1I_1+E_2I_2)$

$P_2 = 0.5q_w blE_2I_2 / (E_1I_1+E_2I_2)$

E_1 = modulus of elasticity of wythe-1

E_2 = modulus of elasticity of wythe-2

I_1 = moment of inertia of wythe-1

I_2 = moment of inertia of wythe-2

σ_1 = axial stress in wythe-1

σ_2 = axial stress in wythe-2

φ_{21} = wythe-1 displacement from its original location due to axial deformation

φ_{22} = wythe-2 displacement from its original location due to axial deformation

τ = shear stress in the middle layer per unit length

N_1 = resultant axial force in wythe-1

A_1 = cross-section area of wythe-1

φ_2 = slip between wythes due to axial deformation

N_2 = resultant axial force in wythe-2

N = resultant axial force in both wythes

K = shear stiffness of the middle layer

$\varphi = \varphi_1 + \varphi_2$ = total slip between wythes

$\varphi_1 = (r_1 + r_2)y'$ = slip due to bending

$r_1 + r_2$ = the distance from the centroid of wythe-1 to the centroid of wythe-2

y = deflection of wythes

$\eta = A_1E_1A_2E_2 / (A_1E_1 + A_2E_2)$

$\chi_B^2 = Kb / \eta$

M_{ex} = External applied bending moment

M_1 = internal bending moment of wythe-1

M_2 = internal bending moment of wythe-2

$D_B = (E_1I_1 + E_2I_2) + (r_1 + r_2)^2\eta$

$\alpha_B^2 = (r_1 + r_2)^2\eta / D_B$

Q_1 = internal shear force on the cross-section for wythe-1

Q_2 = internal shear force on the cross-section for wythe-2

k = middle layer transverse stiffness

$T = bk(y_1 - y_2)$ = middle layer transverse force in unit length

$\beta_B^2 = 1 - \alpha_B^2$

$\lambda^4 = bk(1 / (E_1I_1) + 1 / (E_2I_2))$

l = span length

$A_1 = -(\theta/\gamma^3)\cosh(\gamma l/2)\cos(\gamma l/2) / (\sinh(\gamma l)+\sin(\gamma l))$

$A_4 = -(\theta/\gamma^3)\sinh(\gamma l/2)\sin(\gamma l/2) / (\sinh(\gamma l)+\sin(\gamma l))$

$\theta = bkP_1(1 / (E_1I_1) + 1 / (E_2I_2))$

$\gamma = \lambda / \sqrt{2}$

d_1 = thickness of wythe-1

d_2 = thickness of wythe-2

$\sigma_{1,t/b}$ = top and bottom fiber stresses in wythe-1

$\sigma_{2,t/b}$ = top and bottom fiber stresses in wythe-2

Chapter 5

Granholm's Theory

q_w = external applied uniform pressure

φ_2 = slip between wythes due to axial deformation

E_w = moduli of elasticity of wythes

τ = shear stress in the middle layer

N = resultant axial force in wythe

b = wythe width

d = thickness of wyth

$A = bd$ = cross section area of wythe

K = shear stiffness of the middle layer

$\varphi = \varphi_1 + \varphi_2$ = total slip between wythes

$\varphi_1 = 2ry'$ = slip due to bending

y = total deflection

r = distance from neutral axis of wythe to the overall neutral axis

$\chi^2 = 2Kb / (E_w A)$

M_{ex} = external bending moment

M^{in} = internal bending moment of interior wythe

M^{ex} = internal bending moment of exterior wythe

$I_{sgl} = bd^3 / 12$ = moment of inertia of each wythe

$I_{total} = 2I_{sgl} + 2r^2 A$ = moment of inertia for the whole cross-section

$\alpha^2 = 2r^2 A / I_{total}$

$\beta^2 = 1 - \alpha^2$

k = vertical compressive stiffness of the middle layer

l = span length

$\Psi = \varphi_1{}^0(\varphi_2{}^0 + \varphi_4{}^0) - \varphi_3{}^0(\varphi_2{}^0 - \varphi_4{}^0)$

$\varphi_1{}^0 = \cos\lambda \cdot \cosh\lambda$

$\varphi_2{}^0 = \cos\lambda \cdot \sinh\lambda$

$\varphi_3{}^0 = \sin\lambda \cdot \sinh\lambda$

$\varphi_4{}^0 = \sin\lambda \cdot \cosh\lambda$

$\varphi_1 = \cos\varepsilon \cosh\varepsilon$

$\varphi_3 = \sin\varepsilon \sinh\varepsilon$

$\lambda = \sqrt{2}/4(l/l_0)$

$\varepsilon = \sqrt{2}/4(x/l_0)$

$l_0 = \sqrt[4]{(E_w \cdot i/(2k \cdot b))}$

$i = 2I_{sgl}$

y_f = flexural deflection

y_s = shear deflection

Discrete Model

(Notations are the same with Granholm's model except following)

K_f = the shear stiffness function of the whole structure

K_{in} = the shear stiffness of individual shear connecter

t = length of positive phase

T = period length

$Z_1 = \varphi'$

$Z_2 = \varphi$

$Z_3 = y'$

$Z_4 = y$

$\lambda_1 = 2bK_f / (\beta^2 E_w A)$

$\lambda_2 = 2rM_{ex}' / (\beta^2 E_w I_{total})$

$\lambda_3 = rA / I_{total}$

$\lambda_4 = M_{ex} / (E_w I_{total})$.

Chapter 6

φ_{2c} = concrete beam displacement from its original centroid due to axial deformation

φ_{2s} = strand displacement from its original centroid due to axial deformation

E_c = moduli of elasticity of concrete

E_s = moduli of elasticity of prestressing strand

q = shear force per unit length within the concrete-strand interface

N_c = resultant axial force in the concrete beam

A_c = cross section area of the concrete beam

φ_2 = total slip between concrete and strand due to axial deformation

N_s = resultant axial force in the strand

N = resultant axial force in both the concrete beam and strand

K = shear stiffness of the concrete-strand interface, or bond stiffness for short

$\varphi = \varphi_1 + \varphi_2 + \varphi_3$ = total slip between concrete beam and strand

$\varphi_1 = ey'$ = slip due to bending

$\varphi_3 = \int \varepsilon_{is}\, dx$ = slip due to prestressing strands

e = the distance from the concrete beam centroid to the strand centroid

y = deflection

$\chi_B^2 = K / \eta$

M_{ex} = external applied bending moment

M_c = internal bending moment of the concrete beam

I_c = concrete beam moment of inertia

ε_{is} = initial applied prestrain, before transfer, in the prestressing strand

$D_B = E_c I_c + e^2 \eta$

$\alpha_B^2 = e^2 \eta / D_B$

q_w = external applied uniform pressure

$\beta_B^2 = 1 - \alpha_B^2$

φ_r = total slip between concrete beam and strand of the reinforced concrete beam

N_r = resultant axial force of the reinforced concrete beam

M_r = internal bending moment of the reinforced concrete beam

φ_p = total slip between concrete beam and strand of the prestressed concrete beam

N_p = resultant axial force of the prestressed concrete beam

M_p = internal bending moment of the prestressed concrete beam

$\varepsilon_{cds} = eM_{ex} / D_B$

$f_{cds} = eM_{ex}E_c / D_B$

$\Delta N_{P\text{-}ES}$ = change in axial force due to elastic shortening without slip

$P_{effe\text{-}ES}$ = effective prestress after elastic shortening loss in percentage

$P_{loss\text{-}ES}$ = prestress loss due to elastic shortening in percentage

$\Delta N_{P\text{-}ES\text{-}sp}$ = change in axial force due to elastic shortening considering slip

$\Delta N_{P\text{-}sp}$ = change in axial force due to slip

$P_{loss\text{-}sp}$ = prestress loss due to slip in percentage

γ = the tolerance of axial force at mid-span

L_t = transfer length

$\lambda_t = (1\text{-}\gamma)\ cosh(\chi_B l / (2\beta_B))$

μ_d = factor depending upon individual strand circumference or diameter = 1 for 0.6 inch strands; 0.83 for 0.5 inch strands

n = total number of strands

K_0 = interface shear stiffness of an individual strand

μ_{sl} = factor depending on end slip = 0.67 when $0.08 \leq \varphi_p \leq 0.11$ inch and $\mu_{sl} = 0.5$ when $0.11 < \varphi_p \leq 0.15$

Chapter 7

L_t = transfer length

φ = total slip between concrete beam and strand

$\chi_B^2 = K / \eta$

K = shear stiffness of the concrete-strand interface

$\eta = (A_c E_c A_s E_s) / (A_c E_c + A_s E_s)$

A_c = area of concrete beam

A_s = area of prestressing strand

E_c = moduli of elasticity of concrete

E_s = moduli of elasticity of prestressing strand

e = strand eccentricity

y = deflection

$\alpha_B^2 = e^2\eta / D_B$

M_{ex} = external bending moment

$D_B = E_cI_c + e^2\eta$

ε_{is} = initial applied prestrain

$\beta_B^2 = 1 - \alpha_B^2$

φ_p = slip due to prestressing force

N_p = resultant axial force due to prestressing force

γ = the tolerance of axial force at mid-span

$\lambda_t = (1-\gamma)\ cosh(\chi_B l / (2\beta_B))$

$\mu = \chi_B l / (2\beta_B)$

$\varphi_{pe} = \varphi_p(l/2)$ = end slip due to prestressing force

M_s = resultant bending moment in concrete due to gravity load

M_{ex} = external applied bending moment including self-weight

N_s = resultant axial force due in both concrete and reinforcement or tendons due to gravity load

d = the distance from the centroid to the position of interest

Chapter 1 Introduction

1.1 Introduction

In many fields of structural engineering, for example sandwich structure and prestressed concrete, the design and analysis are primarily based on the classical Euler-Bernoulli beam theory. Once there are issues that cannot be solved by the classical Euler-Bernoulli beam theory, modifications and empirical factors tend to be added based on the Euler-Bernoulli beam solutions to account for those effects. However, it should be recognized that the Euler-Bernoulli beam theory was solely developed for the conventional solid and uniform beam structures, and modern structures may consist of very distinct structural components like the prestressing tendon and concrete in the prestressed concrete structures, or exterior and interior wythes in the sandwich structures. To better understand the behavior of these modern composite structures, analyses may need to be carried from an individual component level, and then coupled together through the interface mechanical properties.

This dissertation makes efforts to define the structures of interest as interacting components under the frame work of engineering mechanics, in which the balance between accuracy and applicability is important. Although there are very advanced physical models available, those models may be too complicated to be applied to engineering practices therefore do not fit into the scope of this dissertation.

The mechanics in this dissertation features the interaction between structural components, and the outcome of which is the Interface / interlayer slip. Interface / interlayer slip occurs in the composite structures such as steel-concrete composite T girders, insulated concrete sandwich structures and prestressed concrete. (Note that “slip” refers to the relative movement between the centroids of

components within the cross section as demonstrated in Figure 1-1). This slip results in many problems that cannot be addressed through classic Euler-Bernoulli beam theory because of the assumptions adopted. For example, due to the existence of relatively flexible shear connections, a considerable amount of slip (longitudinal shear deformation of the middle layer) can occur in composite T girders, sandwich structures and prestressed concrete, which are illustrated in Figure 1-1. This slip or shear deformation makes the plane section assumption invalid.

However, for the sandwich structure illustrated in Figure 1-1, the common practice in design is to assume that the whole cross section participates in the action as a plane first and then assume a composite ratio to deduct the cross section properties. This is may be a good way to simplify the design process but it should be recognized that the sandwich structure cross section is not plane because of the relative slip (shear deformation) between the wythes. Additionally, deformation due to the transverse interaction occurs beside the longitudinal interaction, and the longitudinal and transverse interactions may even be coupled if the two wythes are not identical. Overall, the flexible middle layer and prominent shear deformation results in much more flexible behavior than the corresponding solid structures and makes analysis and design very difficult.

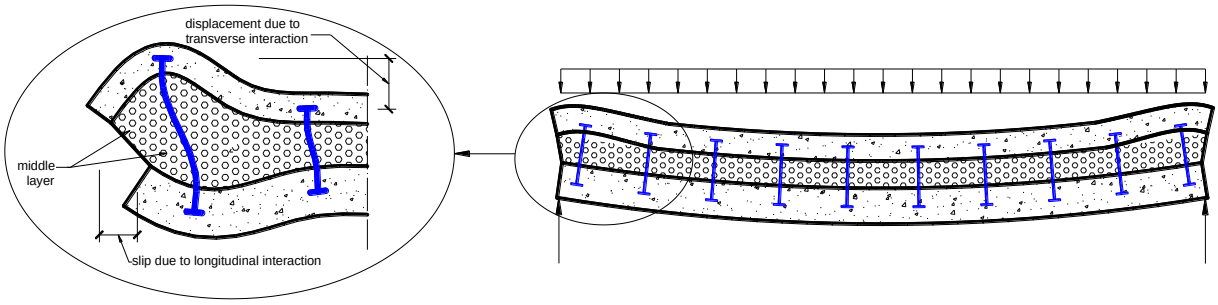

Figure 1-1: Definition of slip, longitudinal and transverse interactions in sandwich structures

Another example of conventional engineering analysis method inadequacy is the design of prestressed concrete structures. Ideally in the prestressed concrete structure design, the concrete and prestressing

tendons are perfectly bonded and interface slip does not occur between them. However, in reality there is always slip occurring between them and the slip results in the phenomenon that prestressing force requires a certain transfer distance (referred to as transfer length) to be fully transmitted to the concrete. Although modern prestressed concrete structural design methodology, to some extent, accounts for the transfer length, the design methodology could not consistently take the bonding condition into consideration and usually needs to assume perfect bond and plane cross section first. Tendons and concrete are very distinct but interactive structural components, and in the design actual bonding condition should be determined instead of being assumed to be perfect and plane cross section assumption is invalid within the transfer zones due to the large interface shear force.

It should be noted that the some design provisions dealing with steel-concrete T girders, insulated sandwich structures, and prestressed concrete may yield unreliable results because of the inappropriate theory used as the basis of the theoretical development. Many of the long debated problems are caused by the interlayer / interface slip that cannot be captured by conventional beam theory. Therefore, this dissertation presents the development of a novel structural analysis theory, namely a composite beam theory that considers the interface / layer slip, and also takes advantage of the developed composite beam theory to shed some light on various long debated issues in structural engineering.

1.2 Research objectives

The first objective of this dissertation research is to develop a new theoretical tool from the perspective of interactive composite theory. This new tool should be in a general form that considers the geometry and material variations of composite structures, meanwhile maintaining a balance between accuracy and applicability. The second objective is to apply the developed composite theory to several areas in structural engineering and to investigate the possibility of replacing some unreliable provisions and recommendations in the popular requirements, design guides and specifications of related fields.

Nevertheless, during the development and application of the composite theory, comprehensive data and results from the literature need to be scrutinized and the theoretical solutions and associated conclusions have to be validated. The overall goal is to make solid advancements in the related fields, and provide insights into existing problems and theoretical guidance for future studies.

1.3 Scope and methodology

This dissertation emphasizes rigorous theoretical development at normal service conditions. Therefore the study is limited to the linear and elastic range of the materials involved and the assumption of small displacements. The research presented in this dissertation includes deriving governing equations, obtaining the closed form solutions, studying the properties of closed form solutions, applying the overall theory to various long lasting structural engineering problems, and validating the theoretical development and its applications against test data. In addition, comparisons, recommendations and conclusions are made based upon the results. The theoretical development is specifically applied to several structure forms, including (1) symmetrical and unsymmetrical wythes insulated concrete sandwich structures; and (2) reinforced and prestressed concrete structures in which the prestress losses and transfer length immediately after transfer are thoroughly defined and discussed.

1.4 Dissertation organization

Chapter 2 provides a literature review of composite theory and applications that are relevant to the full dissertation topic. Chapter 3 introduces and derives composite theory in a general form that is ready for the applications presented in the subsequent chapters. Chapter 4 simplifies the composite theory and applies it to sandwich structures with unsymmetrical wythes. Detailed discussions on the upper and lower bounds of axial forces, bending moments and slip are included. In addition, thorough comparisons with existing theory are also provided. Chapter 5 further simplifies the composite theory presented in Chapter 4 and applies it to sandwich structures with symmetrical wythes. Discussions on the upper and

lower bonds of axial forces, bending moments and slips are also provided. Validations against test data are included. Chapter 6 applies the composite theory to prestressed concrete analysis. Specifically, the immediate prestress losses and transfer length problems are discussed in detail. Validations against testing data are included. Chapter 7 continues the discussion of Chapter 6 and develops two practical approaches to determine and evaluate transfer lengths. Validations against test data are also included. Chapter 8 summarizes the work and conclusions and discusses future steps that should be taken.

Chapter 2 Literature review

2.1 Historical development of composite beam theories

The composite theory in this dissertation features the interactions between different cross section components and therefore can be categorized as interactive composite theory. Its original application can be traced back to the 1940's when Granholm[1] published his theory and work in the field of nailed timber structures. Granholm's theory focused on the equilibrium of axial force within individual layers and overall bending moment of the whole cross section. More than a decade later, Holmberg[2] adopted and improved Granhom's theory by considering additional transverse action and applied it to various concrete structures. However, all of the works done by Granholm and Holmberg focus on the composite structures that have identical wythes, properties (sandwich structures that have identical wythes and properties will be referred as symmetrical wythes sandwich structures since the wythes are symmetrical about the neutral axis, and this is a major assumption that simplifies its derivation of governing equations) and uniform distribution of connectors, and could not be applied to structures with different dimensions and mechanical properties in wythes.

On the other hand, there are also composite theories that depart from the kinematics of middle layer shear deformation and arrive at another form of governing equations and solutions, which describe the structures with a single cross section. Allen[8] and Hartsock[9] respectively published essentially the same governing equations that considered the kinematics relationships between interior and exterior wythes, and overall shear or bending moment equilibrium. Later, based on very similar governing equations of

Hartsock, Ha[10][11] and Davies[12] focused on stiffness matrix formation and development of finite element algorithms.

Surprisingly, these two categories of composite theories would yield almost identical results on the applications of sandwich structures[45]. However, in this dissertation the interactive composite theory is considered to be more versatile in terms of describing the mechanical behaviors because it does not rely on an assumed shape of shear deformation, therefore used as the primary tool of investigation. One of the merits of the interactive composite theory is that it focuses on force equilibrium and does not require an assumed shear deformation. So by using this type of interactive composite theory, the prestressed concrete analysis approaches presented in Chapters 6 and 7 are made possible.

In bridge engineering, two-layer composite structures such as composite steel concrete T beams have been widely used and studied theoretically[3][16]-[20]. In 1951, Newmark[3] published his work on composite T beams; his theory was derived from the strain compatibility of the steel concrete interface. In 1967, Goodman[13] proved that Newmark's theory is the same with Granholm's[1]. Since then, a number of studies targeting different aspects of composite T beam mechanics have been carried out. Girhammar[16] developed a second order analysis approach. Ranzi[6][17][18], Salari[19], and Sousa[20] published studies involving finite element formulation. Fabbrocino[21] employed predefined moment curvature relation and force equilibrium to study the mechanics of composite T beams. Xu[22][23] considered the composite cross-section in a plane stress state and derived theoretical solutions.

However, most available theoretical studies of composite structures focused on the longitudinal interaction and for sandwich structures only identical properties are considered in each wythes. Therefore theory considering variations in components of composite structures and both longitudinal and transverse interactions is developed in this dissertation (Chapters 3 and 4).

2.2 Insulated concrete sandwich structures

The increasing use of Insulated Concrete Sandwich Panels (ICSPs) in building constructions calls for accurate analysis theory. The majority of available literatures focused on experimental studies[24]-[44], although there have also been attempts to define sandwich panel behavior by force equilibrium[24][25], classical beam theory[26][27], and adapting various existing composite theories[28][29]. Most of those theories however are not appropriate for ICSP behavior and not derived rigorously nor validated by experiments. Consequently, few of them properly predict the response behavior of concrete sandwich structures to transverse loading.

ICSP analysis methodologies by others[24][26][27][30] typically consider sandwich structures to be classical Euler-Bernoulli beams with a reduced moment of inertia, and the role of interlayer slip is not completely recognized. Also, there are a number of studies that focus on a particular aspect of sandwich structures construction, such as design optimization, structures with thin or thick wythes[13], and development of various composite elements[14]. Therefore the list of multi-layer composite structures theories is extensive, and a comprehensive review and study of over 1300 publications is available [15].

2.3 Transfer length in prestressing concrete

The transfer length problem in prestressed concrete has been a challenge for decades. Janney[57] appeared to be the first one who described the complicated microscopic bond behaviors observed in a series of tests. In the U.S. detailed experimental investigations of transfer length by Russell[49][87], Barnes[55][86] and Peterman[89][90][91] are frequently referenced. There are also innovative ways of studying transfer length, for example, using linear regression[69] and relating the measured end slip to transfer length[53][54][81][82], designated concrete element[62][63], reliability[58], genetic programming[61] and neural network[59][60]. Additional literature reviews and comparisons can be found in other studies[64][65][66][67]. Due to the difficulties in capturing the complex interactive mechanism in the conventional analysis

methodology and quantification of interface bond condition[92], researchers who study transfer length usually have to make assumptions and develop empirical formulas based upon test data and observations.

Current ACI 318[71] and AASHTO LFRD transfer length provisions[79] are based on Hanson's work[88], and Hanson's results were derived based on the assumptions of average bond stress as well as effective prestress. Guyon[82] also defined the transfer length from another angle, based on end slip data, but assumptions of the linear or parabolic stress within transfer zones had to be made. Those assumptions may have reflected what were observed during the tests but the mechanics behind the observation is still not clearly defined.

Since no proven and reliable analytical model is available, the focus on the experimental studies has resulted in debates over the true prestressing force transfer mechanisms. For example, in the discussions over the influence of concrete strength on the transfer length, some researchers argue that concrete strength has nothing to do with the transfer length[47] whereas others argue that the concrete strength definitely influences the transfer length[48]. Now it is generally accepted that concrete strength influences transfer length. However, the concrete strength can influence both concrete elastic modulus and the interface bonding condition, and which of them is dominant in affecting transfer length is still uncertain. Nevertheless, variables like concrete composition[68] and strand diameter[70][71] all appear to influence transfer length, but determination and quantification of those influences are a big challenge.

After all of the efforts spent by many researchers, the mystery of transfer length is still unsolved. Transfer length actually is the consequence of interface slip between strands and concrete, and a model that fully addresses this behavior should help fundamentally understand transfer length phenomena.

2.4 Prestress losses

On the other hand, immediate prestress losses due to elastic shortening, friction and seating are a relatively mature subject. Although the elastic shortening loss may be overestimated in some cases, for normal design conditions currently used formulas yield reasonable results. Zia[50], as well as other researchers associated with ACI-ASCE Committee 423 (Prior Committee 323), reviewed and proposed approaches for estimating prestress losses that are still being used, although some long term load factors have changed over time. This approach, referred to herein as the conventional approach, is used in PCI Design Handbook[70], ACI-318[71] and AASHTO-LRFD Bridge Design Specifications[79]. The National Cooperative Highway Research Program (NCHRP) also sponsored research[75] on the prestress losses of high-strength concrete bridge girders. There might still be some debates on the long term and time-dependent losses but nobody doubts the methods used for estimating the immediate prestress losses. However, in the present study, it is shown that there is still room to improve the methodologies used to estimate the immediate prestress losses, especially when the reinforcement ratio is large.

2.5 Transfer length by end slip

The idea of measuring end slip to evaluate transfer length is not new and studies have investigated the possibility[82][76][81] and evaluated the reliability[83]. Unlike other theoretical developments in the prestressing transfer problem, correlating end-slip to transfer length has a solid foundation and is theoretically sound. However, two prominent issues must be addressed before this theory can yield sound solution. First, the effective prestressing force must be obtained, and second the distribution of the prestressing force as it transitions to the effective prestressing force from zero within the transfer zone must be obtained. Those two issues can be approximated in a number of ways, for example the use of empirical or semi-theoretical formulas, but there is not a consistent system that can provide sound, reliable and practical solutions.

Among those existing studies on relating end slip to transfer length, the important ones are Guyon's, Russell's and Rose's. Guyon[82] first came up with the idea of relating end slip to transfer length and derived the equation based on different prestressing force distributions inside the transfer zones. Later, Russell[49] and Rose[81] adopted the same approach that assumed linear interface shear stress within the transfer zone based on comprehensive testing observations. The two different assumptions, parabolic or linear only result in the discrepancy in the constant α, which relates transfer length to mechanical properties. A linear distribution assumption results in a constant of α = 2.0 whereas parabolic distribution has the same value as α = 3.0. There are other studies that theoretically and experimentally investigated the possible shear stress distribution and the resulting α values in Guyon's derivation, and Marti-Vargas[83] summarized the results and studied reliability of those conclusions.

Chapter 3 Composite theory in general form

3.1 Introduction and scope

This chapter derives the general composite theory that later chapters rely upon and sets the theoretical foundation. The general form composite theory uses the prestressed concrete beam geometry with draped tendon to demonstrate the derivation procedure. However, as will be discussed and demonstrated in the later chapters, this theory is not limited to prestressed concrete; it can be applied to other composite structures such as steel concrete T girder, and insulated sandwich structures.

3.2 Theoretical development

3.2.1 Assumptions and coordinate system

The assumptions involved in this developed are:

1) Structural behavior is limited to linear elastic material behavior and small displacements.

2) The concrete beam and reinforcement or prestressing tendons are assumed to behave as Euler-Bernoulli beams, and they have the same transverse deflection in the longitudinal interaction.

3) Continuous shear resistance exists between concrete and tendons along the span.

4) Tendon has no bending resistance.

x direction is taken as concrete axial direction and the midspan is taken as the origin.

3.2.2 Axial force equilibrium

Axial strain is equal to the derivative of its axial displacement, and the axial stress is equal to Young's modulus times that strain (bending moment by eccentric tendon may exist, but it will not affect the longitudinal force equilibrium and will be included later in bending moment equilibrium):

$$\sigma_c = E_c \varphi_{2c}^{'} \tag{3.1}$$

$$\sigma_{s,x} = E_s \varphi_{2s,x}^{'} \tag{3.2}$$

where σ_c = axial stress in concrete; $\sigma_{s,x}$ = concrete axial component of axial stress in strand; φ_{2c} = concrete axial component of the concrete beam displacement from its original centroid due to axial deformation; $\varphi_{2s,x}$ = concrete axial component of tendon displacement from its original centroid due to axial deformation; E_c = concrete Young's modulus; and E_s = prestressing tendon Young's modulus.

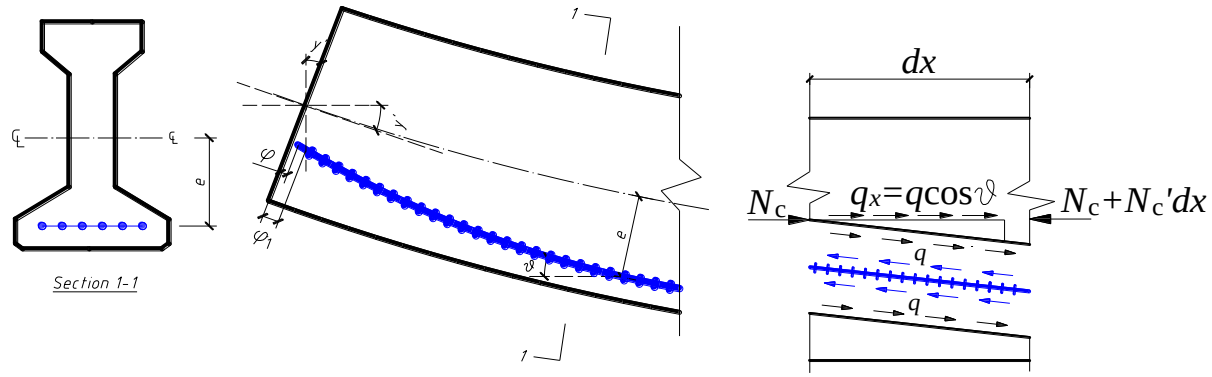

Figure 3-1: Geometry and force equilibrium of differential element

Taking the concrete portion of the beam as example from now on but the same result will be obtained if the tendon is taken. Using the equilibrium of forces in the axial direction of the concrete cross section shown in Figure 3-1:

$$q_x dx = N_c^{'} dx \tag{3.3}$$

where q_x = concrete axial component of shear (bond) force per unit length at the interface and N_c = resultant axial force in the concrete beam. The shear force on the differential unit length now reads:

$$q_x = \left(A_c \sigma_c\right)' \tag{3.4}$$

where A_c = area of the concrete beam. Substituting Equation (3.1) into Equation (3.4), the interface shear force is determined as following:

$$q_x = E_c A_c \varphi_{2c}'' \tag{3.5}$$

The slip is defined as the difference between concrete and tendon displacements:

$$\varphi_{2,x} = \varphi_{2c} + \varphi_{2s,x} \tag{3.6}$$

where $\varphi_{2,x}$ = concrete axial component of the slip (between concrete and tendon) due to axial deformation. On the other hand, the fact that the internal axial forces in the concrete beam and tendon are equal to each other yields following (the sign convention of axial force is not considered since $\varphi_{2,x}$ is a relative movement):

$$N_c = N_{s,x} = N \tag{3.7}$$

where $N_{s,x}$ = concrete axial component of resultant axial force in the tendon, and N = concrete axial component of axial force in both concrete beam and tendon. Equation (3.7) can now be rewritten as:

$$N_c = A_c \sigma_c \tag{3.8}$$

$$N_{s,x} = A_s \sigma_{s,x} \tag{3.9}$$

Substitution of Equation (3.1) into Equation (3.8), and Equation (3.2) into Equation (3.9) respectively will result in:

$$N_c = A_c E_c \varphi'_{2c} \tag{3.10}$$

$$N_{s,x} = A_s E_s \varphi'_{2s,x} \tag{3.11}$$

Differentiating Equation (3.6) twice:

$$\varphi''_{2,x} = \varphi''_{2c} + \varphi''_{2s,x} \tag{3.12}$$

Plugging Equation (3.10) and Equation (3.11) back into Equation (3.7) and differentiating once:

$$A_c E_c \varphi''_{2c} = A_s E_s \varphi''_{2s,x} \tag{3.13}$$

Substitution of φ_{2c}'' and $\varphi_{2s,x}''$ from Equation (3.13) into Equation (3.12) will yield:

$$\varphi''_{2,x} = \left(1 + \frac{A_c E_c}{A_s E_s}\right) \varphi''_{2c} \tag{3.14}$$

$$\varphi''_{2,x} = \left(1 + \frac{A_s E_s}{A_c E_c}\right) \varphi''_{2s,x} \tag{3.15}$$

Considering the equilibrium between interface shear forces and axial force in the horizontal direction:

$$K\varphi_x = q_x \tag{3.16}$$

where K = shear stiffness of the concrete strand interface; $\varphi_x = \varphi_1 + \varphi_{2,x} + \varphi_{3,x}$ = concrete axial component of the total slip; $\varphi_1 = ey'$ = slip due to bending, as in Figure 3-1; e = the eccentricity function between the concrete beam centroid and the strand centroid; y = deflection of concrete beam; and $\varphi_{3,x} = \int(\varepsilon_{is} \cos \vartheta)dx$ = concrete axial component of the slip due to prestressing tendon. Substituting Equation (3.5) into Equation (3.16):

$$K\varphi_x = E_c A_c \varphi''_{2c} \tag{3.17}$$

Substituting φ_{2c}'' from Equation (3.14) into Equation (3.17):

$$K\varphi_x = \frac{E_c A_c}{\left(1+\frac{A_c E_c}{A_s E_s}\right)}\varphi_{2,x}'' \tag{3.18}$$

Also, the total slip along the *x* axis can be written as:

$$\varphi_x = \varphi_1 + \varphi_{2,x} + \varphi_{3,x} \tag{3.19}$$

Plugging $\varphi_1 = ey'$ into Equation (3.19) and rearranging Equation (3.19) results in:

$$\varphi_{2,x} = \varphi_x - ey' - \varphi_{3,x} \tag{3.20}$$

Note that $\varphi_{3,x}$ is the integration of strand strain along the span position. Now differentiating Equation (3.20) twice:

$$\varphi_{2,x}'' = \varphi_x'' - \left(e''y' + ey''' + 2e'y''\right) - \left(\varepsilon_{is}\cos\vartheta\right)' \tag{3.21}$$

where ε_{is} = initial applied strain, before transfer, in the prestressing strand and $\cos\vartheta = 1/\sqrt{(1+(e')^2)}$ = concrete axial component of strand direction, as defined in Figure 3-1. ε_{is} is negative for prestressing strands. Equation (3.21) now takes the form:

$$\varphi_{2,x}'' = \varphi_x'' - \left(e''y' + ey''' + 2e'y''\right) - \varepsilon_{is}\cos'\vartheta \tag{3.22}$$

Substituting Equation (3.22) into Equation (3.18) results in:

$$K\varphi_x = \frac{E_c A_c}{\left(1+\frac{A_c E_c}{A_s E_s}\right)}\left(\varphi_x'' - \left(e''y' + ey''' + 2e'y''\right) - \varepsilon_{is}\cos'\vartheta\right) \tag{3.23}$$

Introducing a new variable:

$$\eta = \frac{A_c E_c}{1+\frac{A_c E_c}{A_s E_s}} = \frac{A_s E_s}{1+\frac{A_s E_s}{A_c E_c}} = \frac{A_c E_c A_s E_s}{A_c E_c + A_s E_s} \tag{3.24}$$

After plugging Equation (3.24) into Equation(3.23), Equation(3.23) takes the form:

$$K\varphi_x = \eta\left(\varphi_x^{''} - \left(e^{''}y^{'} + ey^{'''} + 2e^{'}y^{''}\right) - \varepsilon_{is}\cos^{'}\vartheta\right) \tag{3.25}$$

Rearranging terms and letting $\chi_B^{\,2} = K / \eta$ yields:

$$\varphi_x^{''} - \chi_B^2\varphi_x = e^{''}y^{'} + ey^{'''} + 2e^{'}y^{''} + \varepsilon_{is}\cos^{'}\vartheta \tag{3.26}$$

3.2.3 Bending moment equilibrium

Recall that the distance between the concrete beam centroid and the tendon centroid is e, and then moment equilibrium could be established as:

$$M_{ex} = M_c + eN_{s,x} \tag{3.27}$$

where M_{ex} = external applied bending moment and M_c = internal bending moment of the concrete beam. Equation (3.27) can be rewritten as:

$$M_{ex} = -E_c I_c y^{''} + eN \tag{3.28}$$

where I_c = concrete beam moment of inertia. Differentiating Equation (3.6) once:

$$\varphi_{2,x}^{\,'} = \varphi_{2c}^{\,'} + \varphi_{2s,x}^{'} \tag{3.29}$$

Substituting Equation (3.10) and Equation (3.11) into Equation (3.7) results in the following:

$$A_c E_c \varphi_{2c}^{'} = A_s E_s \varphi_{2s,x}^{'} \tag{3.30}$$

Substituting $\varphi_{2c}^{'}$ and $\varphi_{2s,x}^{'}$ in Equation (3.30) into Equation (3.29) results in:

$$\varphi_{2,x}^{'} = \left(1 + \frac{A_c E_c}{A_s E_s}\right)\varphi_{2c}^{'} \tag{3.31}$$

$$\varphi_{2,x}^{'} = \left(1 + \frac{A_s E_s}{A_c E_c}\right)\varphi_{2s,x}^{'} \tag{3.32}$$

Substituting either Equation (3.31) into Equation (3.10), or Equation (3.32) into Equation (3.11), results in:

$$N = \eta\varphi_{2,x}^{'} \tag{3.33}$$

Equation (3.28) can be rewritten after substitution of Equation (3.33) into it as:

$$M_{ex} = -E_c I_c y^{''} + e\eta\varphi_{2,x}^{'} \tag{3.34}$$

Differentiating Equation (3.20) once:

$$\varphi_{2,x}^{'} = \varphi_x^{'} - \left(e^{'}y^{'} + ey^{''}\right) - \varepsilon_{is}\cos\vartheta \tag{3.35}$$

Then substituting Equation (3.35) into Equation (3.34):

$$M_{ex} = -E_c I_c y^{''} + e\eta\left(\varphi_x^{'} - \left(e^{'}y^{'} + ey^{''}\right) - \varepsilon_{is}\cos\vartheta\right) \tag{3.36}$$

After rearranging terms and letting $D_B = E_c I_c + e^2\eta$ and $\alpha_B^{\,2} = e^2\eta / D_B$, Equation (3.36) can be rewritten as:

$$y^{''} + \frac{\alpha_B^{\,2}}{e}e^{'}y^{'} - \frac{\alpha_B^{\,2}}{e}\varphi_x^{'} = -\frac{M_{ex}}{D_B} - \frac{\alpha_B^{\,2}}{e}\varepsilon_{is}\cos\vartheta \tag{3.37}$$

Finally the set of governing equations is obtained as Equation (3.26) and Equation (3.37):

$$\begin{cases} \varphi_x'' - \chi_B^2 \varphi_x = e'' y' + e y''' + 2e' y'' + \varepsilon_{is} \cos' \vartheta \\ y'' + \dfrac{\alpha_B{}^2}{e} e' y' - \dfrac{\alpha_B{}^2}{e} \varphi_x' = -\dfrac{M_{ex}}{D_B} - \dfrac{\alpha_B{}^2}{e} \varepsilon_{is} \cos \vartheta \end{cases}$$

3.3 Discussion of governing equations

The governing equations derivation focuses on the force equilibrium of concrete axial direction (x direction) and the bending moment equilibrium. In the derivation, all the variables related to the tendon are considered only at the concrete axial direction. This is because if the variables at tendon axial direction are to be considered as well, the derivation of equations such as Equation (3.12) will become practically intractable due to the involvement of the derivatives with respect to the angle and cosine. Therefore, in order to avoid that situation and make the derivation easy to follow, variables related to tendon are all considered directly at concrete axial direction and the results at the tendon actual direction can be determined after solving those concrete axial components variables.

The solution to the governing equations will give the transverse deflection y and axial slip component φ_x. The axial force N_c or $N_{s,x}$ and bending moment M_c are then readily determined. Furthermore, the axial force in the strand N_s and the slip along strand φ can be determined as:

$$N_s = N_c / \cos \vartheta \tag{3.38}$$

$$\varphi = \varphi_x / \cos \vartheta \tag{3.39}$$

$$\varphi_{2s} = \varphi_{2s,x} / \cos \vartheta \tag{3.40}$$

$$q = q_x / \cos \vartheta \tag{3.41}$$

Actually, for most prestressed girders with shallow draping, $\cos\theta$ is small, resulting in a difference in horizontal and actual direction from Equation (3.38) through Equation (3.40) of less than one percent near the end and zero everywhere else.

The applications in the later chapters will be based on the general derivations and governing equations developed in this chapter. However, since the various applications may involve simplifications and varying forms of the governing equations, the specific governing equations used for those applications are also derived in the respective chapters.

Chapter 4 Unsymmetrical sandwich structures

4.1 Introduction and scope

The first application of composite theory is insulated concrete sandwich structures, as illustrated in Figure 4-1. For design purposes, sandwich structures are typically categorized into three types: non-composite, partially composite and fully composite. However, because of the existence of the foam insulation layer and connections between two wythes, all sandwich structures are actually partially composite. In practice, in order to avoid thermal bow, shrinkage, creep and other time dependent effects that are difficult to predict, the unsymmetrical wythes sandwich structures are usually designed to be non-composite, whereas the symmetrical wythes sandwich structures are designed to be partially or fully composite. In order to provide a better understanding of sandwich structures, a new categorization system is suggested herein.

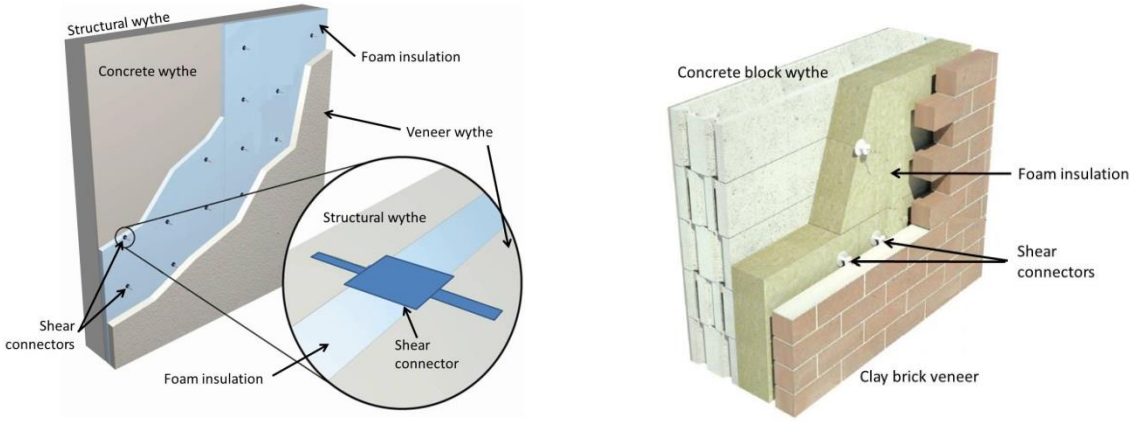

Figure 4-1: Illustrations of unsymmetric sandwich structures (a) precast and (b) masonry

In this dissertation, sandwich structures are differentiated by the analysis approach as symmetrical and unsymmetrical wythes structures. The main difference between symmetrical and unsymmetrical

sandwich structures is that unsymmetrical structures are more difficult to analyze and may have coupled longitudinal and transverse interactions (although it may not be necessary to include the coupled effect) in addition to more prominent transverse interaction than the symmetrical wythes one. Overall, the symmetry of sandwich structures really made both of the longitudinal and transverse interactions easy to quantify.

Generally speaking, symmetrical sandwich structures are much easier to analyze than unsymmetrical sandwich structures, and the most efficient design in terms of resistance and cost. This chapter will focus on the unsymmetrical wythes sandwich structures, and Chapter 5 will simplify the theoretical development of unsymmetrical sandwich structures and apply it to the symmetrical sandwich structures.

4.2 Theoretical development

The longitudinal and transverse interactions are decoupled by decomposing the sandwich structure into the subcases shown in Figure 4-2. Figure 4-2-(b) describes the longitudinal interaction load case; Figure 4-2-(c) and Figure 4-2-(d) are the transverse interaction load cases. In Figure 4-2, q_w = applied uniform pressure, b = width of wythes, $P_1 = 0.5q_w blE_1I_1 / (E_1I_1+E_2I_2)$, $P_2 = 0.5q_w blE_2I_2 / (E_1I_1+E_2I_2)$, E_1 = modulus of elasticity of wythe-1, E_2 = modulus of elasticity of wythe-2, I_1 = moment of inertia of wythe-1, and I_2 = moment of inertia of wythe-2. Following the subscripts on E, I, and P, "wythe-1" is the top wythe, "wythe-2" is the bottom wythe, and "middle layer" refers to the material between wythe-1 and wythe-2 that provides connection between the two wythes.

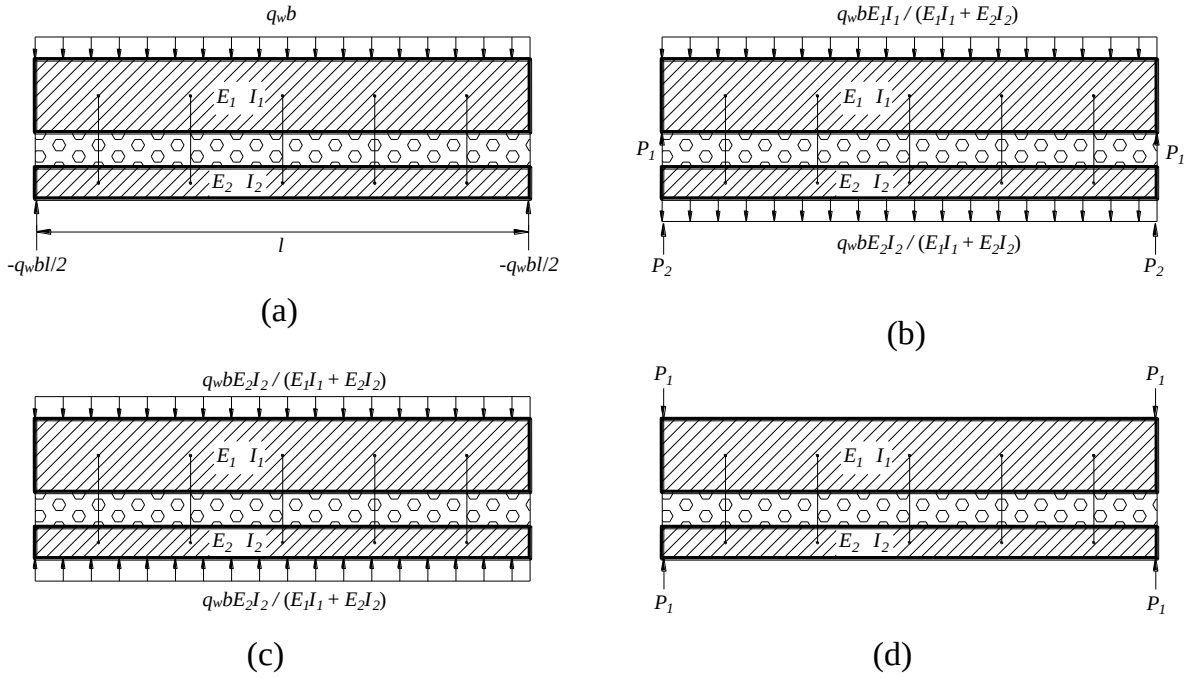

Figure 4-2: Subcases of the uncoupled analysis (compression load case)

It is important to note that, if the loading in Figure 4-2-(a) were changed to that described in Figure 4-3-(a), the analysis procedure would remain the same except that the subcase defined in Figure 4-2-(c) becomes that defined in Figure 4-3-(c). The difference between Figure 4-2-(c) and Figure 4-3-(c) is that the same uniform pressure changes from compressing the sandwich structures to pulling.

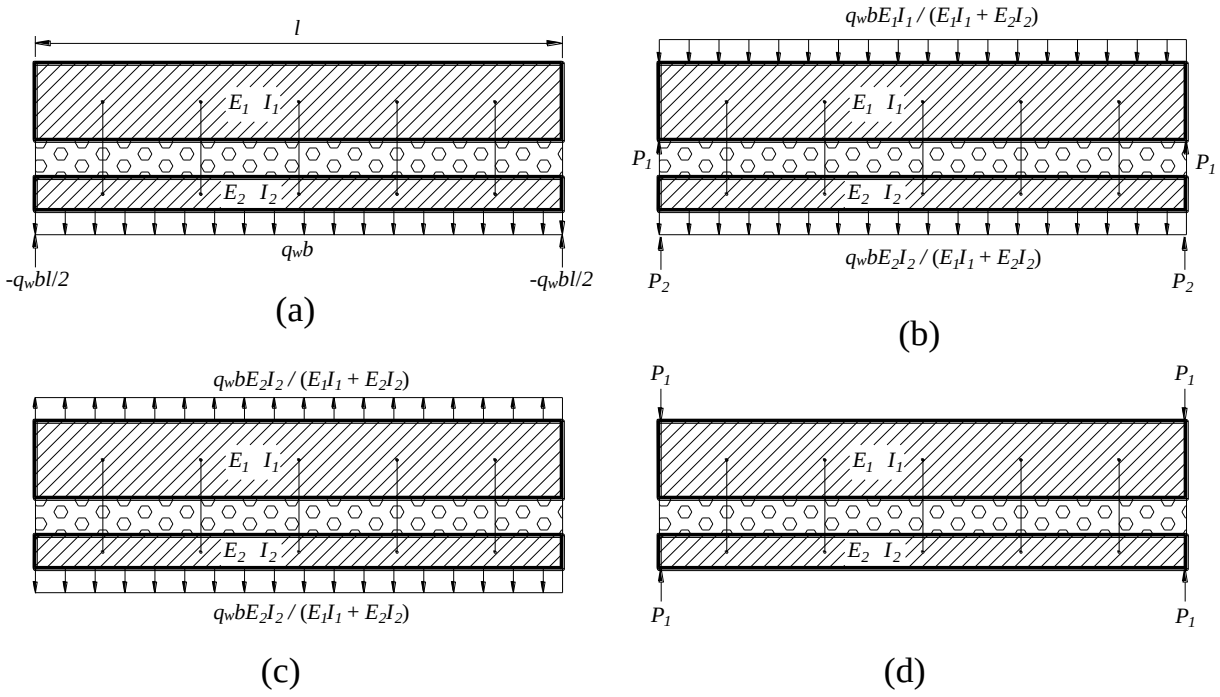

Figure 4-3: Subcases of the uncoupled analysis (tension load case)

4.2.1 Longitudinal interaction

The assumptions and limitations involved in the development of this chapter are the following:

1) Structural behavior is limited to elastic and small displacement, and the constitutive relationships are assumed to be linear.

2) The wythes behave as Euler-Bernoulli beams and have the same deflection and width.

3) Continuous and constant middle layer shear resistance exists along the span. In other words, the shear stiffness of the middle layer is a constant value.

In the derivation that follows, the shear and transverse stiffness of the middle layer, K and k respectively, consists of the stiffness contributions from both the shear connectors and the insulation.

Axial force equilibrium

Axial strain in each wythe is equal to the derivative of its axial displacement, and then the axial stress is equal to Young's modulus times that strain:

$$\sigma_1 = E_1 \varphi_{21}^{'} \tag{4.1}$$

$$\sigma_2 = E_2 \varphi_{22}^{'} \tag{4.2}$$

where σ_1 = axial stress in the first wythe; σ_2 = axial stress in the second wythe; φ_{21} = displacement from its original location of the first wythe (the top one with property of $E_1 I_1$ and A_1 in Figure 4-4) due to axial deformation; φ_{22} = displacement from its original location of the second wythes due to axial deformation;

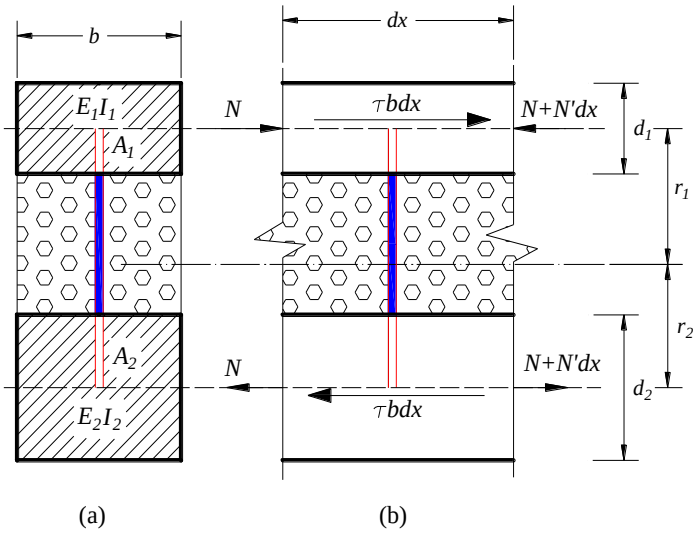

Figure 4-4: (a) cross section; (b) Longitudinal force equilibrium

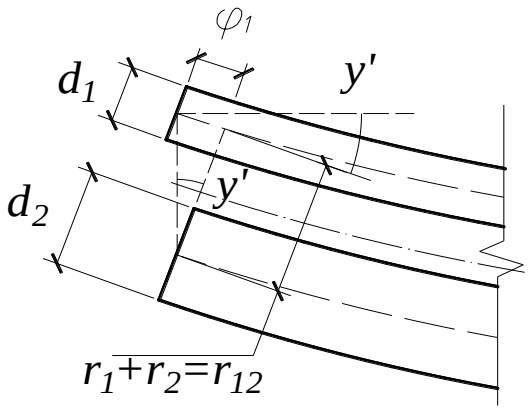

Figure 4-5: Slip due to bending

Wythe-1 is considered, but it should be noted that the same result would be obtained if wythe-2 were considered. Using the equilibrium of forces in axial direction of the wythes shown in Figure 4-4:

$$\tau b dx = N_1^{'} dx \tag{4.3}$$

where τ = shear stress in the middle layer, N_1 = resultant axial force in wythe-1, and b = width of the wythes. The shear of the differential unit length now reads:

$$\tau b = \left(A_1 \sigma_1 \right)' \tag{4.4}$$

where A_1 = cross-section area of wythe-1. Substituting Equation (4.1) into Equation (4.4), the shear stress is determined as:

$$\tau b = E_1 A_1 \varphi_{21}'' \tag{4.5}$$

Rearranging the terms:

$$\tau = \frac{E_1 A_1}{b} \varphi_{21}'' \tag{4.6}$$

Since the slip is the difference between displacements, the slip due to axial deformation is introduced:

$$\varphi_2 = \varphi_{21} + \varphi_{22} \tag{4.7}$$

where φ_2 = slip between wythes due to axial deformation. The fact that the internal axial force in each wythe is equal to each other yields following:

$$N_1 = N_2 = N \tag{4.8}$$

where N_2 = resultant axial force in the second wythe, N = resultant axial force in both wythes. Note that the axial force sign convention is not considered since φ_2 is a relative movement. Equation (4.8) can now be rewritten as:

$$N_1 = A_1 \sigma_1 \tag{4.9}$$

$$N_2 = A_2 \sigma_2 \tag{4.10}$$

Substituting Equation (4.1) and (4.2) into Equations (4.9) and (4.10), respectively, results in:

$$N_1 = A_1 E_1 \varphi_{21}^{'} \tag{4.11}$$

$$N_2 = A_2 E_2 \varphi_{22}^{'} \tag{4.12}$$

Differentiating Equation (4.7) twice:

$$\varphi_2^{''} = \varphi_{21}^{''} + \varphi_{22}^{''} \tag{4.13}$$

Plugging Equation (4.11) and Equation (4.12) into Equation (4.8) and differentiating once:

$$A_1 E_1 \varphi_{21}^{''} = A_2 E_2 \varphi_{22}^{''} \tag{4.14}$$

Substituting φ_{21}'' and φ_{22}'' from Equation (4.14) into Equation (4.13) yields:

$$\varphi_2^{''} = \left(1 + \frac{A_1 E_1}{A_2 E_2}\right) \varphi_{21}^{''} \tag{4.15}$$

$$\varphi_2^{''} = \left(1 + \frac{A_2 E_2}{A_1 E_1}\right) \varphi_{22}^{''} \tag{4.16}$$

Considering the equilibrium between shear connector force and slip:

$$K\varphi = \tau \tag{4.17}$$

where K = shear stiffness of the middle layer; $\varphi = \varphi_1 + \varphi_2$ = total slip between wythes; $\varphi_1 = (r_1 + r_2)y'$ = slip due to bending, as in Figure 4-4 and Figure 4-5; $r_1 + r_2$ = the distance from the centroid of wythe 1 to the centroid of wythe 2 as illustrated; and y = transverse deflection of the wythes. Note that r_1 and r_2 stay together and therefore no need to be computed individually. Again, considering axial force equilibrium of wythe-1 and substituting Equation (4.6) into Equation (4.17):

$$K\varphi = \frac{E_1 A_1}{b} \varphi_{21}^{''} \tag{4.18}$$

Substituting φ_{21}'' in Equation (4.15) into Equation (4.18):

$$K\varphi = \frac{E_1 A_1}{\left(1+\frac{A_1 E_1}{A_2 E_2}\right)b}\varphi_2'' \tag{4.19}$$

Also, the total slip is written as:

$$\varphi = \varphi_1 + \varphi_2 \tag{4.20}$$

Rearranging Equation (4.20) and expressing φ_1 with the relation from Figure 2-5, and plugging $\varphi_1 = (r_1 + r_2)y'$ into Equation (4.20):

$$\varphi_2 = \varphi - (r_1 + r_2)y' \tag{4.21}$$

Differentiating Equation (4.21) twice:

$$\varphi_2'' = \varphi'' - (r_1 + r_2)y''' \tag{4.22}$$

Substituting Equation (4.22) into Equation (4.19):

$$K\varphi = \frac{E_1 A_1}{\left(1+\frac{A_1 E_1}{A_2 E_2}\right)b}\left(\varphi'' - (r_1 + r_2)y'''\right) \tag{4.23}$$

Introducing the variable η:

$$\eta = \frac{A_1 E_1}{1+\frac{A_1 E_1}{A_2 E_2}} = \frac{A_2 E_2}{1+\frac{A_2 E_2}{A_1 E_1}} = \frac{A_1 E_1 A_2 E_2}{A_1 E_1 + A_2 E_2} \tag{4.24}$$

Now plugging Equation (4.24) into Equation (4.23) yields:

$$K\varphi = \frac{\eta}{b}\left(\varphi'' - (r_1 + r_2)y'''\right) \tag{4.25}$$

Rearranging terms and letting $\chi_B^2 = Kb / \eta$ yields:

$$\varphi'' - \chi_B^2 \varphi = (r_1 + r_2)y''' \tag{4.26}$$

Bending moment equilibrium:

Recall that the distances between the resultant axial force in the wythes and the neutral axis are r_1 and r_2, and therefore moment equilibrium can be defined as following:

$$M_{ex} = M_1 + M_2 + r_1 N_1 + r_2 N_2 \tag{4.27}$$

where M_{ex} = external applied bending moment, M_1 = internal bending moment of wythe-1, and M_2 = internal bending moment of wythe-2. Recalling the assumption that both wythes have the same transverse deflection and using Equation (4.8), Equation (4.27) becomes:

$$M_{ex} = -\left(E_1 I_1 + E_2 I_2\right) y'' + \left(r_1 + r_2\right) N \tag{4.28}$$

Differentiating Equation (4.7) once:

$$\varphi_2' = \varphi_{21}' + \varphi_{22}' \tag{4.29}$$

Substituting Equation (4.11) and Equation (4.12) into Equation (4.8):

$$A_1 E_1 \varphi_{21}' = A_2 E_2 \varphi_{22}' \tag{4.30}$$

Substituting φ_{21}' and φ_{22}' in Equation (4.30) back into Equation (4.29) results in:

$$\varphi_2' = \left(1 + \frac{A_1 E_1}{A_2 E_2}\right)\varphi_{21}' \tag{4.31}$$

$$\varphi_2^{'} = \left(1 + \frac{A_2 E_2}{A_1 E_1}\right) \varphi_{22}^{'} \tag{4.32}$$

Substituting either Equation (4.31) into Equation (4.11), or Equation (4.32) into Equation (4.12), results in:

$$N = \eta \varphi_2^{'} \tag{4.33}$$

Equation (4.28) can now be rewritten after substituting Equation (4.33) into it as:

$$M_{ex} = -\left(E_1 I_1 + E_2 I_2\right) y^{"} + \left(r_1 + r_2\right) \eta \varphi_2^{'} \tag{4.34}$$

Differentiating Equation (4.21) once:

$$\varphi_2^{'} = \varphi^{'} - (r_1 + r_2) y^{"} \tag{4.35}$$

Then substituting Equation (4.35) into Equation (4.34):

$$M_{ex} = -\left(E_1 I_1 + E_2 I_2\right) y^{"} + \left(r_1 + r_2\right) \eta \left(\varphi^{'} - (r_1 + r_2) y^{"}\right) \tag{4.36}$$

After rearranging terms and letting $D_B = (E_1 I_1 + E_2 I_2) + (r_1 + r_2)^2 \eta$ and $\alpha_B^{\,2} = (r_1 + r_2)^2 \eta / D_B$, Equation (4.36) is rewritten as:

$$-\frac{M_{ex}}{D_B} = y^{"} - \frac{\alpha_B^{\,2}}{\left(r_1 + r_2\right)} \varphi^{'} \tag{4.37}$$

Finally the governing equations are obtained as Equation (4.26) and Equation (4.37):

$$\begin{cases} \varphi^{"} - \chi_B^{\,2} \varphi = \left(r_1 + r_2\right) y^{'''} \\ y^{"} - \dfrac{\alpha_B^{\,2}}{\left(r_1 + r_2\right)} \varphi^{'} = -\dfrac{M_{ex}}{D_B} \end{cases}$$

4.2.2 Transverse interaction—the 'sandwich pinching' model

The "sandwich pinching" model is obtained by decoupling the transverse action from the longitudinal interaction as shown in Figure 4-2-(d). Its details are further illustrated in Figure 4-6. The assumptions for the transverse interaction are:

1) The longitudinal forces are neglected;

2) The vertical connection through the middle layer remains elastic and constant for both tension and compression.

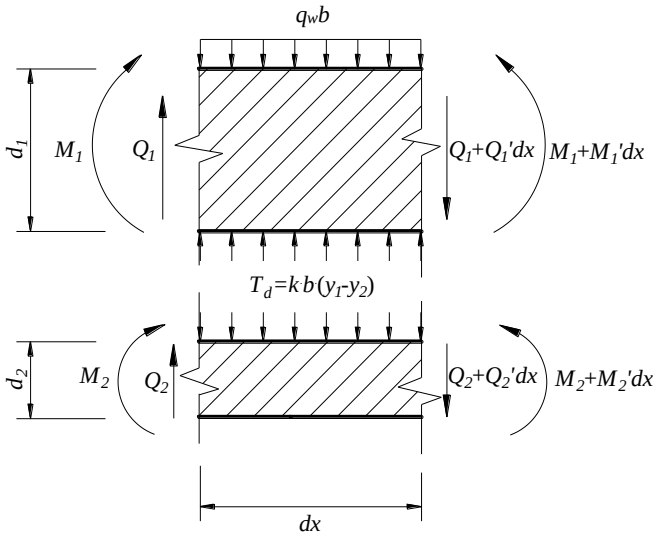

Figure 4-6: Transverse force equilibrium

Individual beam transverse shear equilibrium

Focusing on wythe-1, the transverse shear equilibrium can be established as:

$$Q_1' dx = k\left(y_1 - y_2\right) b dx - q b dx \tag{4.38}$$

where Q_1 = shear force in the cross section of wythe-1 as in Figure 4-6, and k = middle layer transverse stiffness. After rearranging Equation (4.38):

$$Q_1^{'} = bk\left(y_1 - y_2\right) - qb \tag{4.39}$$

Individual beam bending moment equilibrium

Again, focusing on wythe-1, the bending moment must reach equilibrium within the wythe. So sum the bending moment about the left side of the differential element to obtain:

$$M_1^{'}dx = -q_w bdx\left(dx/2\right) + k(y_1 - y_2)bdx\left(dx/2\right) + \left(Q_1 + dQ_1\right)dx \tag{4.40}$$

After eliminating the second order infinitesimal terms,

$$M_1^{'} = Q_1 \tag{4.41}$$

Differentiating Equation (4.41) once:

$$M_1^{''} = Q_1^{'} \tag{4.42}$$

Substituting Equation (4.39) into Equation (4.42) yields:

$$M_1^{''} = bk\left(y_1 - y_2\right) - qb \tag{4.43}$$

Introducing the well-known Euler-Bernoulli beam equation:

$$y_1^{''} = -M_1/\left(E_1 I_1\right) \tag{4.44}$$

Differentiating Equation (4.44) twice:

$$y_1^{(4)} = -M_1^{''}/\left(E_1 I_1\right) \tag{4.45}$$

Substituting Equation (4.43) into Equation (4.45) and rearranging terms:

$$y_1^{(4)} + \left(bk/\left(E_1 I_1\right)\right)\left(y_1 - y_2\right) = q_w b/\left(E_1 I_1\right) \tag{4.46}$$

Similarly, applying the same procedure to the second wythe, its transverse shear and moment equilibrium equations can be obtained as:

$$Q_2^{'} = -bk\left(y_1 - y_2\right) \tag{4.47}$$

where Q_2 = shear force in the second wythe as in Figure 4-6, which is determined as:

$$M_2^{'} = Q_2 \tag{4.48}$$

In the same manner, the governing equation for the second wythe reads:

$$y_2^{(4)} - \left(bk/\left(E_2 I_2\right)\right)\left(y_1 - y_2\right) = 0 \tag{4.49}$$

Equation (4.46) and Equation (4.49) are coupled and therefore will result in difficulties for obtaining a closed form solution. However, they can be simplified by transforming deflections into the transverse forces in the middle layer, T_d. Subtracting Equation (4.46) by Equation (4.49):

$$\left(y_1^{(4)} - y_2^{(4)}\right) + bk\left(1/\left(E_1 I_1\right) + 1/\left(E_2 I_2\right)\right)\left(y_1 - y_2\right) = q_w b/\left(E_1 I_1\right) \tag{4.50}$$

Multiplying Equation (4.50) by width b and middle layer transverse stiffness k:

$$bk\left(y_1^{(4)} - y_2^{(4)}\right) + bk\left(1/\left(E_1 I_1\right) + 1/\left(E_2 I_2\right)\right)bk\left(y_1 - y_2\right) = \left(q_w b\right)\left(kb\right)/\left(E_1 I_1\right) \tag{4.51}$$

Given that there is no uniform pressure for this case (d) of Figure 4-2, q_w is equal to zero. Also only point loads are applied at the two ends of this particular model, which can be conveniently treated as boundary conditions. Thus the governing equation is now written as:

$$T_d^{(4)} + \lambda^4 T_d = 0 \tag{4.52}$$

where $T_d = bk(y_1 - y_2)$ and $\lambda^4 = bk(1/(E_1 I_1) + 1/(E_2 I_2))$.

4.3 Solutions

The following solutions are based on a simply supported beam subjected to uniform pressure on the top (above wythe-1). $M_{ex} = q_w b l^2(1 - (2x / l)^2) / 8$, l = span length, and $x = 0$ is located at the mid-span.

4.3.1 Case b

Upon inspection of the longitudinal governing equations, Equation (4.26) and Equation (4.37), the first impression may be that five boundary conditions are needed since the set of governing equations includes third derivative of deflection and second derivative of slip. However, after mathematical manipulation, only four boundary conditions are actually needed. Firstly, differentiating Equation (4.37) once results in:

$$y''' = \frac{\alpha_B{}^2}{(r_1 + r_2)} \varphi'' - \frac{M_{ex}'}{D_B} \tag{4.53}$$

Substituting Equation (4.53) back into Equation (4.26), the new fourth order governing equations are now:

$$\begin{cases} \varphi'' - \dfrac{\chi_B{}^2}{\beta_B^2} \varphi = -\left(\dfrac{r_1 + r_2}{\beta_B^2 D_B} \right) M_{ex}' \\ y'' - \dfrac{\alpha_B{}^2}{(r_1 + r_2)} \varphi' = -\dfrac{M_{ex}}{D_B} \end{cases}$$

where $\beta_B{}^2 = 1 - \alpha_B{}^2$. For simply supported beams subjected to uniformly distributed pressure, the symmetry boundary conditions at mid-span are slip and slope equal to zero, $\varphi(0) = y'(0) = 0$. Then at the end, deflection and curvature are both zero, so $y(l/2) = y''(l/2) = 0$. As a result, the solutions can be obtained as:

Deflection

$$y_{11} = y_{12} = \frac{5}{384}\frac{q_w b l^4}{D_B}\left[1 - \frac{24}{5}\left(\frac{x}{l}\right)^2 + \frac{16}{5}\left(\frac{x}{l}\right)^4\right]$$
$$+ \frac{1}{16}\frac{q_w b l^4}{D_B}\left(\frac{\alpha_B}{\beta_B}\right)^2\left(\frac{2\beta_B}{\chi_B l}\right)^2\left[\left(\frac{2\beta_B}{\chi_B l}\right)^2\left(\frac{\cosh\frac{\chi_B}{\beta_B}x}{\cosh\frac{\chi_B l}{2\beta_B}} - 1\right) + \frac{1}{2}\left(1 - \left(\frac{2x}{l}\right)^2\right)\right] \quad (4.54)$$

Slip

$$\varphi = \frac{1}{4}\frac{q_w b l^3}{D_B}\left(\frac{r_1 + r_2}{2}\right)\left(\frac{2\beta_B}{\chi_B l}\right)^2 \frac{1}{{\beta_B}^2}\left[\frac{2\beta_B}{\chi_B l}\left(\frac{\sinh\frac{\chi_B}{\beta_B}x}{\cosh\frac{\chi_B l}{2\beta_B}}\right) - \frac{2x}{l}\right] \quad (4.55)$$

Bending Moment

$$M_{11} = \frac{1}{4}q_w b l^2 \frac{E_1 I_1}{\left(E_1 I_1 + E_2 I_2\right)}\left[{\alpha_B}^2\left(\frac{2\beta_B}{\chi_B l}\right)^2\left(1 - \frac{\cosh\frac{\chi_B}{\beta_B}x}{\cosh\frac{\chi_B l}{2\beta_B}}\right) + \frac{1}{2}{\beta_B}^2\left(1 - \left(\frac{2x}{l}\right)^2\right)\right] \quad (4.56)$$

$$M_{12} = \frac{1}{4}q_w b l^2 \frac{E_2 I_2}{\left(E_1 I_1 + E_2 I_2\right)}\left[{\alpha_B}^2\left(\frac{2\beta_B}{\chi_B l}\right)^2\left(1 - \frac{\cosh\frac{\chi_B}{\beta_B}x}{\cosh\frac{\chi_B l}{2\beta_B}}\right) + \frac{1}{2}{\beta_B}^2\left(1 - \left(\frac{2x}{l}\right)^2\right)\right] \quad (4.57)$$

Axial Force

$$N_{11} = -N_{12} = -\frac{1}{4}\frac{q_w b l^2}{\left(r_1 + r_2\right)}{\alpha_B}^2\left[-\left(\frac{2\beta_B}{\chi_B l}\right)^2\left(1 - \frac{\cosh\frac{\chi_B}{\beta_B}x}{\cosh\frac{\chi_B l}{2\beta_B}}\right) + \frac{1}{2}\left(1 - \left(\frac{2x}{l}\right)^2\right)\right] \quad (4.58)$$

Shear Force per Unit Length

$$\tau = \frac{1}{2}\frac{q_w l}{\left(r_1 + r_2\right)}\alpha_B^2\left[\frac{2\beta_B}{\chi_B l}\left(\frac{\sinh\frac{\chi_B}{\beta_B}x}{\cosh\frac{\chi_B l}{2\beta_B}}\right) - \frac{2x}{l}\right] \tag{4.59}$$

4.3.2 Case c

This is a relatively simple case, however it should be noted that since the deflection of each wythe is computed from the centroid of the middle layer, the stiffness is $2k$.

$$y_{21} = -y_{22} = \frac{q_w E_2 I_2}{2k\left(E_1 I_1 + E_2 I_2\right)} \tag{4.60}$$

$$T_c = \frac{q_w b E_2 I_2}{E_1 I_1 + E_2 I_2} \tag{4.61}$$

4.3.3 Case d

The longitudinal interaction is also a fourth order differential equation of the middle layer transverse force. The boundary conditions are obtained according to Figure 4-2-(d). Since $T_d = bk(y_1 - y_2)$, at mid-span, slopes of both wythes are zero so $T_d'(0) = 0$, and no distributed pressure on both wythes so $T_d'''(0) = 0$. At the end, bending moment of each wythe is zero so $T_d''(l/2) = 0$, and two opposite point loads as $T_d'''(l/2) = bkP_1(1/(E_1I_1)+1/(E_2I_2))$. Finally, the middle layer transverse force per unit length is determined as:

$$T_d = A_1\cosh\left(\gamma x\right)\cos\left(\gamma x\right) + A_4\sinh\left(\gamma x\right)\sin\left(\gamma x\right) \tag{4.62}$$

where $A_1 = -(\theta/\gamma^3)\cosh(\gamma l/2)\cos(\gamma l/2)/(\sinh(\gamma l)+\sin(\gamma l))$; $A_4 = -(\theta/\gamma^3)\sinh(\gamma l/2)\sin(\gamma l/2)/(\sinh(\gamma l)+\sin(\gamma l))$; $\theta = bkP_1(1/(E_1I_1)+1/(E_2I_2))$; and $\gamma = \lambda/\sqrt{2}$.

4.4 Properties of solutions

4.4.1 Upper and lower bounds of deflection

In the solutions, from Equation (4.54) to Equation (4.59), the shear stiffness of middle layer K is incorporated into the parameter χ. Therefore the upper and lower bounds of Equation (4.54) can be solved theoretically by setting K to zero and infinity, respectively, as:

$$\lim_{K\to 0} y_1 = y_2 = \frac{5}{384}\frac{q_w b l^4}{\left(E_1 I_1 + E_2 I_2\right)}\left[1 - \frac{24}{5}\left(\frac{x}{l}\right)^2 + \frac{16}{5}\left(\frac{x}{l}\right)^4\right] \tag{4.63}$$

$$\lim_{K\to \infty} y_1 = y_2 = \frac{5}{384}\frac{q_w b l^4}{D_B}\left[1 - \frac{24}{5}\left(\frac{x}{l}\right)^2 + \frac{16}{5}\left(\frac{x}{l}\right)^4\right] \tag{4.64}$$

Equations (4.63) and (4.64) demonstrate that, when the shear stiffness of the middle layer is small enough, the wythes withstand local flexural deformation independently. However, if the shear stiffness of the middle layer is large enough, the wythes will act together as a fully composite beam.

4.4.2 Upper and lower bounds of slip

The bounds of relative slip can be found based from Equation (4.65) and Figure 2-5:

$$\varphi = \varphi_1 + \varphi_2 = \left(r_1 + r_2\right) \times y' + \varphi_2 \tag{4.65}$$

For non-composite beams, φ_2 is zero since the axial force is zero for each wythe. y is obtained from Equation (4.63). For fully composite beams, it is reasonable to assume that the relative slip is zero when considering the assumption made by Euler-Bernoulli beam theory that the plane's normal remains coincident with the beam centroid while bending. Finally, the upper and lower bounds of relative slip can be obtained as:

$$\lim_{K\to 0}\varphi = \frac{5}{384}\frac{(r_1+r_2)q_w bl^3}{(E_1I_1+E_2I_2)}\left[-\frac{48}{5}\left(\frac{x}{l}\right)+\frac{64}{5}\left(\frac{x}{l}\right)^3\right] \tag{4.66}$$

$$\lim_{K\to\infty}\varphi = 0 \tag{4.67}$$

4.4.3 Upper and lower bounds of shear stress

Although the bounds of slip have already been derived, the bounds of shear stress cannot be simply obtained by using the product of slip and shear stiffness. This is because slip will approach zero while the longitudinal shear stiffness will approach infinity when the upper bound is of interest. Consequently, the upper limit is not straightforward. Firstly, from examining Equation (4.19), the lower bound is for non-composite structures, and thus there is no shear stress in the middle layer:

$$\lim_{K\to 0}\tau = 0 \tag{4.68}$$

Now consider the upper bound, fully composite structure. In this case, $\varphi = \varphi_1 + \varphi_2 = 0$, so φ_2 can be determined as:

$$\varphi_2 = -(r_1+r_2)y' \tag{4.69}$$

Plugging Equation (4.69) into Equation (4.19), and recalling that $K\varphi = \tau$ and $\eta = A_1E_1A_2E_2 / (A_1E_1 + A_2E_2)$:

$$\lim_{K\to\infty}\tau = -\eta\left(\frac{r_1+r_2}{b}\right)y''' \tag{4.70}$$

In order to make Equation (4.70) comparable with existing solid beam formula, it must be further transformed by substituting $-E_1I_1y''' = Q_1$ or $-E_2I_2y''' = Q_2$ into Equation (4.70) and again using $\eta = A_1E_1A_2E_2 / (A_1E_1 + A_2E_2)$ and $-E_1I_1y''' = Q_1$:

$$\lim_{K\to\infty}\tau=\frac{Q_1}{I_1 b}\frac{A_1\left(r_1+r_2\right)}{\left(1+A_1E_1/\left(A_2E_2\right)\right)} \tag{4.71}$$

Equation (4.71) takes the same form with the shear in the equivalent Euler- Bernoulli beam, and it is especially obvious when $A_1E_1 = A_2E_2$, which is the symmetrical case that classical beam theory usually considers.

4.4.4 Upper and lower bounds of internal forces

The upper and lower bounds that moment and axial forces at mid-span converge to are based on Equation (4.56) and Equation (4.58):

$$\lim_{K\to 0}M_1=\frac{q_w bl^2}{8}\frac{E_1I_1}{\left(E_1I_1+E_2I_2\right)} \tag{4.72}$$

$$\lim_{K\to 0}M_2=\frac{q_w bl^2}{8}\frac{E_2I_2}{\left(E_1I_1+E_2I_2\right)} \tag{4.73}$$

$$\lim_{K\to\infty}M_1=\left(\frac{q_w bl^2}{8}\beta_B{}^2\right)\frac{E_1I_1}{\left(E_1I_1+E_2I_2\right)} \tag{4.74}$$

$$\lim_{K\to\infty}M_2=\left(\frac{q_w bl^2}{8}\beta_B{}^2\right)\frac{E_2I_2}{\left(E_1I_1+E_2I_2\right)} \tag{4.75}$$

$$\lim_{K\to 0}N_1=-N_2=0 \tag{4.76}$$

$$\lim_{K\to\infty}N_1=-N_2=-\left(\frac{q_w bl^2}{8}\alpha_B{}^2\right)\Big/\left(r_1+r_2\right) \tag{4.77}$$

Where $\alpha_B{}^2$ and $\beta_B{}^2$ represent the ratios of the middle layer bending stiffness and wythes bending stiffness over the overall bending stiffness, respectively. The bending moment is a result of the wythes'

local bending, and the axial force is the result of composite action by shear connectors' forces. Internal forces will be distributed according to the bending stiffness ratio only when fully composite action is achieved. For partially composite structures, internal forces will be distributed according to the equilibrium achieved between shear connectors' deformation and wythes' bending.

4.5 Comparison with existing theories

Many popular literatures in steel concrete composite T girder or other types of composite structures are more or less related to the Newmark model, which includes only the longitudinal interaction. The methodology presented here is similar to Newmark's model[3] in the longitudinal interaction as well, but the transverse interaction was not considered by Newmark.

Longitudinal interaction in Newmark's model

In order to compare with other theories, the set of governing equations are reorganized into a general form. Equation (4.26) and Equation (4.37) are combined to eliminate the terms containing slip. Firstly, differentiating Equation (4.37) once and rearrange terms:

$$y''' = \frac{\alpha_B^2}{r_1 + r_2}\varphi'' - \frac{M_{ex}'}{D_B} \tag{4.78}$$

Substituting Equation (4.78) into Equation (4.26):

$$\varphi'' - \frac{\chi_B^2}{\beta_B^2}\varphi = -\frac{r_1 + r_2}{D_B \beta_B^2} M_{ex}' \tag{4.79}$$

then differentiating Equation (4.79) once:

$$\varphi''' - \frac{\chi_B^2}{\beta_B^2}\varphi' = -\frac{r_1 + r_2}{D_B \beta_B^2} M_{ex}'' \tag{4.80}$$

Also Equation (4.37) can be written as:

$$\varphi' = \left(y'' + \frac{M_{ex}}{D_B} \right) \frac{r_1 + r_2}{\alpha_B^2} \tag{4.81}$$

Differentiating Equation (4.81) twice:

$$\varphi''' = \left(y^{(4)} + \frac{M_{ex}''}{D_B} \right) \frac{r_1 + r_2}{\alpha_B^2} \tag{4.82}$$

Substituting Equation (4.81) and Equation (4.82) into Equation (4.80) and rearranging terms:

$$\left(E_1 I_1 + E_2 I_2 \right) y^{(4)} - \chi_B^2 \left(D_B y'' + M_{ex} \right) = -M_{ex}'' \tag{4.83}$$

On the other hand, Newmark's model is adopted with symbols from this study as:

$$N'' - \frac{K_n}{s} \frac{D_B}{\eta \left(E_1 I_1 + E_2 I_2 \right)} N = -\frac{K_n}{s} \frac{r_1 + r_2}{E_1 I_1 + E_2 I_2} M_{ex} \tag{4.84}$$

where K_n = shear stiffness of an individual connector and s = connector spacing. Then the axial force can be related to deflection as:

$$y'' = -\frac{M_{ex} - N \left(r_1 + r_2 \right)}{E_1 I_1 + E_2 I_2} \tag{4.85}$$

Equation (4.84) and Equation (4.85) together are the governing equations of Newmark's model. Similarly, axial force terms must be eliminated to arrive at a general form. Firstly, from Equation (4.85), N can be expressed as:

$$N = \frac{M_{ex} + y'' \left(E_1 I_1 + E_2 I_2 \right)}{r_1 + r_2} \tag{4.86}$$

Differentiating Equation (4.86) twice:

$$N^{"} = \frac{M_{ex}^{"} + y^{(4)}\left(E_1 I_1 + E_2 I_2\right)}{r_1 + r_2} \tag{4.87}$$

Substituting Equation (4.86) and Equation (4.87) back into Equation (4.84) and rearranging terms:

$$\left(E_1 I_1 + E_2 I_2\right) y^{(4)} - \frac{K_n}{s\eta}\left(D_B y^{"} + M_{ex}\right) = -M_{ex}^{"} \tag{4.88}$$

In Newmark's model, K_n is the stiffness of an individual connector and in this study, K is the average stiffness over the interface area and therefore $Kb = K_n/s$ and $K_n/(s\eta) = \chi_B^2$. Upon inspecting Equation (4.83) and Equation (4.88), it can be concluded that the longitudinal interaction governing equations derived in this study are comparable to Newmark's model. However, it is worth mentioning that Newmark's solutions are complicated and do not necessarily reveal some important resistance characteristics, whereas the solutions developed through the present research can be easily decomposed into the flexural (fully-composite) and shear (inter-layer slip compensation) components. In this manner, many attributes can be simplified for neglecting the shear related compensation terms when the structures are essentially fully composite.

4.6 Stress and results discussion

The internal forces solutions are already given in the solution section 4.3 and therefore the longitudinal stresses of top and bottom fibers are:

$$\sigma_{1,t/b} = \frac{N_{11}}{A} \pm \frac{M_1}{I}\left(\frac{d_1}{2}\right) \tag{4.89}$$

$$\sigma_{2,t/b} = \frac{N_{12}}{A} \pm \frac{M_2}{I}\left(\frac{d_2}{2}\right) \tag{4.90}$$

However, for the present approach, the bending moments M_1 and M_2 require special consideration because the additional transverse deformation will cause additional bending moments in the wythes. Therefore starting from the transverse force, which takes the form:

$$T_d = kb(y_1 - y_2) \tag{4.91}$$

Differentiating Equation (4.91) twice results in:

$$T_d^{''} = kb\left(y_1^{''} - y_2^{''}\right) \tag{4.92}$$

Using $y_1^{''}$ = -M_1 / (E_1I_1) and $y_2^{''}$ = -M_2 / (E_2I_2), Equation (4.92) can be rewritten as:

$$-\frac{M_1}{E_1I_1} + \frac{M_2}{E_2I_2} = \frac{T_d^{''}}{kb} \tag{4.93}$$

From bending moment equilibrium:

$$M_1 + M_2 = M_{ex} - N\left(r_1 + r_2\right) \tag{4.94}$$

Dividing Equation (4.94) with E_2I_2 and E_1I_1:

$$\frac{M_1}{E_2I_2} + \frac{M_2}{E_2I_2} = \frac{M_{ex} - N\left(r_1 + r_2\right)}{E_2I_2} \tag{4.95}$$

$$\frac{M_1}{E_1I_1} + \frac{M_2}{E_1I_1} = \frac{M_{ex} - N\left(r_1 + r_2\right)}{E_1I_1} \tag{4.96}$$

Through Equation (4.93), Equation (4.95) and Equation (4.96), the total wythes bending moments considering the transverse effects M_1 and M_2 can be determined as:

$$M_1 = \left(\frac{M_{ex} - N\left(r_1 + r_2\right)}{E_2I_2} - \frac{T_d^{''}}{kb}\right)\frac{E_1I_1E_2I_2}{E_1I_1 + E_2I_2} \tag{4.97}$$

$$M_2 = \left(\frac{M_{ex} - N\left(r_1 + r_2\right)}{E_1 I_1} + \frac{T_d^{''}}{kb} \right) \frac{E_1 I_1 E_2 I_2}{E_1 I_1 + E_2 I_2} \tag{4.98}$$

Furthermore, the top and bottom longitudinal stresses in the two wythes are determined as:

$$\sigma_{1,t/b} = N/A_1 \pm E_1 \left(\frac{M_{ex} - N\left(r_1 + r_2\right)}{E_2 I_2} - \frac{T_d^{''}}{kb} \right) \frac{E_2 I_2}{E_1 I_1 + E_2 I_2} \left(\frac{d_1}{2} \right) \tag{4.99}$$

$$\sigma_{2,t/b} = -N/A_2 \pm E_2 \left(\frac{M_{ex} - N\left(r_1 + r_2\right)}{E_1 I_1} + \frac{T_d^{''}}{kb} \right) \frac{E_1 I_1}{E_1 I_1 + E_2 I_2} \left(\frac{d_2}{2} \right) \tag{4.100}$$

Also, the bending moment solutions of the Newmark approach and current approach are given in Equations (4.56) and (4.57), and Equations (4.97) and (4.98). Several things are worth noting; first Equation (4.56) and Equation (4.57) only include the bending moments from the longitudinal interaction. On the other hand, Equation (4.97) and Equation (4.98) include the resultant bending moments from both the longitudinal and transverse interactions.

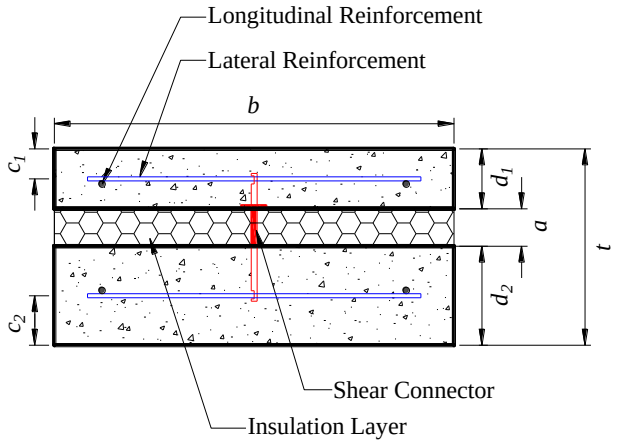

Figure 4-7: Precast sandwich structure cross section.

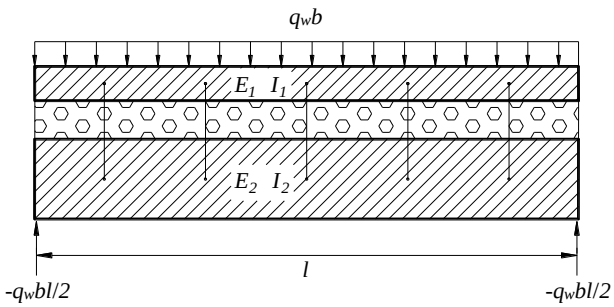

Figure 4-8: Scenario 1

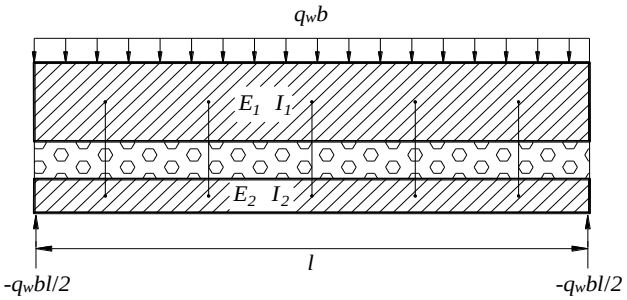

Figure 4-9: Scenario 2

Two scenarios are investigated as in Figure 4-8 and Figure 4-9, the only difference between the two scenarios is that the top and bottom wythes are switched. The basic parameters and dimensions of sandwich structure employed for numerical comparison purposes are defined in Figure 4-8. In the following numerical results and discussion, the baseline dimensions are: a = 2 inches, b = 16 inches, t = 11 inches, d_1 = 3 inches, d_2 = 6 inches, c_1 = 1.5 inches, c_2 = 3 inches, the structure is simply supported with 120 inches span and uniform pressure of 1.5 psi is applied along the span. Young's modulus of top and bottom wythe are 4074.6 ksi and 3886.9 ksi, respectively. The longitudinal and transverse shear stiffnesses are 1740 (lbf/in) and 13921 (lbf/in^3). Note in all the following plots, only the right half of the span is plotted because of symmetry. "0" and "1" along the horizontal axis represent the mid-span and end support respectively. First the middle layer transverse force, which combines the solutions from subcase-c and subcase-d of Figure 4-2, is plotted by using the present methodology.

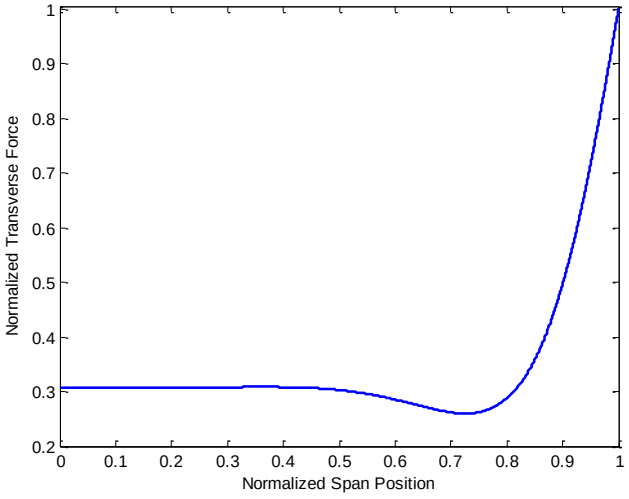

Figure 4-10: Transverse force of scenario 1. T_{max}=69.25 (lbf/in)

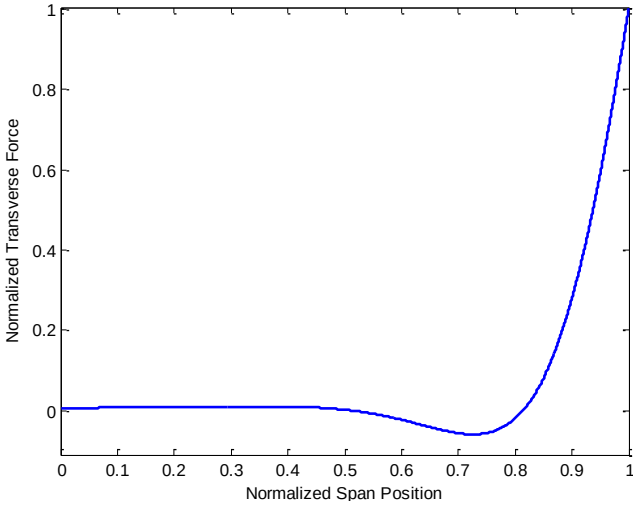

Figure 4-11: Transverse force of scenario 2. T_{max}=369.32 (lbf/in)

It can be observed from Figure 4-10 and Figure 4-11 that at the end support the transverse force reaches the maximum value but decreases to its minimum value within about one third of the half span. However, in the Figure 4-10 scenario 1 the transverse force is in compression whereas in the Figure 4-11 scenario 2 near the quarter span tensile transverse force (negative values) starts to develop. In Figure 4-11 the tensile force occurs because the tensile force from the subcase-d of Figure 4-2-(d) overrides the compressive pressure from the subcase-c of Figure 4-2-(c) near the quarter span. Also, another interesting observation is that the transverse force in scenario 2 is more than four times larger than it is in scenario 1 at the end support. For the two scenarios, the bending moment in the two wythes are plotted in Figure 4-12 to Figure 4-15.

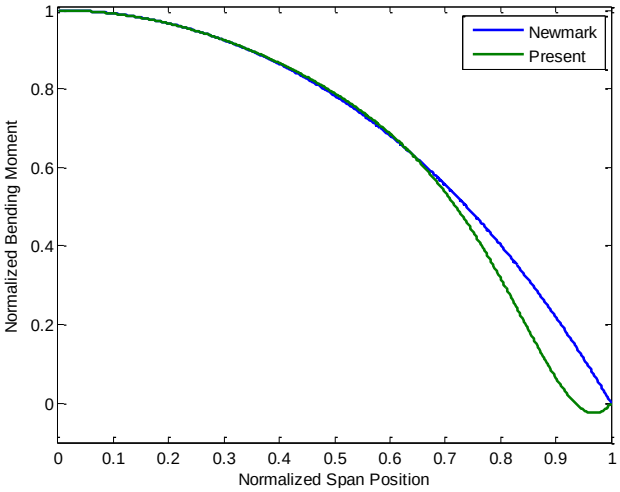

Figure 4-12: Wythe-1 bending moments of scenario 1. M_{max}=2407 (lbf-in)

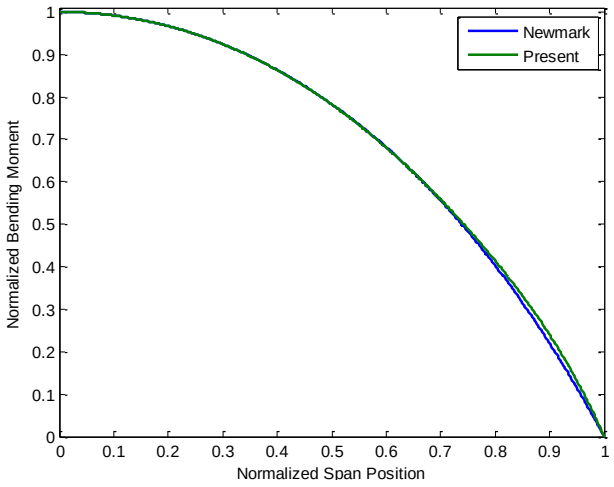

Figure 4-13: Wythe-2 bending moments of scenario 1. M_{max}=18370 (lbf-in)

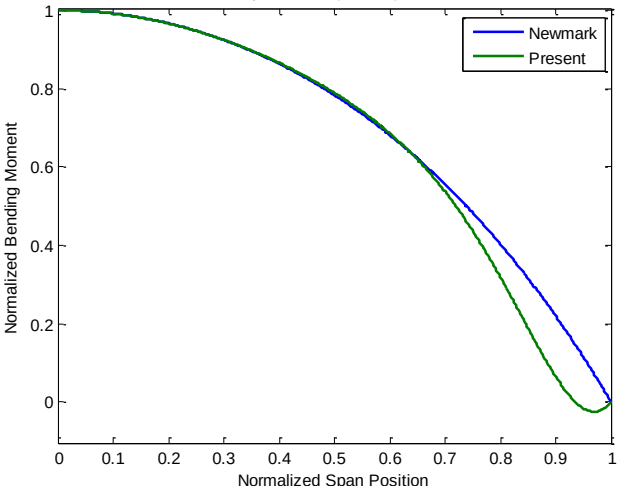

Figure 4-14: Wythe-1 bending moments of scenario 2. M_{max}=18367 (lbf-in)

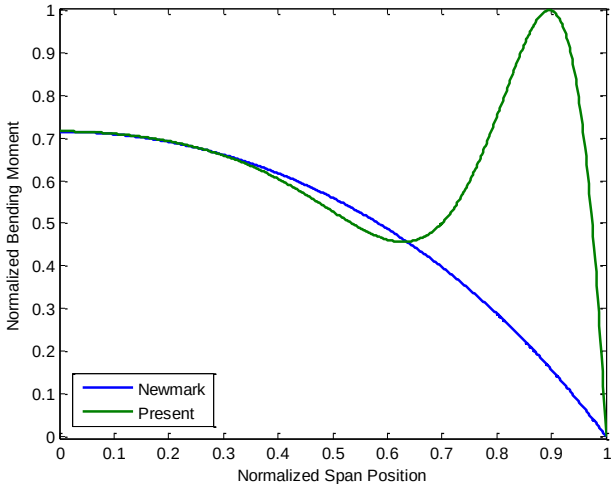

Figure 4-15: Wythe-2 bending moments of scenario 2. M_{max}=3365 (lbf-in)

From Figure 4-12 to Figure 4-15, the present approach and Newmark's approach result in very obvious difference in bending moments, as much as 500% for wythe-2 near the end support. However, near the mid-span the difference almost vanishes since the influence of transverse interaction can hardly reach there. Additionally, it is worth noting that among the two different wythes the thin wythe tends to bear the larger difference between the two methodologies. For example, in Figure 4-12 and Figure 4-13, different approaches result in larger difference on wythe-1. However, in Figure 4-14 and Figure 4-15, two different approaches result in larger difference on wythe-2. This makes sense given the fact that the

main difference between the two approaches is that the present methodology considers the bending moment caused by the transverse interaction whereas Newmark's methodology does not. Therefore when the two wythes are subjected to the same external loads as in the subcase-(d) of Figure 4-2, the thinner wythe will have more prominent transverse interaction and therefore larger bending moment associated with the transverse interaction. Stresses in the top and bottom fibers of the two wythes are plotted in Figure 4-16 to Figure 4-23.

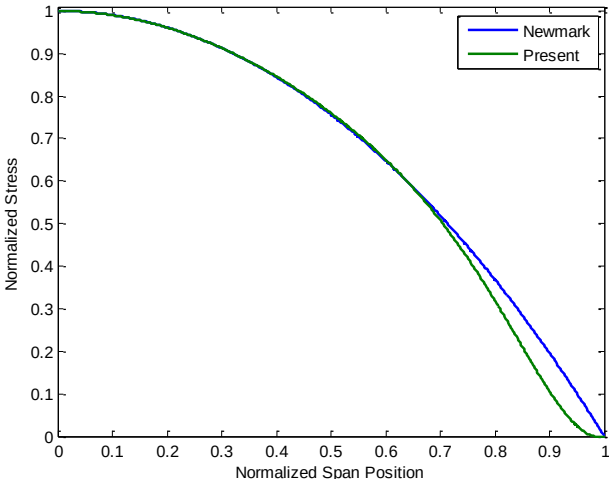

Figure 4-16: Top fiber stress of wythe-1 for scenario 1. σ_{max}=172.15 (psi)

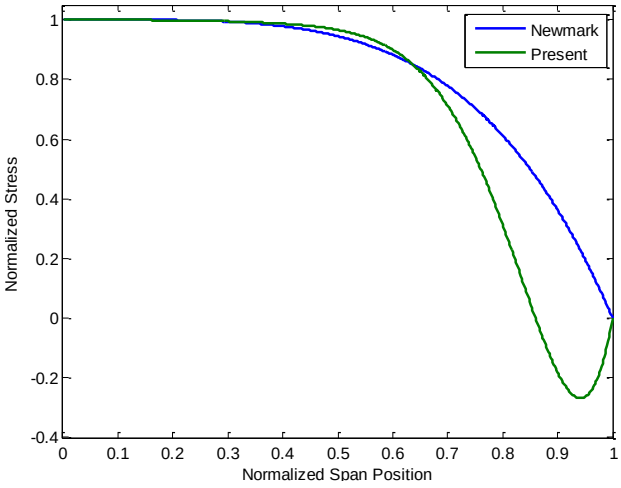

Figure 4-17: Bottom fiber stress of wythe-1 for scenario 1. σ_{min}=-28.41 (psi)

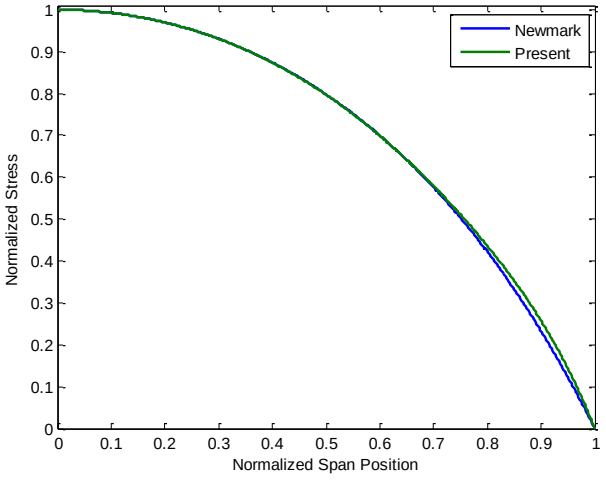

Figure 4-18: Top fiber stress of wythe-2 for scenario 1. σ_{max}=155.42 (psi)

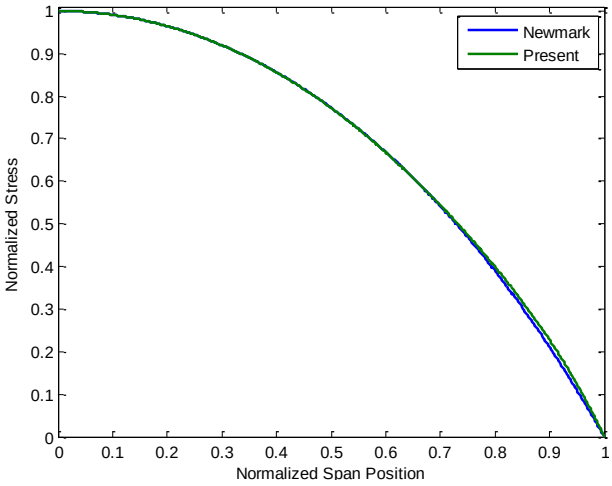

Figure 4-19: Bottom fiber stress of wythe-2 for scenario 1. σ_{min}=-227.29 (psi)

As in Figure 4-16 to Figure 4-19, for scenario one, at the thinner wythe, wythe-1, two approaches yield apparent difference in terms of stress, but for the thicker wythe, wythe-2, the difference between the two approaches is smaller than wythe-1. This is due to the bending moment difference between the two wythes. In Figure 4-17 near the end support, note that the transverse interaction will result in compressive stress whereas, if the transverse interaction is not considered as in Newmark's approach, the stress is still tensile. Furthermore the compressive stress is about 25% of the maximum stress at the mid-span in Figure 4-17.

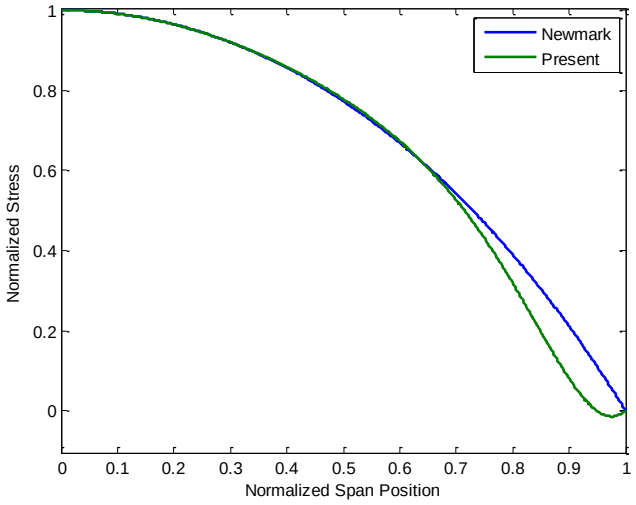

Figure 4-20: Top fiber stresses of wythe-1 for scenario 2. σ_{max}= 227.26 (psi)

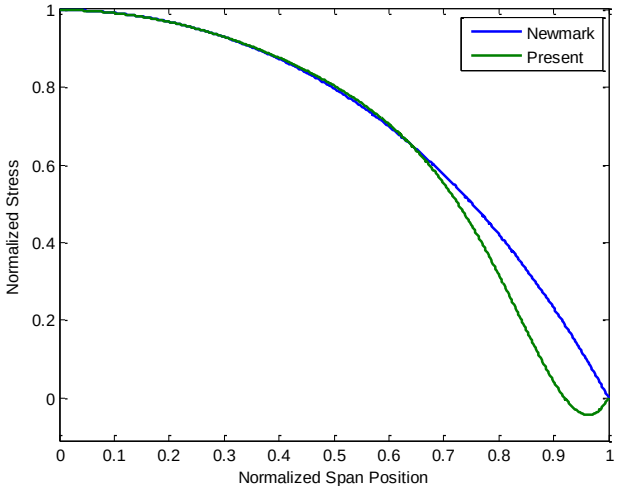

Figure 4-21: Bottom fiber stresses of wythe-1 for scenario 2. σ_{min}=-155.39 (psi)

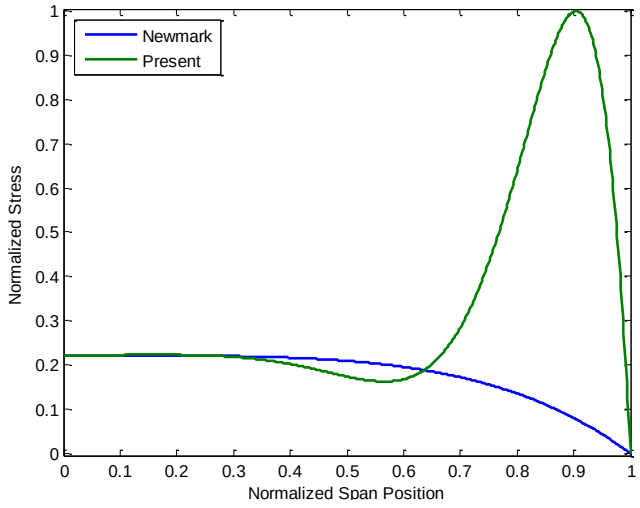

Figure 4-22: Top fiber stresses of wythe-2 for scenario 2. σ_{max}=128.54 (psi)

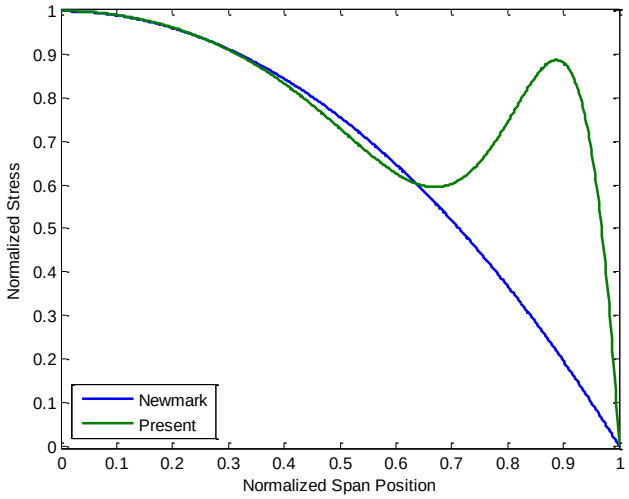

Figure 4-23: Bottom fiber stresses of wythe-2 for scenario 2. σ_{min}=-172.26 (psi)

As seen in Figure 4-20 to Figure 4-23, again for scenario 2 the thinner wythe, wythe-2, also bear larger difference between the two approaches than the thicker wythe. However the difference is more obvious than it is in scenario 1. This is again mainly because the transverse interaction in subcase-d of Figure 4-2-(d) is larger and the resultant bending moments is greater for the thin wythe but Newmark's approach does not consider this resultant bending moment from transverse interaction. Therefore, as this transverse interaction associated bending moment becomes larger, the difference between the two approaches increases.

4.7 Conclusions

A new analysis procedure and associated subcases for analyzing partially composite structures with non-symmetric wythes are presented to break the complicated behaviors into the the simple subcases illustrated in Figure 4-2 and Figure 4-3. Two sets of governing equations are derived to capture the longitudinal and transverse behaviors of partially composite sandwich structures. The longitudinal governing differential equations derived in this study are an extension of Granholm's governing equations, which were originally derived only for nailed timber structures with identical timber layers. It has now been generalized to accommodate a wide range of structures, including the capability to deal with arbitrary properties and materials such as foam insulated sandwich structures, steel concrete T girders, etc. The transverse governing equations are derived to consider subcase (d) in Figure 4-2 and Figure 4-3. Furthermore, this study provides mathematical discussion that links theories such as the Newmark model to the present model. The differences between the two models are thoroughly inspected and discussed.

It is demonstrated that the present approach captures transverse interaction and results in more reasonable results than Newmark's approach, especially in terms of bending moment. The resultant

stresses also show apparent difference between the two approaches. The model developed through the present research balances the complexity and accuracy by supplementing important transverse interaction as a decoupled load case. Another important aspect of this study is that the governing equations are all solved with closed form solutions, which lends convenience to future application to practical design and analysis. Also the upper and lower bounds of those solutions are derived and provided in closed forms, and in that way the estimation of internal forces in any partially composite structures is made possible.

This analysis approach in this chapter decouples the longitudinal land transverse interactions and investigates them separately. However, the longitudinal and transverse effects are actually coupled. The discussion and evaluation on the mechanics of coupling needs thorough investigation so future study will include that aspect. Other future work will also include transforming the theory presented here into design methodology and additional discussion of nonlinear properties associated with sandwich structures.

Chapter 5 Symmetrical sandwich structures

5.1 Introduction and scope

Symmetrical sandwich structures can be regarded as a special case of unsymmetrical structures, and the governing equations and solutions of unsymmetrical cases are applicable to the symmetrical structures. Since the internal forces and stresses have been thoroughly discussed in Chapter 4, this chapter will emphasize the deflection, and other symmetrical sandwich structures behavior. Furthermore, unlike unsymmetrical sandwich structures, the deflection associated with transverse interaction in symmetrical sandwich structures is usually negligible compared to the deflection associated with the longitudinal effect. Therefore only the longitudinal behaviors are discussed in this chapter.

5.2 Theoretical development

After simplifying the theory developed in Chapter 4 and applying it to symmetrical structures, the governing equations now take the form:

$$\varphi'' - \chi^2 \varphi = 2ry''' \tag{5.1}$$

$$y'' - \frac{\alpha^2}{2r}\varphi' = -\frac{M_{ex}}{E_w I_{total}} \tag{5.2}$$

The solution cases can still be derived from Figure 4-2, but in case of symmetrical wythes the load cases are simplified as illustrated in Figure 5-1.

.

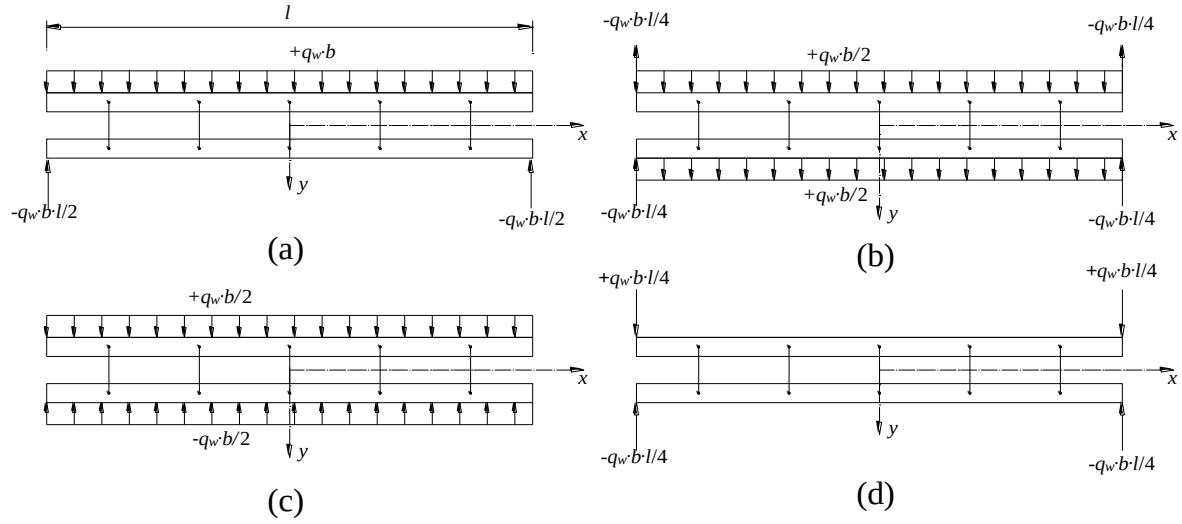

Figure 5-1: Load Cases of symmetrical sandwich structures

In Figure 5-1, q_w = applied uniform pressure. The case shown in Figure 5-1-(b) determines the deflection shared by both wythes, then the second and third cases shown in Figure 5-1-(c) and Figure 5-1-(d), respectively, determine the relative vertical compression between the wythes. All of the three cases are presented here, but the second and third cases are regarded as beam bending on soft medium, the details of which can also be found from related references. In this study, those later two cases are considered to be trivial for symmetrical wythes sandwich structures.

5.3 Solutions

In this section, the solutions of the longitudinal interaction as in Figure 5-1-(a) are considered.

Deflection:

$$y_1 = \frac{5}{384}\frac{q_w b l^4}{E_w I_{total}}\left[1-\frac{24}{5}\left(\frac{x}{l}\right)^2+\frac{16}{5}\left(\frac{x}{l}\right)^4\right] + \frac{1}{16}\frac{q_w b l^4}{E_w I_{total}}\left(\frac{\alpha}{\beta}\right)^2\left(\frac{2\beta}{\chi l}\right)^2\left[\left(\frac{2\beta}{\chi l}\right)^2\left(\frac{\cosh\frac{\chi}{\beta}x}{\cosh\frac{\chi l}{2\beta}}-1\right)+\frac{1}{2}\left(1-\left(\frac{2x}{l}\right)^2\right)\right] \quad (5.3)$$

$$y_2 = \pm \frac{q_w}{4k} \tag{5.4}$$

where: $\beta = \sqrt{(1-\alpha^2)}$; k = vertical compressive stiffness of middle layer; l = span length.

$$y_3 = \pm \frac{\sqrt{2}}{2} \frac{q_w b l}{E_w I_{total}} \frac{l_0}{\beta^2} \frac{1}{\psi} \left(\varphi_1^0 \varphi_1 + \varphi_3^0 \varphi_3 \right) \tag{5.5}$$

where: $\Psi = \varphi_1{}^0(\varphi_2{}^0 + \varphi_4{}^0) - \varphi_3{}^0(\varphi_2{}^0 - \varphi_4{}^0)$; $\varphi_1{}^0 = \cos\lambda \cdot \cosh\lambda$; $\varphi_2{}^0 = \cos\lambda \cdot \sinh\lambda$; $\varphi_3{}^0 = \sin\lambda \cdot \sinh\lambda$; $\varphi_4{}^0 = \sin\lambda \cdot \cosh\lambda$; $\varphi_1 = \cos\varepsilon \cosh\varepsilon$; $\varphi_3 = \sin\varepsilon \sinh\varepsilon$; $\lambda = \sqrt{2}/4(l/l_0)$; $\varepsilon = \sqrt{2}/4(x/l_0)$; and $l_0 = \sqrt[4]{(E_w \cdot i/(2k \cdot b))}$; $i = 2I_{sgl}$.

The solution can be represented as:

$$\begin{cases} y^{ex} = |y_1| + |y_2| + |y_3| \\ y^{in} = |y_1| - |y_2| - |y_3| \end{cases} \tag{5.6}$$

Bending moment in the wythes:

$$M_1 = \frac{1}{8} q_w b l^2 \left[\alpha^2 \left(\frac{2\beta}{\chi l} \right)^2 \left(1 - \frac{\cosh \frac{\chi}{\beta} x}{\cosh \frac{\chi l}{2\beta}} \right) + \frac{1}{2} \beta^2 \left(1 - \left(\frac{2x}{l} \right)^2 \right) \right] \tag{5.7}$$

$$M_2 = 0 \tag{5.8}$$

$$M_3 = -\frac{\sqrt{2}}{4} q_w b l^2 \frac{l_0}{l} \frac{1}{\psi} \left(\varphi_3^0 \varphi_1 - \varphi_1^0 \varphi_3 \right) \tag{5.9}$$

The solution can be represented as:

$$\begin{cases} M^{ex} = |M_1| - |M_3| \\ M^{in} = |M_1| + |M_3| \end{cases} \tag{5.10}$$

Axial force in the wythes (prestressing force not included):

$$N_1 = \frac{1}{8}\frac{q_w b l^2}{r}\alpha^2\left[-\left(\frac{2\beta}{\chi l}\right)^2\left(1-\frac{\cosh\frac{\chi}{\beta}x}{\cosh\frac{\chi l}{2\beta}}\right)+\frac{1}{2}\left(1-\left(\frac{2x}{l}\right)^2\right)\right] \tag{5.11}$$

$$N_2 = 0 \tag{5.12}$$

$$N_3 = 0 \tag{5.13}$$

The solution can be represented as:

$$\begin{cases} N^{ex} = -N_1 \\ N^{in} = N_1 \end{cases} \tag{5.14}$$

Slip between the wythes:

$$\varphi = \frac{1}{4}\frac{q_w r b l^3}{E_w I_{total}}\left(\frac{2\beta}{\chi l}\right)^2\frac{1}{\beta^2}\left[\frac{2\beta}{\chi l}\left(\frac{\sinh\frac{\chi}{\beta}x}{\cosh\frac{\chi l}{2\beta}}\right)-\frac{2x}{l}\right] \tag{5.15}$$

Middle layer shear stress:

$$\tau = \frac{1}{4}\frac{q_w l}{r}\alpha^2\left[\frac{2\beta}{\chi l}\left(\frac{\sinh\frac{\chi}{\beta}x}{\cosh\frac{\chi l}{2\beta}}\right)-\frac{2x}{l}\right] \tag{5.16}$$

Or alternatively

$$\tau = K\varphi \tag{5.17}$$

5.4 Property of solution

5.4.1 Upper and lower bounds of deflection

The upper and lower bounds of Equation (5.3) can be solved theoretically as:

$$\lim_{K\to 0} y = \frac{5}{384}\frac{q_w b l^4}{E_w\left(2I_{\text{sgl}}\right)}\left[1-\frac{24}{5}\left(\frac{x}{l}\right)^2+\frac{16}{5}\left(\frac{x}{l}\right)^4\right] \tag{5.18}$$

$$\lim_{K\to \infty} y = \frac{5}{384}\frac{q_w b l^4}{E_w I_{total}}\left[1-\frac{24}{5}\left(\frac{x}{l}\right)^2+\frac{16}{5}\left(\frac{x}{l}\right)^4\right] \tag{5.19}$$

Equations (5.18) and (5.19) mean that when the shear stiffness of the middle layer is sufficiently small, the wythes withstand local flexural deformation independently. However, if the shear stiffness of middle layer is sufficiently large, the wythes will act together as a fully composite beam.

5.4.2 Upper and lower bounds of slip

The bounds of relative slip can be calculated based on Equation (5.20):

$$\varphi = \varphi_1 + \varphi_2 = 2r \times y' + \varphi_2 \tag{5.20}$$

For non-composite beams, φ_2 is zero since the axial force is zero for each wythe. y is obtained from Equation (5.18). For fully composite beams, it is reasonable to assume that the relative slip is zero when considering the assumption made by Euler-Bernoulli beam theory that the plane's normal remains coincident with the beam centroid while bending. Finally, the upper and lower bounds of relative slip can be obtained as:

$$\lim_{K\to 0} \varphi = \frac{5}{384}\frac{r q_w b l^3}{E_w I_{\text{sgl}}}\left[-\frac{48}{5}\left(\frac{x}{l}\right)+\frac{64}{5}\left(\frac{x}{l}\right)^3\right] \tag{5.21}$$

$$\lim_{K\to\infty} \varphi = 0 \tag{5.22}$$

5.4.3 Upper and lower bounds of internal forces

The upper and lower bounds in which the mid-span moment and axial forces converge to are based upon Equations (5.7) and Equation (5.11):

$$\lim_{K\to 0} M = \frac{(q_w/2)bl^2}{8} \tag{5.23}$$

$$\lim_{K\to\infty} M = \left(\frac{q_w bl^2}{8}\beta^2\right)\Big/ 2 \tag{5.24}$$

$$\lim_{K\to 0} N = 0 \tag{5.25}$$

$$\lim_{K\to\infty} N = \left(\frac{q_w bl^2}{8}\alpha^2\right)\Big/ (2r) \tag{5.26}$$

where $\alpha^2 = 2r^2A/I_{total}$, $\beta^2 = 1\text{-}\alpha^2$. α^2 and β^2 represent the ratios of middle layer bending stiffness, and wythes bending stiffness over the overall bending stiffness respectively. The bending moment is a result of the local bending in the wythes, and the axial force is the result of composite action through the resistance provided by the shear connectors. Internal forces will be distributed according to bending stiffness ratio only when fully composite action is achieved. For partially composite structures, internal forces will be distributed according to equilibrium achieved between shear connector deformation and wythe bending.

5.5 Theory for discrete shear connectors

As in the section 3.2.1, one of the common assumptions is that the shear stiffness is constant and continuous along the span. However, in reality, this is an unrealistic assumption since discrete, perhaps

with non-uniform spacing, shear connector distributions are often used. Therefore, an arbitrary shear stiffness function is implemented in the present research. By doing so, any form of shear connector pattern can be analyzed, but as a result, the governing equations are nonlinear and can only be solved numerically.

In this study, a rectangle wave is chosen to represent the stiffness of discrete shear connecters. Therefore the constant shear stiffness K is replaced by a shear stiffness function K_f, which is obtained through Fourier Transform as:

$$K_f(x) = K_{in}\left\{\frac{t}{T} + \sum_{n=1}^{\infty}\frac{1}{n\pi}\sin\left(\frac{2\pi n}{T}\right)\cos\left(\frac{2\pi n}{T}x\right) + \sum_{n=1}^{\infty}\frac{1}{n\pi}\left(1-\cos\left(\frac{2\pi n}{T}\right)\right)\sin\left(\frac{2\pi n}{T}x\right)\right\} \quad (5.27)$$

where K_f = the shear stiffness function of the whole structure; K_{in} = the shear stiffness of individual shear connecter; t = length of positive phase; T = period length. It is suggested that $K_{in} = K(T/t)$ when the dimension of shear connecter cannot be accurately obtained. In this way, the total shear stiffness of all the shear connecters remains constant, even though the shear connecter width varies. The rectangular wave function with $T = l/6$ (l = span length), and $t = 0.05T$ is used in this study, which is normalized and plotted in Figure 5-2.

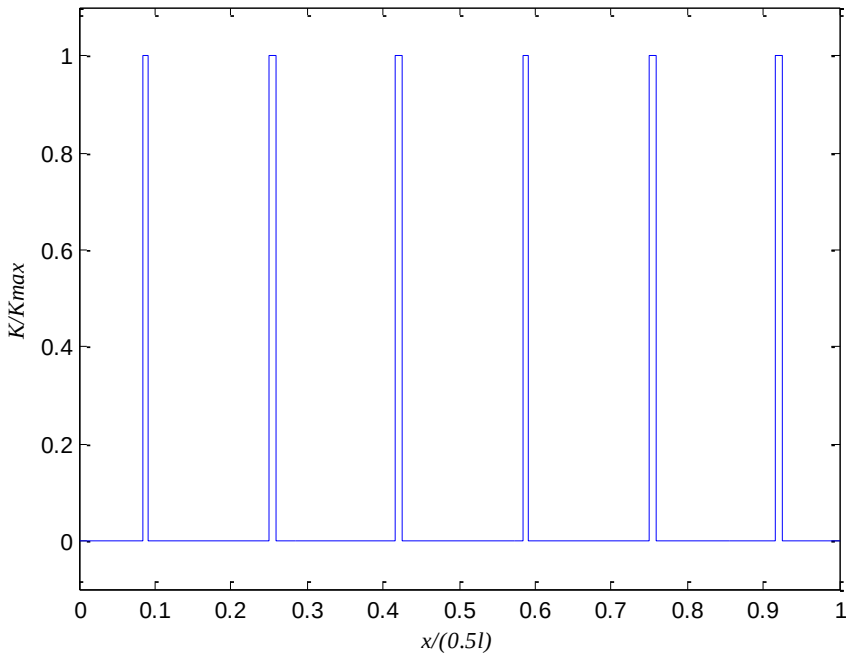

Figure 5-2: Shear stiffness function

K is then replaced with K_f in the governing equations, and the first governing equation is obtained as:

$$\frac{2bK_f}{E_w A}\varphi - \varphi'' = -2ry''' \tag{5.28}$$

The new set of governing equations is now rewritten by replacing Equation (5.1) with Equation (5.28) as:

$$\begin{cases} \varphi'' - \dfrac{2bK_f}{E_w A}\varphi = 2ry''' \\ y'' - \dfrac{\alpha^2}{2r}\varphi' = -\dfrac{M_{ex}}{E_w I_{total}} \end{cases}$$

In order to solve the coupled governing equations, Equation (5.28) is mathematically manipulated to the second order by eliminating the third order term of deflection. The processed set of governing equations is determined as:

$$\varphi'' - \frac{2bK_f}{\beta^2 E_w A}\varphi = -\frac{2r}{\beta^2 E_w I_{total}} M'_{ex} \tag{5.29}$$

$$y'' - \frac{rA}{I_{total}}\varphi' = -\frac{M_{ex}}{E_w I_{total}} \tag{5.30}$$

where $\beta^2 = (1-\alpha^2)$. Then the first order standard form of the governing equations is determined based on Equations (5.29) and (5.30) for numerical solution as:

$$Z_1' = \lambda_1 \cdot Z_2 - \lambda_2 \tag{5.31}$$

$$Z_2' = Z_1 \tag{5.32}$$

$$Z_3' = \lambda_3 \cdot Z_1 - \lambda_4 \tag{5.33}$$

$$Z_4' = Z_3 \tag{5.34}$$

where: $Z_1 = \varphi'$; $Z_2 = \varphi$; $Z_3 = y'$; $Z_4 = y$; $\lambda_1 = 2bK_f/(\beta^2 E_w A)$; $\lambda_2 = 2rM_{ex}'/(\beta^2 E_w I_{total})$; $\lambda_3 = rA/I_{total}$; and $\lambda_4 = M_{ex}/(E_w I_{total})$.

Finally, Equations (5.31) through (5.34) can be solved with specific boundary conditions as a Boundary Value Problem (BVP), and numerical schemes such as finite difference can be employed.

Granholm's theory does not involve those additional assumptions and is mechanically closer to ICSPs but yields complexity in both of the governing equations and solution. However, they both have an unrealistic assumption of constant and continuous shear stiffness in the middle layer along the span length. Finally, the arbitrary shear resistance theory developed herein is better conditioned in terms of shear stiffness but can only be solved numerically.

Comparison between continuous and discrete models

The continuous model refers to Granholm's Model or the first case of Holmberg's solution. Equations (5.31) through (5.34) can be solved with simply supported beam boundary conditions, which are given in

Equations (5.35). Note that among these boundary conditions, $Z_2(0) = 0$, $Z_3(0) = 0$, and $Z_4(l/2) = 0$ are directly obtained from the fact that slip and slope are zero at the mid-span, and deflection is zero at the end support. However, $Z_1(l/2) = 0$ is derived from Equation (5.30), with the conditions of both external applied bending moment M_{ex} and internal bending moment $-E_W I_{sgl} y''$ equal to zero at the ends.

$$Z_1(l/2) = Z_2(0) = Z_3(0) = Z_4(l/2) = 0 \tag{5.35}$$

The normalized results of deflection, slip, bending moment and axial force (normalized to 0.39) of both models for half of the span are compared and plotted in Figure 5-3. As can be noted, deflection and relative slip are not significantly affected by the Discrete Models. However, the internal forces, such as axial force and bending moment, are significantly affected at the vicinity of the shear connectors. Furthermore, two parameters, t and T as defined in Equation (5.27), will affect the results, even though the total shear stiffness remains constant. The ratio of t / T is usually referred to as "duty cycle," which ranges from zero to one. The greater the duty cycle is the smoother the results will become. When the duty cycle is equal to 1, the discrete model becomes the continuous model. For example, in Figure 5-3, the Discrete Model has a duty cycle of 0.05 and the Continuous Model can be regarded as the Discrete Model with duty cycle of 1, and they all have the same middle layer total shear stiffness. Therefore it is generally sound to conclude that the continuous shear connector model is adequate for general analysis; however, the maximum stress may no longer occur at mid-span, but rather in the vicinity of shear connectors near mid-span, and actual stress near the shear connecters may be larger than predicted by the continuous model. Special attention should be paid to the problems with large shear stiffness, but small duty cycle.

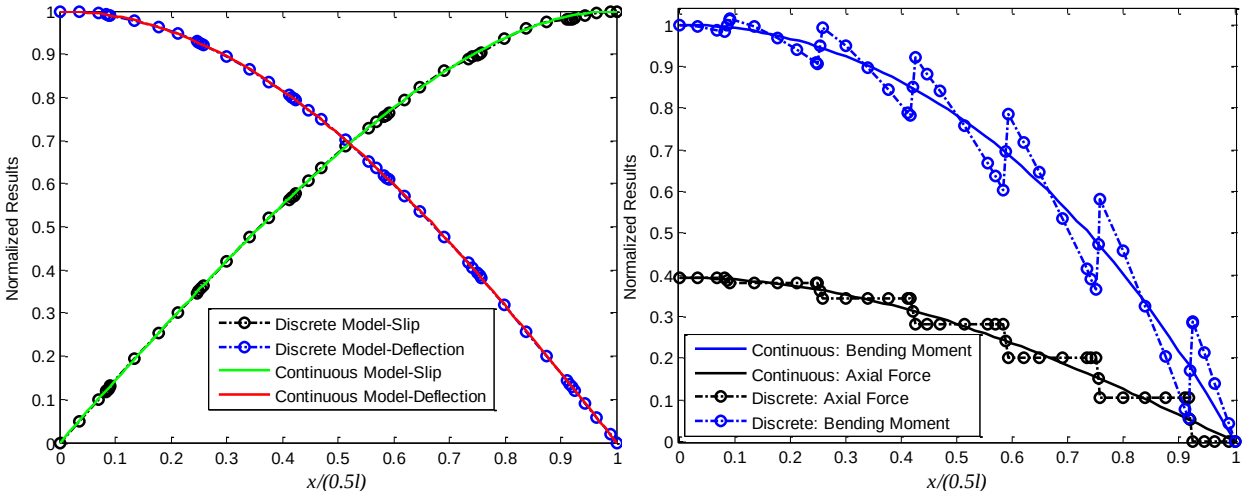

Figure 5-3: Comparison of different models

5.6 Experiment setup and validation

Holmberg's solution is employed for the validation since the Discrete Model will yield the same deflection and slip results. Also, the sandwich panels tested have very large vertical resistances; therefore the second and third terms are trivial.

$$y = y^{in} = y^{ex} = y_1 \tag{5.36}$$

5.6.1 Consideration of prestressing forces

Prestressing forces are considered as a pair of axial forces plus a pair of additional bending moments if eccentric prestressing tendons are present. For this study, the prestressing tendons are in the center of each wythe, therefore only a pair of axial forces is considered. Since this study is limited to small displacement and linear elastic behaviors, curvature and deflection will not be affected by this pair of axial forces.

5.6.2 Experiment setup

Data from experiments conducted by Naito[25][31]-[34] are used for validation. Displacements were measured as a distributed load was applied by a load tree apparatus that simulated uniform pressure.

The test apparatus and cross section properties of tested sandwich panels are illustrated in Figure 5-4, Table 5-1 and Table 5-2. The span length of all specimens is 304.8 cm (120 inches).

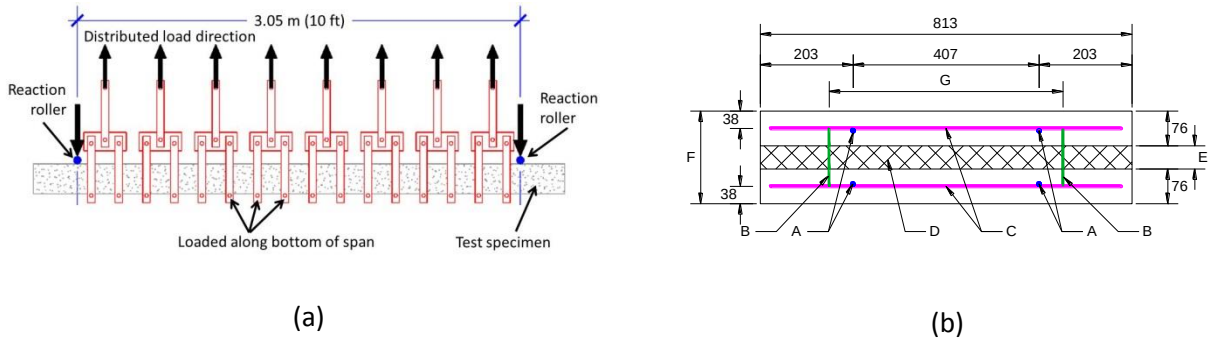

Figure 5-4: a) Test apparatus **b) Cross sections (Unit: mm)**

Table 5-1: Cross section details

	A kN (kips)	B	C	D	E mm (in)	F mm (in)	G mm (in)
PCS 1	9.525mm(3/8") Ø @71.62(16.1)	Steel C Shape	WWR	EPS	51 (2)	203 (8)	2@508 (20)
PCS 2	9.525mm(3/8") Ø @71.62(16.1)	Carbon Mesh	WWR	EPS	51 (2)	203 (8)	2@508 (20)
PCS 3	2×200mm^2(#5) bars &9.525mm(3/8")Ø @71.62(16.1)	Carbon Mesh	WWR	EPS	51 (2)	203 (8)	2@508 (20)
PCS 4	9.525mm(3/8") Ø @66.28(14.9)	Metal C-pins	71mm^2(#3) @ 45.72cm(18")	XEPS	76 (3)	229 (9)	3@305 (12)
PCS 5	9.525mm(3/8") Ø @66.28(14.9)	Composite Pin	71mm^2(#3) @ 45.72cm(18")	XEPS	76 (3)	229 (9)	2@508 (20)
PCS 6	9.525mm(3/8") Ø @71.62(16.1)	Carbon Mesh	WWR	XEPS	76 (3)	229 (9)	2@508 (20)

Where: A is the longitudinal prestressing tendon; B is the shear connector; C is the reinforcement; D is the type of insulation foam; E is the thickness of insulation layer; F is the total thickness of the sandwich beam; G is the space between shear connectors.

Table 5-2: Material properties

	Young's Modulus of Wythes GPa (ksi)	Insulation Foam Stiffness kN/m^3 (lb/in^3)	Shear Connector Stiffness kN/m^3 (lb/in^3)
PCS 1	35.63 (5167)	84517 (311.36)	3042 (11.21)
PCS 2	36.01 (5223)	84517 (311.36)	196723 (724.72)
PCS 3	36.03 (5226)	84517 (311.36)	196723 (724.72)
PCS 4	36.91 (5353)	56347 (207.58)	952 (3.51)
PCS 5	36.86 (5346)	56347 (207.58)	8490 (31.28)
PCS 6	36.61 (5310)	56347 (207.58)	374678 (1380.30)

5.6.3 Mid-span deflection validation

The upper and lower bounds of deflection are given in Equations (5.18) and (5.19). Erroneous sensor data and deflection associated with seating of the samples were eliminated.

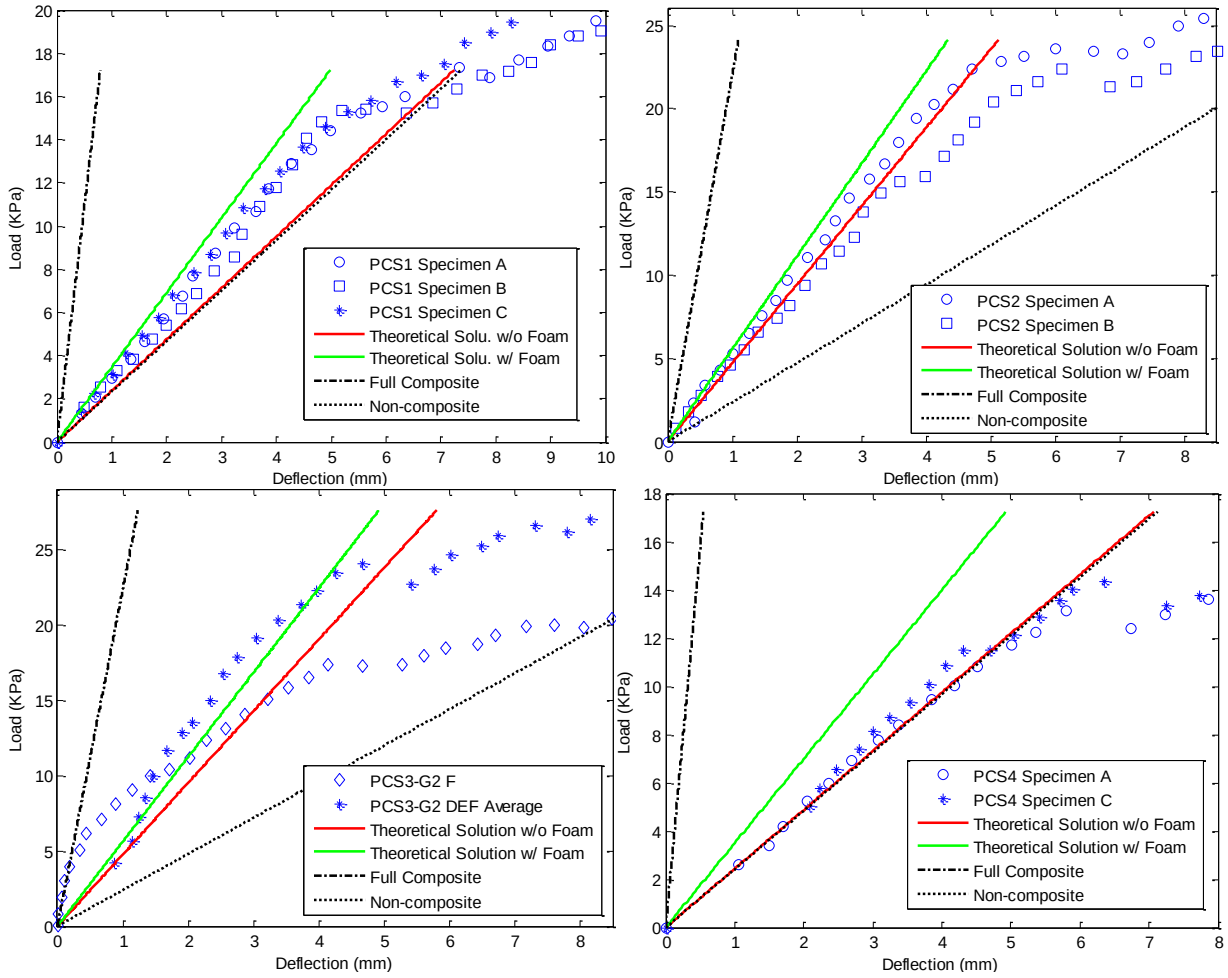

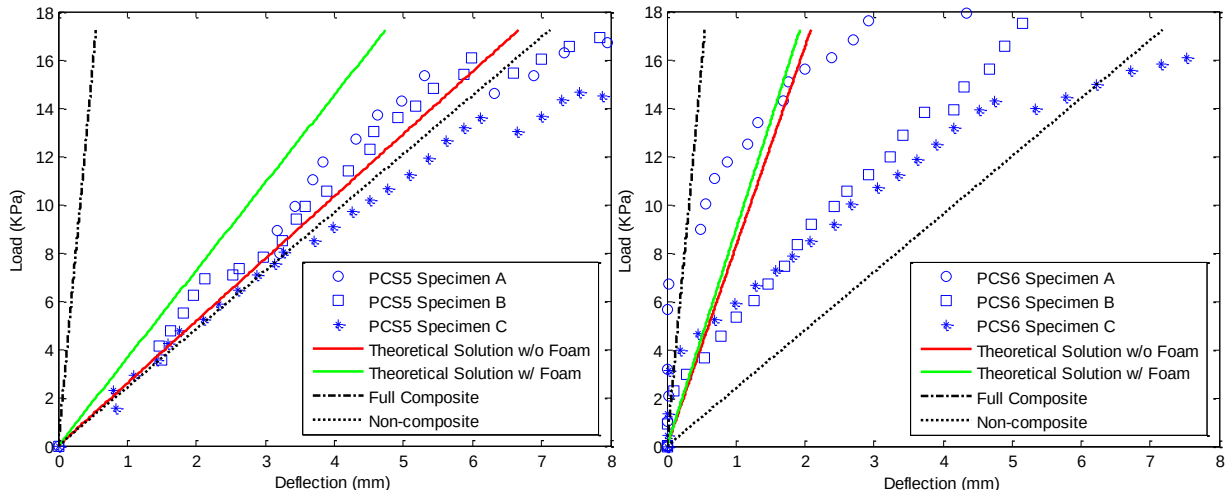

Figure 5-5: Deflection-resistance comparisons

Several characteristics of behavior can be observed in Figure 5-5. Firstly, the testing results will usually fall between the theoretical solutions with and without the middle layer foam, although it has not yet been studied to what extent the foam shear stiffness is effective. Secondly, the comparisons between the testing results and the theoretical solutions confirm that the stiffness influences the deflection in a nonlinear way. For example, the comparison of PCS1 and PCS2 shows that the same foam will help reduce the deflection more effectively for specimens with small existing shear connecter stiffness compared to the one with large existing shear connecter stiffness. Furthermore, the behavior related to a common manufacturing flaw of concrete sandwich structures, poor embedment of the shear connectors, can be observed from the PCS6 specimens. Although, the shear stiffness of PCS6 is large, as defined in Table 5-2, all three tested samples show non-composite behaviors shortly after loading begins. For example, the theoretically predicted slopes of deflection are much larger than that demonstrated by the testing results, and the slopes of the testing results are actually very close to the lower bound, non-composite action. This is because when the poor bonding of the shear connecter embedment is smaller than the demand exerted by the applied load, shear connecter embedment failure occurs and the two concrete wythes act independently as non-composite structures. Nonetheless, the deflection comparisons of Figure 5-5 demonstrate that the developed methodology can capture the characteristic

of sandwich structures with reasonable accuracy considering the random characteristics of concrete structures and uncontrollable factors associated with the manufacturing process.

5.6.4 End slip validation

The upper and lower bounds of end slip are given in Equations (5.21) and (5.22). It can be noted from Figure 5-6 that the relative slip predicted at the ends of the specimens correlates well with the test results. However due to manufacturing imperfections, the slip at one end may differ slightly from the slip at the other end.

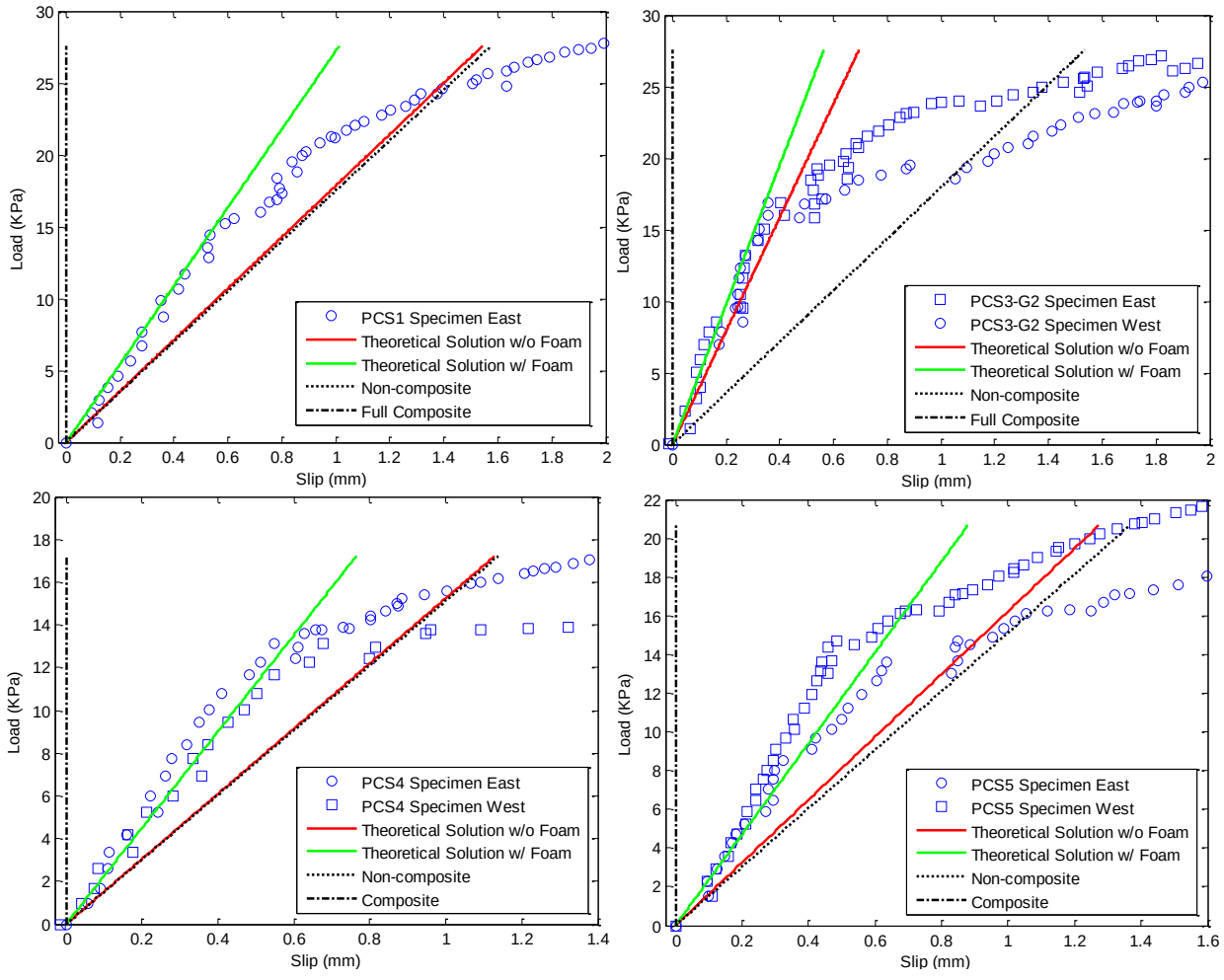

Figure 5-6: Load-slip relationship

5.7 Discussions based on theory

5.7.1 Pattern of internal forces and stresses

The dimensions of PCS1 under pressure of 10.34 KPa is taken as an example. The internal forces and stresses are plotted using 60 times the true stiffness of the shear connectors to emphasize the effect. Figure 5-7 shows how the shear connector stiffness influences the internal forces and the related stress pattern. As expected, the bending moment decreases and the axial force increases to their bounds, respectively, when shear connectors become sufficiently stiff. Then, at the normalized stiffness of 2.1, exterior wythe stresses are plotted with both Continuous and Discrete Models. It should be noticed that the discrete model will yield larger stresses near shear connectors and the maximum value exists at the first one or two connectors from the mid-span.

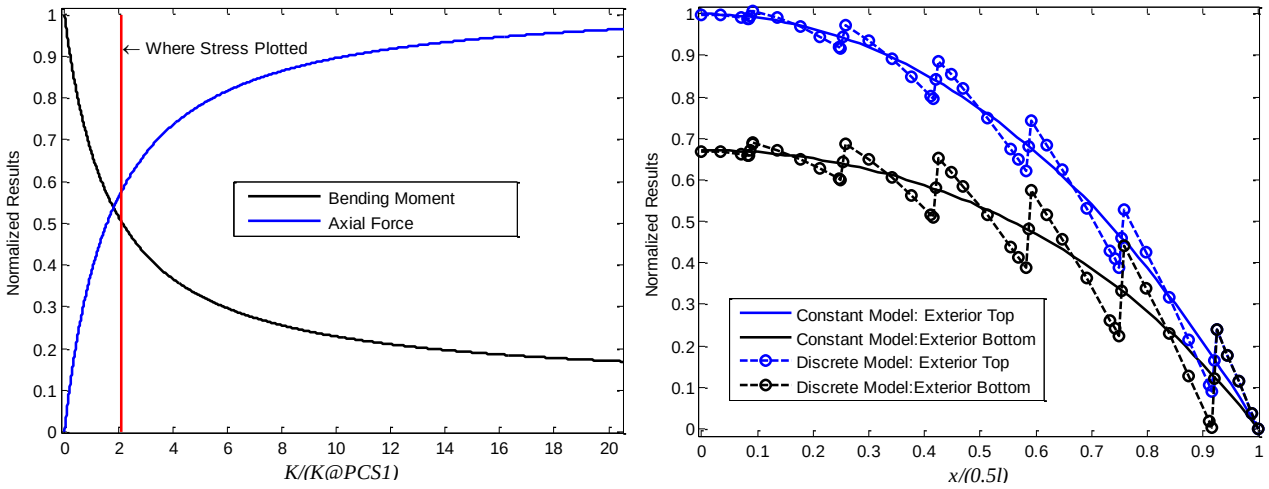

(a) (b)

Figure 5-7: Mid-span internal forces and stresses

5.7.2 Influence of different insulation layer thickness on overall behavior

Five insulation setups are considered as illustrated in Figure 5-8. The insulation layers' thicknesses vary but the concrete wythes' dimensions are the same. Also, the assumption is that the same type of shear connectors and insulation foam are used, but their heights can vary according to different middle layer thickness.

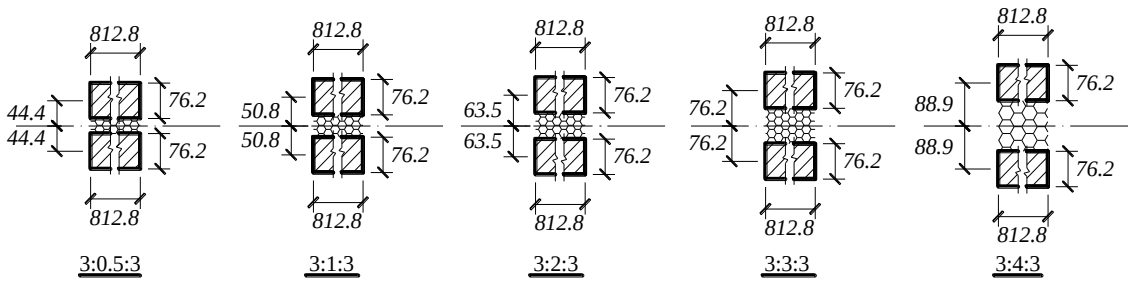

Figure 5-8: Cross-section and dimension ratios considered (Unit: mm)

In order to study the effect of insulation layer thickness variation, the assumption that the shear connectors' ends are built into the wythes as fixed boundary conditions is made. In that case,

$$K = \tau / \varphi = \frac{p}{A} \Big/ \frac{p\left(2r-d\right)^3}{12EI} = \frac{12EI}{A} \frac{1}{\left(2r-d\right)^3} \tag{5.37}$$

It can be observed in Equation (5.37) that K, as a function of thickness of the middle layer $2r$-d, changes exponentially. The deflection is plotted in Figure 5-9 as a function of middle layer stiffness for the five cross-sections. Parameters and dimensions of PCS6 are taken under 10.34 KPa pressure for demonstration. Figure 5-9 demonstrates that for relatively thick insulation layers, it is more difficult to achieve fully composite action than for thin insulation layers (the 3-4-3 panel would need about 3 times the number of connectors compared to the 3-3-3 panel, and 5 times compared to 3-2-3). After achieving fully composite action, the 3-4-3 panel would be stiffer and have less deflection due to the larger moment of inertia, but for average sandwich panel design, the deflection associated with shear dominates and consequently a thicker insulation layer results in a larger deflection. Therefore it is not sound to conclude that a larger moment of inertia would help reduce deflection in sandwich structures.

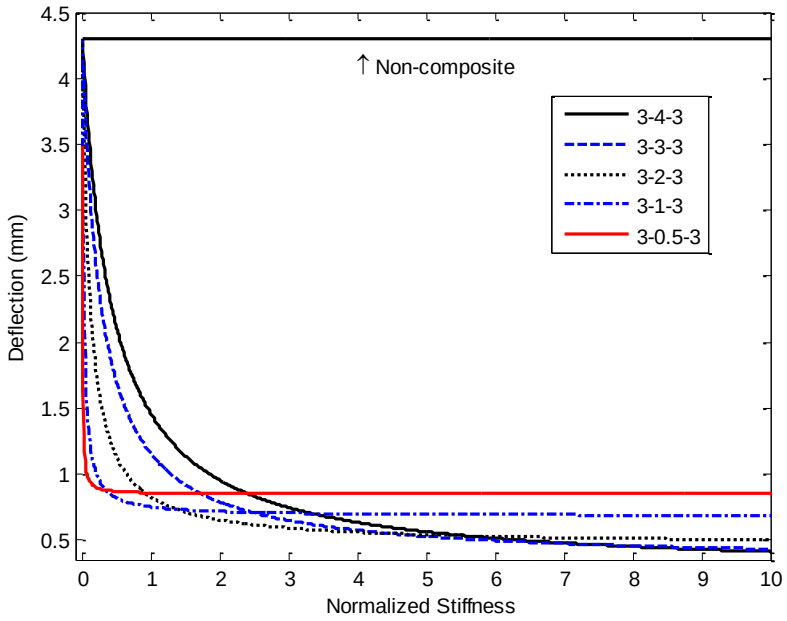

Figure 5-9: Influence of middle layer on the mid-span deflection

5.8 Conclusions

This chapter derives a rigorous discrete analysis model for composite structures. Most importantly, it addresses the absence of reliable analysis methodology in the ICSP industry. Key findings and accomplishments of the work include:

1. The Discrete Model can improve the stress calculation accuracy near shear connectors and capture the key characteristic of ICSP structures.

2. Sandwich structures deflection is decomposed and classified as flexural and shear components. Furthermore, the upper and lower bounds of deflection, end slip and internal forces are derived and verified against full-scale test data.

3. The deflection associated with shear deformation can be so large that it can dominate the deflection when the middle layer stiffness is relatively small (demonstrated in Figure 5-9).

Chapter 6 Transfer length and immediate prestress losses in prestressed concrete

6.1 Introduction and scope

Another application of the composite theory developed in Chapter 3 is addressing problems of transfer length and the prestress losses immediately after release of the presstressing tendons in prestressed concrete structures. As discussed in Chapter 2, transfer length is not completely understood by the prestressing concrete industry. Many research efforts and resources have been spent on this subject during the development of the prestressing concrete industry over several decades but nowadays the methods used for predicting and understanding it are still under development. However, transfer length is one of the most important issues in prestressed concrete design and analysis since the applicability of plane cross section assumption relies on it.

Unlike conventionally reinforced concrete structures, in prestressed concrete structures the large amount of prestressing forces, which are transferred to the concrete within the transfer zones, results in large concentrated forces that are applied to the concrete. These concentrated forces in the transfer zones make the assumption of plane cross section invalid. However, away from the transfer zones, the tendons have no interaction with the concrete as the concrete / tendon interface shear force becomes zero (Figure 6-1). The transfer zones essentially serves as anchorage, and the prestressing force out of transfer zones is transfer by the “anchorage” concrete in the transfer zones instead of tendons. Therefore the plane cross section assumption is only valid out of transfer zones, as illustrated in Figure 6-1.

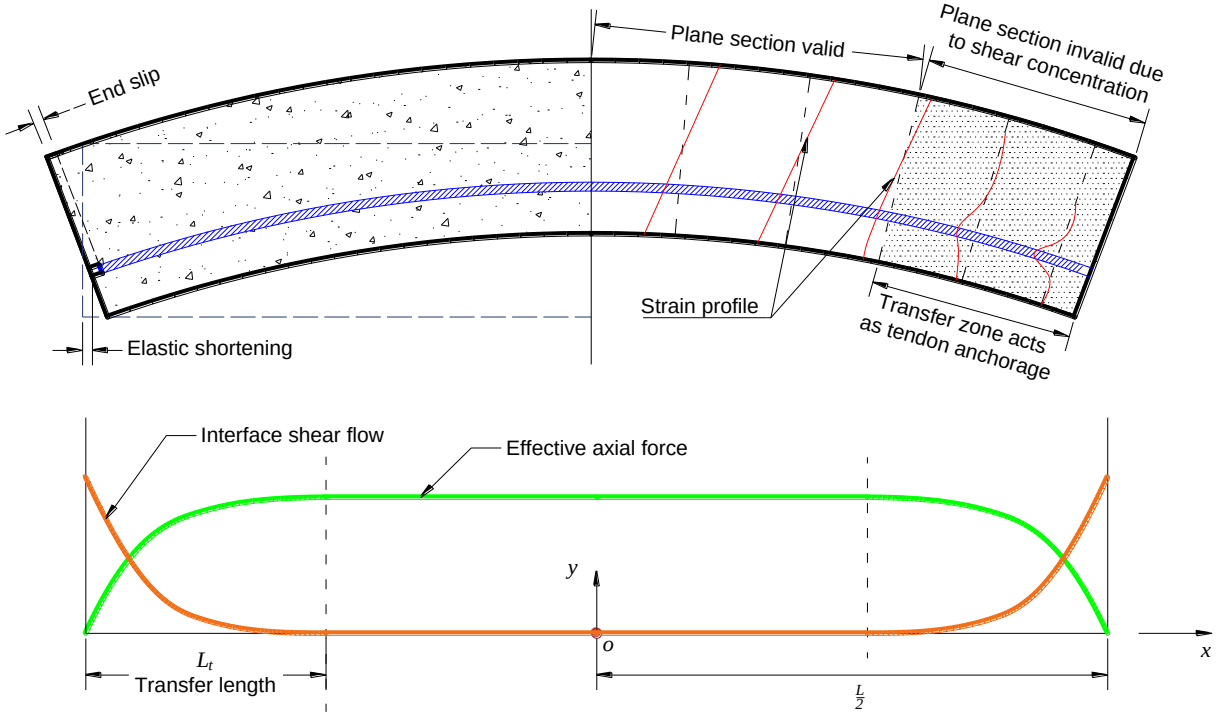

Figure 6-1: Prestressed concrete and force equilibrium in pretensioned concrete girder

The theoretical development is based on the composite theory presented in Chapter 3. However due to the constant eccentricity of prestressed tendon in this chapter, the theoretical development presented will therefore be slightly different from that presented in Chapter 3.

6.2 Theoretical development

6.2.1 Assumptions and limitations

Assumptions involved in the following development include:

1) Structural behavior is limited to elastic and small displacement and constitutive relationships are assumed to be linear;

2) The concrete beam and reinforcement or prestressing strands behave as Euler-Bernoulli beams and have the same transverse deflection;

3) Strands have no bending resistance; and

4) Continuous and constant shear stiffness exists along the surfaces of the strands.

The last assumption may not reflect the true bond condition when slip exceeds the elastic threshold; however the idea is to average the possible nonlinear bond-slip relationship by using a constant value to capture the trend within acceptable accuracy. If more accurate results are desired, a numerical model that considers the nonlinear bond-slip relationship must be employed.

6.2.2 Axial force equilibrium

Axial strain is equal to the derivative of its axial displacement, and then the axial stress is equal to Young's modulus times that strain:

$$\sigma_c = E_c \varphi_{2c}^{'} \tag{6.1}$$

$$\sigma_s = E_s \varphi_{2s}^{'} \tag{6.2}$$

where φ_{2c} = concrete beam displacement from its original centroid due to axial deformation; φ_{2s} = strand displacement from its original centroid due to axial deformation; E_c = modulus of elasticity of concrete; and E_s = modulus of elasticity of prestressing strand. Bending moment caused by strand eccentricity may be present, but it will not affect the longitudinal equilibrium and will be included later.

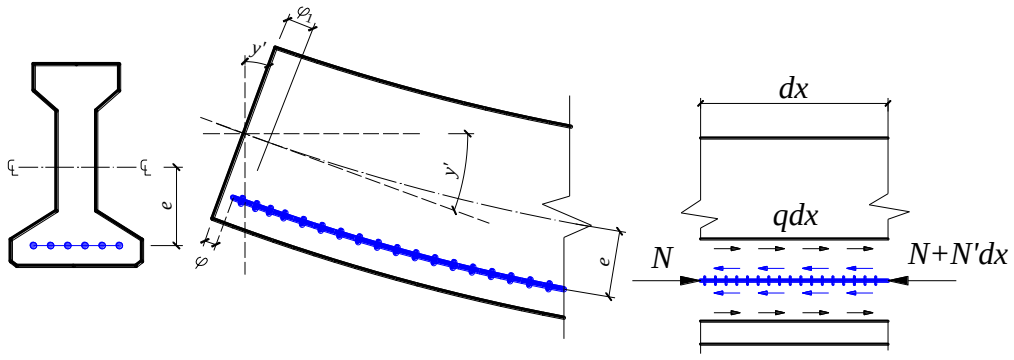

Figure 6-2: Geometry and force equilibrium

The first focus will be on the concrete girder but the same result will be obtained for the strand. Using the equilibrium of forces in the axial direction of the cross section shown in Figure 6-2:

$$qdx = N_c^{'}dx \tag{6.3}$$

where q = shear force per unit length within the concrete/strand interface and N_c = resultant axial force in the concrete beam. The shear force within the differential unit length:

$$q = \left(A_c\sigma_c\right)^{'} \tag{6.4}$$

where A_c = cross section area of the concrete beam. Substituting Equation (6.1) into Equation (6.4), the shear force per unit length is defined as:

$$q = E_c A_c \varphi_{2c}^{''} \tag{6.5}$$

Since the slip is the difference in displacements, the slip can be written as:

$$\varphi_2 = \varphi_{2c} + \varphi_{2s} \tag{6.6}$$

where φ_2 = slip between concrete and strand due to axial displacement. Note that φ_2 includes slip from curvature and prestressed strands. The fact that internal axial forces in the concrete beam and strands are equal to each other yields following:

$$N_c = N_s = N \tag{6.7}$$

where N_s = resultant axial force in the strand and N = resultant axial force in both the concrete beam and strand. Note that the axial force sign convention is not considered since φ_2 is a relative movement. Equation (6.7) can now be rewritten as:

$$N_c = A_c\sigma_c \tag{6.8}$$

$$N_s = A_s \sigma_s \tag{6.9}$$

Substituting Equation (6.1) into Equation (6.8), and Equation (6.2) into Equation (6.9) respectively results in:

$$N_c = A_c E_c \varphi_{2c}^{'} \tag{6.10}$$

$$N_s = A_s E_s \varphi_{2s}^{'} \tag{6.11}$$

Differentiating Equation (6.6) twice:

$$\varphi_2^{''} = \varphi_{2c}^{''} + \varphi_{2s}^{''} \tag{6.12}$$

Plugging Equation (6.10) and Equation (6.11) back into Equation (6.7) and differentiating once:

$$A_c E_c \varphi_{2c}^{''} = A_s E_s \varphi_{2s}^{''} \tag{6.13}$$

Substituting of φ_{2c}'' and φ_{2s}'' in Equation (6.13) into Equation (6.12) yields:

$$\varphi_2^{''} = \left(1 + \frac{A_c E_c}{A_s E_s}\right) \varphi_{2c}^{''} \tag{6.14}$$

$$\varphi_2^{''} = \left(1 + \frac{A_s E_s}{A_c E_c}\right) \varphi_{2s}^{''} \tag{6.15}$$

Now, considering the equilibrium between interface shear force and slip:

$$K\varphi = q \tag{6.16}$$

where K = shear stiffness of the concrete-strand interface, or bond stiffness for short; $\varphi = \varphi_1 + \varphi_2 + \varphi_3$ = total slip between concrete beam and strand; $\varphi_1 = ey^{'}$ = slip due to bending, as in Figure 6-2; e = the distance from the concrete beam centroid to the strand centroid; y = deflection. $\varphi_3 = \int \varepsilon_{is}\, dx$ = slip due

to prestrained strands. Again, taking the concrete beam as an example and substituting Equation (6.5) into Equation (6.16):

$$K\varphi = E_c A_c \varphi_{2c}^{''} \tag{6.17}$$

Substituting $\varphi_{2c}^{''}$ in Equation (6.14) into Equation (6.17):

$$K\varphi = \frac{E_c A_c}{\left(1+\frac{A_c E_c}{A_s E_s}\right)} \varphi_2^{''} \tag{6.18}$$

Also, the total slip is written as:

$$\varphi = \varphi_1 + \varphi_2 + \varphi_3 \tag{6.19}$$

Rearranging Equation (6.19) and expressing φ_1 with *e* and *y* as shown in Figure 6-2. φ_3 is also easily obtained but it is not necessary in this step. Plugging $\varphi_1 = ey^{'}$ into Equation (6.19):

$$\varphi_2 = \varphi - ey^{'} - \varphi_3 \tag{6.20}$$

Noted that φ_3 is a linear function of span position since the prestrain is constant in the strands and the relative slip is the integration of strain along the span length. Now differentiating Equation (6.20) twice:

$$\varphi_2^{''} = \varphi^{''} - ey^{'''} \tag{6.21}$$

φ_3 is consequently eliminated. Substituting Equation (6.21) into Equation (6.18):

$$K\varphi = \frac{E_c A_c}{\left(1+\frac{A_c E_c}{A_s E_s}\right)} \left(\varphi^{''} - ey^{'''}\right) \tag{6.22}$$

Introducing a new variable:

$$\eta = \frac{A_c E_c}{1 + \frac{A_c E_c}{A_s E_s}} = \frac{A_s E_s}{1 + \frac{A_s E_s}{A_c E_c}} = \frac{A_c E_c A_s E_s}{A_c E_c + A_s E_s} \tag{6.23}$$

After plugging Equation (6.23) into Equation (6.22):

$$K\varphi = \eta\left(\varphi'' - ey''\right) \tag{6.24}$$

Rearranging terms and letting $\chi_B{}^2 = K/\eta$ yields:

$$\varphi'' - \chi_B{}^2 \varphi = ey'' \tag{6.25}$$

6.2.3 Bending moment equilibrium

Recalling that the distance from the centroid of concrete beam to the centroid of the strand is e, the moment equilibrium can be established as:

$$M_{ex} = M_c + eN_s \tag{6.26}$$

where M_{ex} = external applied bending moment and M_c = internal bending moment of the concrete beam. On the left side of Equation (6.26) are the applied known loads, and on the right side of Equation (6.26) are the unknown variables. Equation (6.26) can be rewritten as:

$$M_{ex} = -E_c I_c y'' + eN \tag{6.27}$$

where I_c = concrete beam moment of inertia. Differentiating Equation (6.6) once:

$$\varphi_2' = \varphi_{2c}' + \varphi_{2s}' \tag{6.28}$$

Substituting Equation (6.10) and Equation (6.11) into Equation (6.7):

$$A_c E_c \varphi_{2c}' = A_s E_s \varphi_{2s}' \tag{6.29}$$

Substituting $\varphi_{2c}^{'}$ and $\varphi_{2s}^{'}$ in Equation (6.29) back into Equation (6.28):

$$\varphi_2^{'} = \left(1 + \frac{A_c E_c}{A_s E_s}\right)\varphi_{2c}^{'} \tag{6.30}$$

$$\varphi_2^{'} = \left(1 + \frac{A_s E_s}{A_c E_c}\right)\varphi_{2s}^{'} \tag{6.31}$$

Substituting either Equation (6.30) into Equation (6.10), or Equation (6.31) into Equation (6.11), results in the following:

$$N = \eta\varphi_2^{'} \tag{6.32}$$

Now Equation (6.27) can be rewritten after substituting Equation (6.32) into it:

$$M_{ex} = -E_c I_c y^{"} + e\eta\varphi_2^{'} \tag{6.33}$$

In Equation (6.33), $\varphi_2^{'}$ represents the total axial slip, which includes the slip due to bending and prestrained strands. Differentiating Equation (6.20) once:

$$\varphi_2^{'} = \varphi^{'} - ey^{"} - \varepsilon_{is} \tag{6.34}$$

where ε_{is} = initial applied prestrain, before transfer, in the prestressing strand. For prestressed strands, ε_{is} is negative. Then substituting Equation (6.34) into Equation (6.33):

$$M_{ex} = -E_c I_c y^{"} + e\eta\left(\varphi^{'} - ey^{"} - \varepsilon_{is}\right) \tag{6.35}$$

After rearranging terms and letting $D_B = E_c I_c + e^2\eta$ and $\alpha_B^2 = e^2\eta / D_B$, Equation (6.35) can be rewritten as:

$$y^{"} - \frac{\alpha_B^2}{e}\varphi^{'} = -\frac{M_{ex}}{D_B} - \frac{\alpha_B^2}{e}\varepsilon_{is} \tag{6.36}$$

When prestressing force exists, the additional resultant strain term is added to take prestressing force into account. So finally the set of governing equations is obtained as Equation (6.25) and Equation (6.36):

$$\begin{cases} \varphi'' - {\chi_B}^2 \varphi = e y''' \\ y'' - \dfrac{{\alpha_B}^2}{e} \varphi' = -\dfrac{M_{ex}}{D_B} - \dfrac{{\alpha_B}^2}{e} \varepsilon_{is} \end{cases}$$

The governing equations are applicable to both conventionally reinforced concrete and prestressed concrete structures. When conventionally reinforced concrete structures are the subject of interest, the prestrain should be set to zero. Also, there are three possible scenarios for the eccentricity of prestressed strands:

1) The simplest case is that the eccentricity e is zero, meaning that the prestressing strand is placed at the centroid of concrete beam, which is not common in prestressed beams and girders but occurs in other structures such as prestressed insulated sandwich panels and prestressed poles. Actually, for this scenario, the set of governing equations is reduced to one simple homogeneous differential equation governing the longitudinal interaction, as in Equation (6.37). The second governing equation becomes the well-known Euler-Bernoulli beam curvature relationship when e is zero. The solutions can be determined by setting e to zero in the related solutions in Section 6.3.

$$\varphi'' - {\chi_B}^2 \varphi = 0 \tag{6.37}$$

2) The eccentricity e is constant, which means that the prestressing strand is straight and placed near the bottom of the beam, which is common for prestressed beams and girders. The conventionally reinforced and prestressed scenarios are both represented by the governing equations derived in this study. For case 2, the set of governing equations is linear and its closed form solutions will be provided in Section 6.3.

3) The eccentricity e is neither zero nor constant. Ideally, the eccentricity e, is draped to the farthest allowed to increase the resistance of girder at mid-span and closest to the centroid of the concrete girder at the end support to avoid excessive stress by prestressing force near the end support. This case involves higher order deformation and nonlinearities and the governing equations will be nonlinear and no closed form solutions will be available, as derived already in Chapter 3.

6.3 Closed form solutions

The origin of the x axis is at the mid-span, so for a simply supported beam subjected to uniformly distributed pressure of q_w on unit length, the boundary conditions are: $\varphi(0) = y''(l/2) = 0$ (additionally, $y(l/2) = y'(0) = 0$ when deflection is desired).

6.3.1 Reinforced concrete beam

For analysis of conventionally reinforced concrete, the term associated with prestrain is dropped and only the externally applied bending moment is kept.

Slip

$$\varphi_r = \frac{1}{8}\frac{q_w l^3 e}{D_B}\left(\frac{2\beta_B}{\chi_B l}\right)^2 \frac{1}{{\beta_B}^2}\left[\frac{2\beta_B}{\chi_B l}\left(\frac{\sinh\frac{\chi_B}{\beta_B}x}{\cosh\frac{\chi_B l}{2\beta_B}}\right) - \frac{2x}{l}\right] \tag{6.38}$$

where ${\beta_B}^2 = 1 - {\alpha_B}^2$.

Axial force

$$N_r = \frac{1}{4}\frac{q_w l^2}{e}{\alpha_B}^2\left[-\left(\frac{2\beta_B}{\chi_B l}\right)^2\left(1-\frac{\cosh\frac{\chi_B}{\beta_B}x}{\cosh\frac{\chi_B l}{2\beta_B}}\right)+\frac{1}{2}\left(1-\left(\frac{2x}{l}\right)^2\right)\right] \tag{6.39}$$

Bending moment

$$M_r = \frac{1}{4} q_w l^2 \left[\alpha_B{}^2 \left(\frac{2\beta_B}{\chi_B l} \right)^2 \left(1 - \frac{\cosh \frac{\chi_B}{\beta_B} x}{\cosh \frac{\chi_B l}{2\beta_B}} \right) + \frac{1}{2} \beta_B{}^2 \left(1 - \left(\frac{2x}{l} \right)^2 \right) \right] \tag{6.40}$$

6.3.2 Prestressed concrete beam

For prestress caused response, the applied bending moment is set to zero and a prestrain ε_{is} is added to account for the forces in the prestressing strands. Note that in the sign convention adopted for this study, ε_{is} is negative for prestressed concrete.

Slip

$$\varphi_p = \frac{\beta_B \varepsilon_{is}}{\chi_B} \frac{\sinh \frac{\chi_B}{\beta_B} x}{\cosh \frac{\chi_B l}{2\beta_B}} \tag{6.41}$$

Axial force

$$N_p = -\beta_B^2 \eta \varepsilon_{is} \left(1 - \frac{\cosh \frac{\chi_B}{\beta_B} x}{\cosh \frac{\chi_B l}{2\beta_B}} \right) \tag{6.42}$$

Bending moment

$$M_p = e \beta_B^2 \eta \varepsilon_{is} \left(1 - \frac{\cosh \frac{\chi_B}{\beta_B} x}{\cosh \frac{\chi_B l}{2\beta_B}} \right) \tag{6.43}$$

6.4 Applications and discussions

6.4.1 Additional force gain by the curvature change

Equation (6.39) represents the elastic gain of strand force due to curvature change in the corresponding prestressing strand location and is relatively small when compared to the axial force caused by prestressing strands. Equation (6.39) can be decomposed into two components, the perfect bonding component (also referred as fully composite component) and interface slip compensation component:

$$N_r = \frac{1}{8}\frac{q_w l^2}{e}\alpha_B{}^2\left(1-\left(\frac{2x}{l}\right)^2\right)-\frac{1}{4}\frac{q_w l^2}{e}\alpha_B{}^2\left(\frac{2\beta_B}{\chi_B l}\right)^2\left(1-\cosh\frac{\chi_B}{\beta_B}x\Big/\cosh\frac{\chi_B l}{2\beta_B}\right) \qquad (6.44)$$

In Equation (6.44), the gain or 'add-back' portion of the strand force consists of two components. The first component is associated with the bending moment induced curvature and the second component is associated with the bonding condition between the prestressing strands and the concrete. In other words, the first term is valid when the strand and concrete have fully composite action, showing very little slip over the span. The second term accounts for the scenario where fully composite action is not achieved due to poor bonding between strands and concrete. The second bonding condition related term is usually negative, meaning that the 'add-back' force with slip involved will be smaller than the perfect bonding condition without slip. The good news is that, for typical strands and concrete used in practice, the bonding is quite strong and the second term can be neglected at the mid-span, which may only result in less than one percent difference. Additionally, even if the bonding is not good, the first term will yield an upper bound. Therefore, neglecting the slip compensation and only considering perfect bonding related axial force, the axial force is determined as:

$$N_r = \frac{1}{8}\frac{q_w l^2}{e}\alpha_B{}^2\left(1-\left(\frac{2x}{l}\right)^2\right) \qquad (6.45)$$

Recall that the bending moment is $(q_w l^2/8)(1-(2x/l)^2)$ at the mid-span so Equation (6.45) can be further generalized as:

$$N_r = \frac{M_{ex}}{e}\alpha_B{}^2 \tag{6.46}$$

The development in Equation (6.46) will now be compared to the corresponding elastic gain due to self-weight in Equation 5-65 and due to superimposed loads in Equations 5-66 and 5-67 of the PCI Design Handbook, 7th edition[70]. Plugging $\alpha_B{}^2 = e^2\eta/D_B$ into Equation (6.46), and rearranging the terms to arrive at this form:

$$N_r = \varepsilon_{cds}\eta \tag{6.47}$$

where $\varepsilon_{cds} = eM_{ex}/D_B$. ε_{cds} is the strain caused by the external applied bending moment at the location of prestressing strands. In order to compare with the existing formula of elastic gain mentioned above, Equation (6.47) can also be written as:

$$N_r = A_s f_{cds}\frac{A_c E_s}{A_s E_s + A_c E_c} \tag{6.48}$$

where $f_{cds} = eM_{ex}E_c/D_B$. f_{cds} is the stress caused by the external applied bending moment at the location of prestressing strands. Given that A_sE_s is usually smaller compared to A_cE_c, Equation (6.48) is simplified by eliminating A_sE_s from the denominator as:

$$N_r/A_s = f_{cds}\frac{E_s}{E_c} \tag{6.49}$$

Equation (6.49) is now comparable to the formula used in Equations 5-66 and 5-67 of PCI Design Handbook, 7th edition. Note that the gain is integrated in the concrete elastic shortening (ES) and creep (CR) losses in the PCI Design Handbook, 7th edition.

Equation (6.46) is a closed form solution and does not involve any of the potentially unrealistic assumptions. The major importance is that Equation (6.46) facilitates a better understanding of the mechanics and does not include assumptions or approximations that can result in significant errors out of normal design conditions. In other words, Equation (6.46) is theoretically pure yet concise. On the other hand, the curvature gain formula presented in the PCI Design Handbook is only invalid for unusual design situations, for example, when reinforcement ratio is large or the cross section area of concrete beam is relatively small. In those cases, neglecting $A_s E_s$ from the denominator in Equation (6.48) will result in considerable error. Details and discussion are provided in the Section 6.6.3.

6.4.2 Bending moment resulting in zero curvature

There is a special case of when the externally applied bending moment is balanced by the prestress force resulting in zero curvature. This condition was conventionally analyzed by calculating the curvature or stresses of concrete cross sections due to prestress force, after estimate of immediate prestress loss, and then plugging it back to calculate the external bending moment associated with that curvature or stress. The prestress force is related to the external applied bending moment through curvature or stress of the specific cross section. Now, with the formulation developed in this study, this zero curvature bending moment can be directly determined without involving cross section properties and prestress loss estimate by setting the right hand side of Equation (6.36) to be zero. The bending moment is canceled with the prestress force and the resulting curvature is zero:

$$-\frac{M_{ex}}{D_B}-\frac{{\alpha_B}^2}{e}\varepsilon_{is}=0 \tag{6.50}$$

Therefore, from Equation (6.50), the bending moment is determined as:

$$M_{ex}=-e\eta\varepsilon_{is} \tag{6.51}$$

The bending moment represented by Equation (6.51) does not involve bending action or interface slip related properties because the curvature is zero and slip related loss is canceled out. As a result, it takes a very simple form. Note that Equation (6.51) has already considered prestress losses and the prestrain is the initial strain before prestress transfer and immediate losses. Therefore it simplifies the way this bending moment is computed while having much better accuracy by not involving prestress loss estimate and cross section properties.

6.4.3 Immediate prestress losses

Immediate prestress losses, namely elastic shortening, anchorage seating and friction, are relatively mature subjects. Anchorage seating is often compensated for by overjacking. Friction loss occurs because of curvature and is only applicable for posttensioning components. Therefore elastic shortening is discussed in this section. In addition to the immediate losses, a new category of immediate prestress loss, loss due to slip, is defined in this section, as illustrated in Figure 6-3. This slip associated loss is similar to the anchorage seating loss, and could be regarded as seating of strands in concrete. Note, in this section, elastic shortening refers to the portion caused by prestressing force only. So the gain due to self-weight, which can be determined by Equation (6.47), is not included.

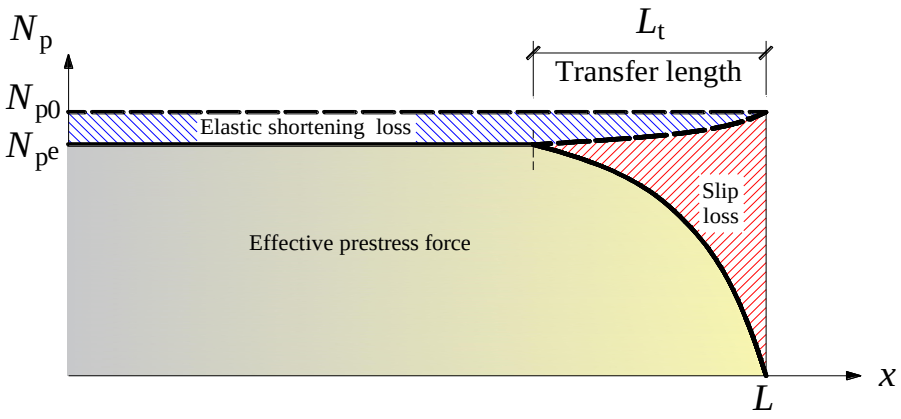

Figure 6-3: Immediate prestress losses of bonded construction

Elastic shortening loss

Elastic shortening is an important issue, and conventional analysis approaches can achieve reasonable accuracy when applied to normal design conditions. However, the conventional method is mechanically accurate only at one specific point due to the constant factor used in concrete stress calculation. Specifically, in Equations 5-64 and 5-65 of the PCI Design Handbook, 7th edition[70] for elastic shortening loss, f_{cir} (net compressive stress in concrete at center of gravity of prestressing force immediately after the prestress has been applied to the concrete) is calculated by the initial prestress force P_i multiplied by a constant factor K_{cir} of 0.9. From a mechanical perspective, f_{cir}, in Equation 5-65 in the PCI Design Handbook should be calculated by the actual force after elastic shortening loss. In other words, this approach assumes 10% elastic shortening loss in its calculation and is mechanically correct only when the elastic shortening loss eventually turns out to be 10%. Better accuracy can be achieved through iteration. However, in this study, a concise closed form solution is derived. Additionally, the cross section properties should consider the existence of prestressing strands and its eccentricity in an appropriate way. Detailed validation and comparison are provided in the Section 6.6.

A pure mechanical model based on the prior theoretical development is presented. It is difficult to separate the loss due to pure elastic shortening and loss due to slip from the total immediate loss, therefore the derivation begins with perfect bonding condition and no prestress force is lost through slip. This is the most useful case for normal design conditions since this assumption is valid outside of the transfer zones. In that case, the effective prestressing force is determined as $-\beta_B^2 \eta \varepsilon_{is}$ and prestressing force loss due to elastic shortening is constant through the beam, which can be written as:

$$\Delta N_{P\_ES} = \left(-\varepsilon_{is} A_s E_s\right) - \left(-\beta_B^2 \eta \varepsilon_{is}\right) \tag{6.52}$$

Alternatively, after sorting terms:

$$\Delta N_{P\_ES} = -\varepsilon_{is} A_s E_s \left(1 - \frac{\beta_B{}^2 A_c E_c}{A_s E_s + A_c E_c}\right) = -\varepsilon_{is} A_s E_s \left(\frac{A_s E_s + \alpha_B{}^2 A_c E_c}{A_s E_s + A_c E_c}\right) \tag{6.53}$$

Now the remaining effective prestressing force, in percentage, due to the elastic shortening can be written as:

$$P_{effe-ES} = \frac{\beta_B{}^2 A_c E_c}{A_s E_s + A_c E_c} \tag{6.54}$$

Accordingly, the prestressing force loss, in percentage, due to elastic shortening is determined as:

$$P_{loss-ES} = \frac{A_s E_s + \alpha_B{}^2 A_c E_c}{A_s E_s + A_c E_c} \tag{6.55}$$

As reflected in Equations (6.54) and (6.55), the effective component of prestressing force or the lost component of prestressing force accounts for the eccentricity by including the factor β_B. If β_B is one (or α_B is zero), there is no eccentricity and the expression for the prestress loss reduces to:

$$P_{loss-ES} = \frac{A_s E_s}{A_s E_s + A_c E_c} \tag{6.56}$$

To define the elastic shortening considering slip, Equation (6.53) is reduced by a factor depending on slip as:

$$\Delta N_{P\_ES\_sp} = -\varepsilon_{is} A_s E_s \left(\frac{A_s E_s + \alpha_B{}^2 A_c E_c}{A_s E_s + A_c E_c}\right)\left(1 - \cosh\frac{\chi_B}{\beta_B} x \Big/ \cosh\frac{\chi_B l}{2\beta_B}\right) \tag{6.57}$$

The percentage of loss or remaining effective prestressing force with existence of slip can be determined similarly based on Equation (6.57), instead of Equation (6.53) when without slip. Equation (6.57) implies that elastic shortening is dependent on the slip in the transfer zone, similar to that discussed by Guyon[82], Russell[49] and Barnes[55].

Loss due to slip

Perfect bond is typically assumed in conventional analyses. Therefore, the loss due to slip at the strand-concrete interface cannot be defined using conventional analyses approach, whereas this slip loss is actually the reason that the transfer length exists. In the prestressed concrete components of bonded construction, if the bonding condition is ideal (infinitely large interface stiffness), the axial force induced by the prestressing strands will be constant everywhere in the beam and there will not be prestress loss due to slip. However, that degree of bonding between concrete and steel strands is not possible and therefore there is always prestress loss due to slip within the transfer zones. The loss due to slip at any position is therefore determined as:

$$\Delta N_{P\_sp} = -\varepsilon_{is} A_s E_s \left(\cosh \frac{\chi_B}{\beta_B} x \middle/ \cosh \frac{\chi_B l}{2\beta_B} \right) \tag{6.58}$$

The percentage of prestress loss due to the slip can also be expressed as:

$$P_{loss-sp} = \cosh \frac{\chi_B}{\beta_B} x \middle/ \cosh \frac{\chi_B l}{2\beta_B} \tag{6.59}$$

As seen in Equation (6.58), the mid-span will have the minimum slip induced loss and the end of the girder will suffer the maximum slip loss. For other locations between them, the loss will vary monotonically from minimum to maximum values. At the mid-span, Equation (6.58) becomes:

$$\Delta N_{P\_sp}(0) = -\frac{\varepsilon_{is} A_s E_s}{\cosh \frac{\chi_B l}{2\beta_B}} \tag{6.60}$$

At the end support, Equation (6.58) becomes:

$$\Delta N_{P\_sp}(l/2) = -\varepsilon_{is} A_s E_s \tag{6.61}$$

As shown in Equation (6.60), if the bonding is large enough or the span is long enough to allow the bond to build up, the prestress force loss due to slip will be very small at the mid-span, which is the case for most prestressed girders. However, for short components or strands with very poor bond, the denominator in Equation (6.60) is relatively large and the prestress force loses a significant amount of force at the mid-span. At the end support, as in Equation (6.61), the axial force is zero and all of the prestress force is lost due to slip.

6.4.4 Transfer length

For bonded prestressing strand, a certain distance is required for the prestressing force to fully transfer from the end to the concrete girder, numerically from zero to the effective prestressing force, which is referred to as the transfer length. If this distance is calculated beyond the service condition at the structure's ultimate resistance, it is called development length, which is longer than transfer length. Development length will require nonlinear properties and will be included in a future study.

According to the definition of transfer length, the distance that axial force increases from zero to the effective value can be considered as transfer length. So plugging the axial force in Equation (6.42) and assuming a tolerance that is associated with effective force, the equilibrium associated with transfer length can be established as:

$$-\beta_B^2 \eta \varepsilon_{is} \left(1 - \frac{\cosh \frac{\chi_B}{\beta_B} x}{\cosh \frac{\chi_B l}{2\beta_B}} \right) = -\gamma \beta_B^2 \eta \varepsilon_{is} \tag{6.62}$$

where γ is the tolerance of axial force at mid-span, which can be assumed as 0.95 to be consistent with the 95% AMS method[49]. γ is added on the one hand because in Equation (6.42) the axial force N_p can only reach the value exactly at the mid-span. On the other hand, it is added to be consistent with the

popular AMS method. Therefore a certain tolerance is given to ensure that the calculation yields meaningful results instead of only mid-span results. Equation (6.62) can be rewritten as:

$$\cosh\frac{\chi_B}{\beta_B}x=(1-\gamma)\cosh\frac{\chi_B l}{2\beta_B} \tag{6.63}$$

The transfer length L_t can now be solved as:

$$L_t=l/2-\frac{\beta_B}{\chi_B}\ln\left(\lambda_t+\sqrt{\lambda_t^{\,2}-1}\right) \tag{6.64}$$

where $\lambda_t = (1\text{-}\gamma)\ cosh(\chi_B l/(2\beta_B))$.

6.5 Validation and discussion

6.5.1 Transfer length by average interface bonding stiffness

As discussed in Chapter 2, the transfer length has been investigated by many researchers over several decades. Most studies have focused on experimental work and establishing empirical formulation or simplified definitions of force equilibrium. The methodology developed herein will now be compared with testing data presented in the literature. For illustration purposes, the interface stiffness K is kept the same for all specimens, even though the data suggests that the bond may vary between specimens due to various reasons such as the mixture of concrete and other uncertainties involved in the testing. The interface stiffness K is calculated based on:

$$K=n\mu_d K_0 \tag{6.65}$$

where n = total number of strands; μ_d = factor depending upon individual strand circumference or diameter, for example μ_d = 1.0 was used for 0.6 inch strands so 0.83 was used for 0.5 inch strands; and K_0 = interface shear stiffness of an individual strand, which is determined based on 0.6 inch strand from

reported testing[72] [78]. In the literature, Dang[72] and Floyd[78] conducted the pull-out test on 0.6 inch strand, and the average pull-out loads of 16 inch specimens corresponding to 0.01 inch slip from the two tests are 14047 lb and 14490 lb. However, according to the pullout force-slip relationship reported in Dang's test this load at 0.01 inch of slip only represents the upper bound of linear and elastic interface stiffness and slip measured in realistic girders may reach well beyond that 0.01 inch. So in the present study, the interface stiffness is taken as the average interface stiffness of both 0.01 inch slip and 0.1 inch slip, or alternatively for simplification it can be calculated as half of the interface stiffness at 0.01 inch slip to approximately compensate for nonlinearity in the bond-slip relationship. Note that for every batch of strands and concrete, K_0 could vary due to many factors associated with the manufacture, storage and construction processes. Therefore pull-out tests, ASTM A1081[80], may be a good way to verify the condition of bond and confirm applicability of constants and factors used here.

Specimen data from FC150, FC350, FA550, FC160, FC360, and FC560 were extracted from Russell[49]. In the specimen names, the first letter F refers to fully bonded specimen; the second letter C refers to rectangular cross section and A refers to AASHTO type cross section; the first numeral digit denotes the number of strands; the last two numeral digits represent the diameter of strands, in tenth inch. For example, FC150 refers to a fully bonded rectangular beam containing one 0.5-inch strand.

For rectangular cross sections (FC150, FC350, FC160, FC360, and FC560), specimens were uniformly supported on the ground without any external loading except the prestressing force in the strands, but the AASHTO type beams (FA550) were additionally subjected to its self-weight due to eccentric prestressing force caused camber. All of the grade 270 strands were prestressed to 75% of their tensile strength. For rectangular cross sections, strands and strain gages were placed at the beam centroid. For AASHTO beams, strands were placed 2.5 inches from the bottom and strain gauges were placed 1.5 inches above bottom flange. Additional details can be found in Russell[49].

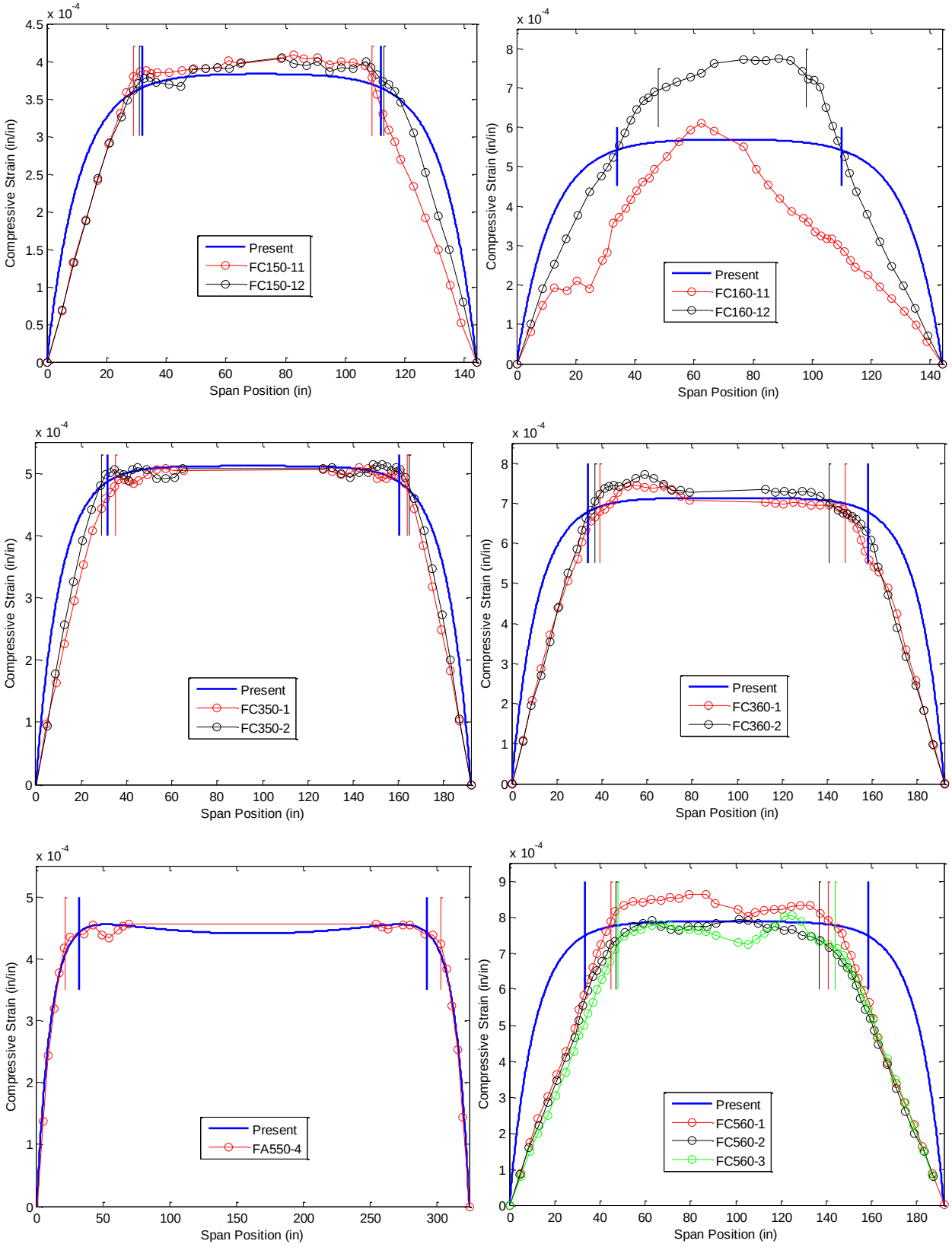

Figure 6-4: Compressive strain at the strain gauge. (Blue vertical lines indicate end of transfer length by present approach, Eq. (6.64), and red, black and green vertical lines indicate values reported by Russell[49])

The comparisons to test results are presented in Figure 6-4. Generally speaking, the predicted results both strain and transfer length are close to the values reported in testing. However, from the strain profile, 0.6-inch strands may have less bonding stiffness than theoretically calculated whereas 0.5-inch strands have results that are close to the predicted values, the predicted transfer length of 0.6 inch strand is shorter than reported in the testing. For example, the FC160, FC360 and FC560 results will correlate better if the interface stiffness is reduced, as in Figure 6-6. One of the possible reasons is, as seen from the plots, 0.6-inch strands are associated with higher level of strain. The higher strain level will make the bond stiffness, determined by averaging bond-slip relation between concrete and strands, smaller. So in the next section, the 0.6-inch strand results are recalibrated using an additional factor that considers the bond-slip relationship. Additionally, the effective prestress is calculated with excellent accuracy; for example effective prestress strain from the testing data and prediction is generally within 10%.

6.5.2 Transfer length considering bond-slip relation

The bond-slip relationship at the steel concrete interface is a complicated matter. It has been reported by a number of studies that the bond-slip relationship exhibits nonlinear behaviors, for example a linear, nonlinear and softening portion. Figure 6-5 illustrates an idealized bond-slip relationship between steel reinforcement and concrete. Therefore, the accuracy of the value used for the bond stiffness K in calculations can be improved according to the strand slip if precise results are needed. However, it is not necessary to include all of the complicated nonlinear and microscopic properties of the bond behavior. An averaging factor is sufficient to represent the overall behavior, and the engineering applicability goals of the work can be met while maintaining sufficient accuracy through concise closed form solutions. The goal is achieved by averaging the nonlinear or discontinuous properties at the strand/concrete interfaces by a constant. This approach, validated against testing data, simplifies the nonlinear problem into a linear approach. Therefore K should consider the end slip as:

$$K = n\mu_{sl}\mu_d K_0 \tag{6.66}$$

where μ_{sl} = factor depending on end slip. Based on the data from Russell's test data[49] and bond-slip studies in the literature[72][74], μ_{sl} = 0.67 when $0.08 \leq \varphi_p \leq 0.11$ inch and μ_{sl} = 0.5 when $0.11 < \varphi_p \leq 0.15$, are used in generating the data presented in Figure 6-6. Based on the complexity of this bond-slip behavior reported in literature, it may benefit from researches at the microscopic level. In this study, FC360 and FC560 are recalibrated and plotted in Figure 6-6 to take the additional slip into consideration.

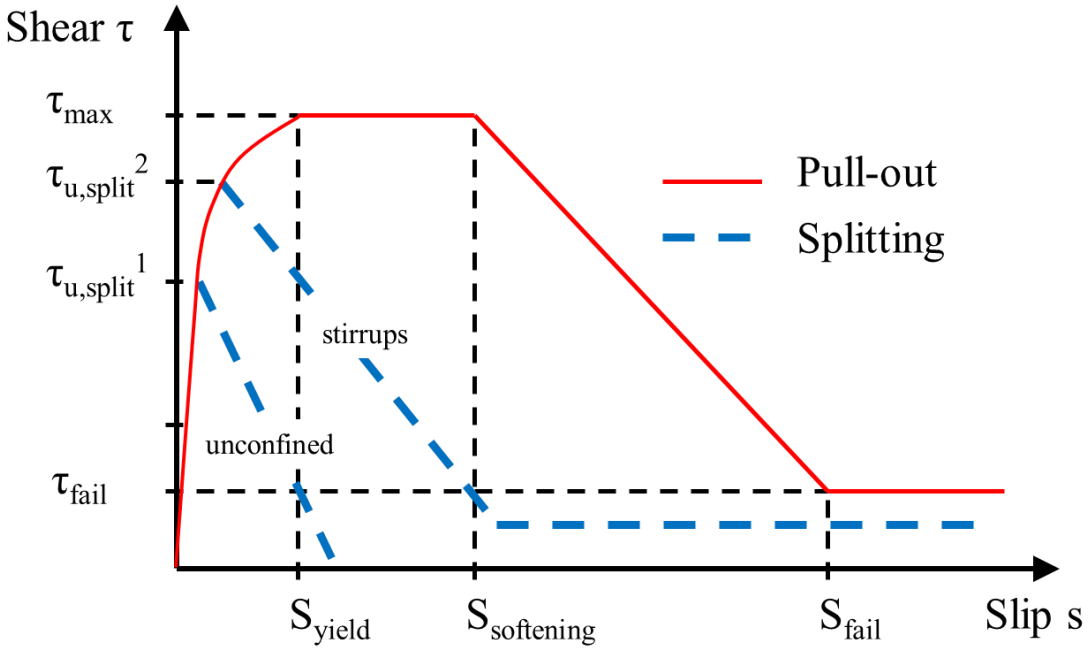

Figure 6-5: Typical bond-slip relationship

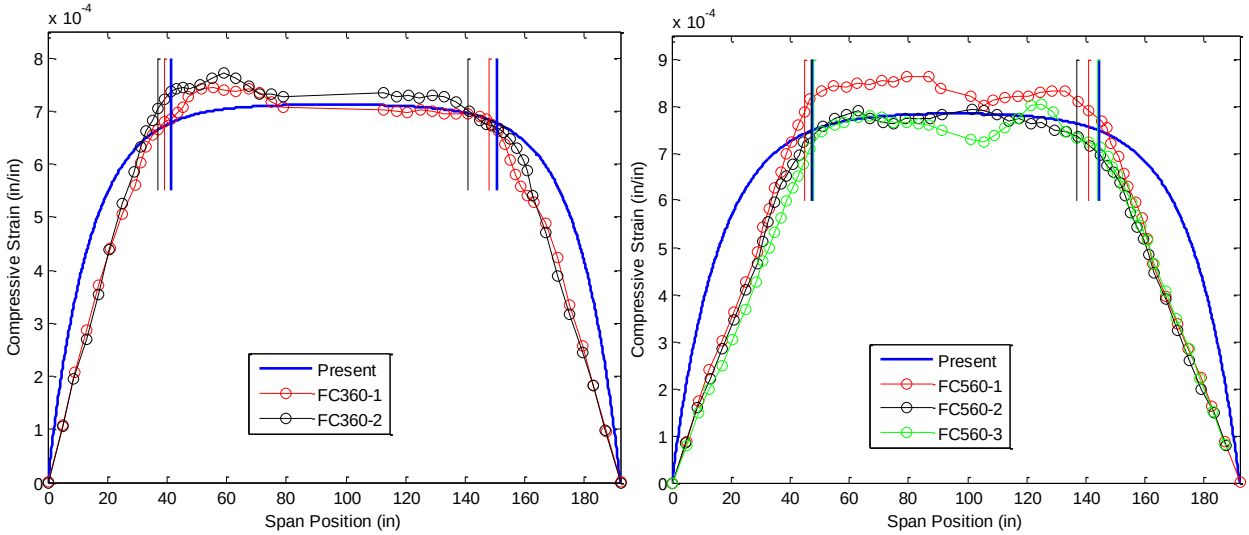

Figure 6-6: Recalibrated results for 0.6 inch strand girders

Table 6-1: Transfer length results and comparison with Russell[49]

Specimen	Transfer length reported (in) North end	Transfer length reported (in) South end	Average of all specimens (in)	Present (recalibrated) (in)
FC150-11	29	35	30.5	32.0
FC150-12	31	31		
FC350-1	35	28	29.8	31.7
FC350-2	29	27		
FC160-11	-	-	47.0	34.2
FC160-12	48	46		
FC360-1	39	44	42.8	33. 8 (41.4)
FC360-2	37	51		
FC560-1	45	51	49.0	33.6 (47.5)
FC560-2	47	55		
FC560-3	48	48		
FA550-4	21	21	21.0	31.7

Table 6-1 demonstrates that the reported transfer length results agree well with results determined from Equation (6.64) for all specimens except FC160. From the results in Figure 6-4, FC160 has very long transfer length, which indicates unusually poor bond. The absolute difference in transfer length for FA550 may appear large, but it is acceptable when considering the very long span length.

6.5.3 Prestress loss due to elastic shortening

Validation and discussion

Prestress loss due to elastic shortening in Equation (6.54) is validated against the data from Kaar[47] because Kaar's tests include a wide range of strand diameters and concrete strengths. Specimens 0.25-1660, 0.25-5000, 0.6-1660, and 0.6-5000 are used for validation. The first number represents the strand diameter and the second number indicates concrete strength. For specimens with concrete strength of 1660 psi, two strands were placed symmetrically along the centroid of a 3 inch by 4.1875 inch rectangular cross section. For 5000 psi concrete strength specimens, six strands were placed symmetrically through the centroid of a 7.5 inch by 10.5 inch rectangular cross section. No external load was applied; the specimens were uniformly supported by the ground.

Table 6-2: Immediate prestress loss comparison with Kaar[47]

Specimen	Strand stress before transfer (ksi)	Strand stress after transfer (ksi)	Loss (%)	Average loss of A & B (%)	Zia, PCI and ACI (%)	Present (%)
0.25-1660-A	194.1	178.8	7.9	7.6	7.6	7.7
0.25-1660-B	194.1	179.8	7.4			
0.25-5000-A	195.7	167.0	14.7	14.5	15.1	14.4
0.25-5000-B	195.7	167.7	14.3			
0.6-1660-A	182.0	172.7	5.1	5.6	5.7	5.9
0.6-1660-B	182.0	170.8	6.2			
0.6-5000-A	177.7	153.8	13.5	13.7	12.4	12.1
0.6-5000-B	177.7	153.1	13.8			

In Table 6-2, the prestress losses calculated using the PCI Design Handbook[70] and ACI 318-11[71] methodologies, which are both based on the work of Zia[50], and Equation (6.54) are essentially the same. Therefore, in order to demonstrate the advantage of the approach developed herein over the PCI Design Handbook and ACI 318-11 methodologies, specimen 0.25-5000 is taken as an example in Figure 6-7, with increasing the total number of 0.25-inch strands from one to eighteen. Additionally, since the

number of strands influences the difference between the formulation presented herein and the formula proposed by Zia, a normalized unit and an additional specimen 0.25-1600 are introduced to demonstrate the difference in Figure 6-8. The large number of strands is used here to study their influence on prestress loss, but it may not necessarily reflect a realistic design scenario.

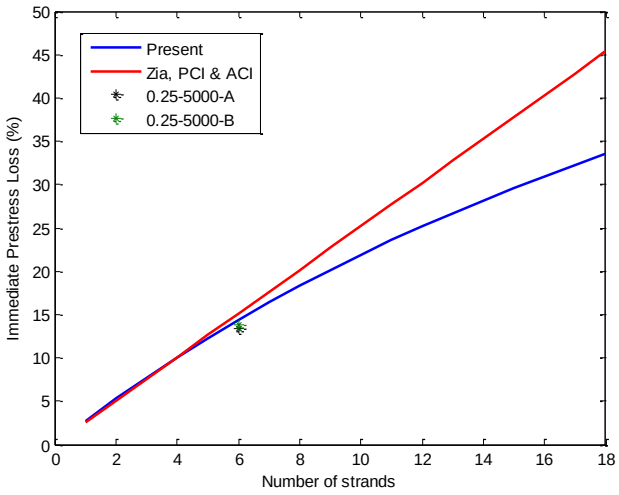

Figure 6-7: Prestress loss due to elastic shortening as a function of number of strands for 0.25-5000.

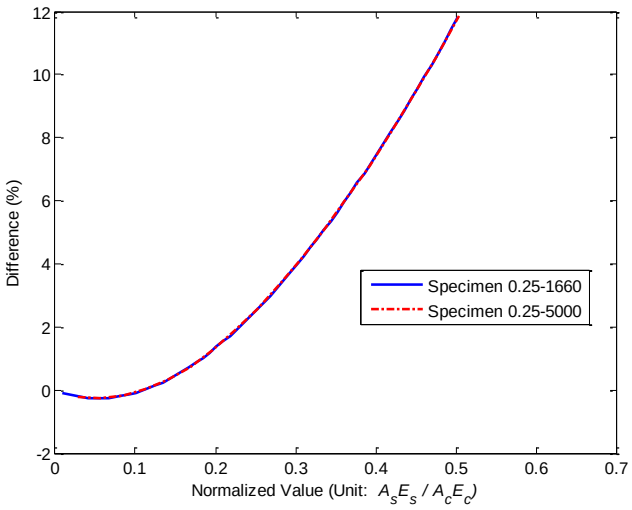

Figure 6-8: Difference between two approaches for elastic shortening loss as a function of normalized unit.

Figure 6-7 and Figure 6-8 demonstrate that the accuracy of the existing formula depends on the number of strands, or more fundamentally $A_sE_s/(A_cE_c)$. When $A_sE_s/(A_cE_c)$ is small, say below 0.1, the difference is basically zero. However, when $A_sE_s/(A_cE_c)$ increases, the difference becomes larger and eventually the existing formula predicts 45% of loss versus the 33% based upon the approach developed herein. Note that the theoretical solution derived in this study and Zia's method yield the same results at 10% immediate prestress loss, which is because Zia assumes 10% losses by using a load factor of 0.9 in the formula. Mathematical proof is provided from Equation (6.67) to Equation (6.73).

In Figure 6-7 and Figure 6-8, however, specimens 0.25-5000 and 0.25-1660 both had strands placed symmetrically about the cross section centroid so there is no bending moment acting on the specimen. In order to study the influence of eccentricity and bending moments on the prestress loss due to elastic

shortening, specimen FA550 from Russell's tests is taken in Figure 6-9 and Figure 6-10 for comparison between the two approaches. Specimen FA550 had five 0.5 inch strands with overall eccentricity e of 9.19 inches from the girder bottom. In Figure 6-7 and Figure 6-8, the total number of 0.5 inch strands is increased from one to thirty to illustrate how strand quantity variation affects the prestress loss due to elastic shortening by different methodologies.

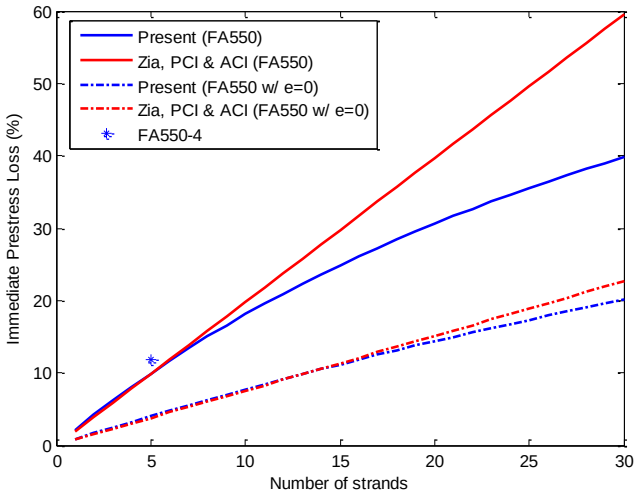

Figure 6-9: Prestress loss due to elastic shortening as a function of number of strands for FA550.

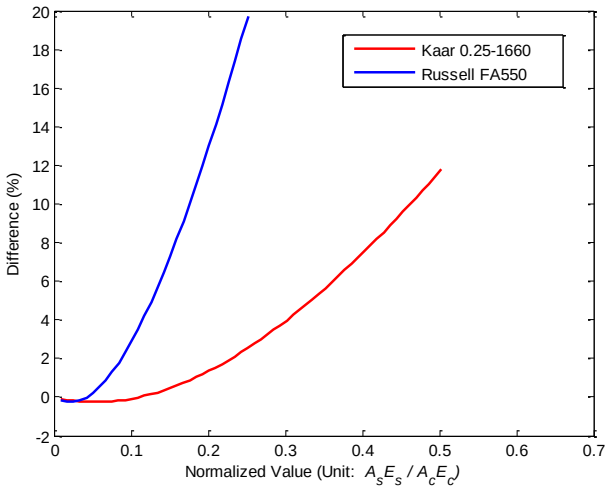

Figure 6-10: Difference between two approaches for elastic shortening loss as a function of normalized unit.

In Figure 6-9 and Figure 6-10, when the total number of strands is below seven the two approaches yield almost the same results on the prestress loss due to elastic shortening. However, as the number of strands increases, the difference becomes larger. For example, at thirty strands, Zia's approach overestimates the loss by 50%. Again, regardless of whether eccentricity is considered or not, at 10% loss the theoretical solution derived in this study and Zia's approach would intersect with each other because the load factor 0.9 used by Zia.

The eccentricity e is set to zero in the dot-dash lines Figure 6-9 to demonstrate the influence of bending moments on the prestress loss due to elastic shortening. The results demonstrate that the shortening caused by bending moment contributes approximately 50% of the overall immediate loss in FA550. The

effect of bending moment on the overall elastic shortening is better illustrated in Figure 6-10 where the difference between the two approaches are plotted with specimens from Kaar and Russell as functions of normalized unit $A_sE_s/(A_cE_c)$. Kaar's 0.25-1660 specimen has symmetrical strands resulting in no eccentricity whereas Russell's FA550 has maximum eccentricity. Therefore, the 0.25-1660 specimen only has elastic shortening loss due to axial compression but FA550 specimen has elastic shortening loss due to both axial and bending compression. This demonstrates that when $A_sE_s/(A_cE_c)$ is relatively large for eccentric specimens, the present and Zia approaches will have larger difference.

Comparison with currently used design formula

Since Equation (6.55) does not involve interface slip, it is possible to derive the same results based on conventional approach. In the PCI Design Handbook[70], the elastic shortening is calculated, with notations adopted in this study, as:

$$ES = K_{es}\left(E_s/E_c\right) f_{cir} \tag{6.67}$$

where: K_{es} = 1.0 for pretensioned components; f_{cir} = net compressive stress in concrete at the center of gravity of prestressing force immediately after the prestress has been applied to the concrete.

$$f_{cir} = K_{cir}\left(\frac{N_i}{A_c} + \frac{N_i e^2}{I_c}\right) - \frac{M_c}{I_c} \tag{6.68}$$

where: K_{cir} = 0.9 for pretensioned components; N_i = initial prestress force; M_c = bending moment due to dead weight of the prestressed component and any other permanent loads in place at the time of prestressing. Equation (6.67) reflects the mechanics well, however Equation (6.68) does not. In Equation (6.68), the initial applied prestress force N_i multiplied by K_{cir} = 0.9 is used to calculate the concrete stress. Therefore, with the constant load factor K_{cir} = 0.9, the formula implies that it is only correct when elastic shortening is 10%, and otherwise it is an approximation; this can be observed in Figure 6-7 and

Figure 6-9 (results by two methodologies only intersect at 10% loss). It may be improved by iteration; however there is a much better way to obtain the closed form solution. Consider the scenario of e = 0 for simplification and elastic gain due to self-weight not considered. In Equation (6.68), replacing K_{cir} with P_{effe} results in:

$$f_{cir} = P_{effe} \frac{N_i}{A_c} \tag{6.69}$$

Substituting Equation (6.69) into Equation (6.67):

$$ES = K_{es} \left(E_s / E_c \right) P_{effe} \frac{N_i}{A_c} \tag{6.70}$$

Equation (6.70) is further transformed by multiplying (A_s / N_i) to both sides and neglecting K_{es} = 1.0:

$$P_{loss} = p_{effe} \frac{A_s E_s}{A_c E_c} \tag{6.71}$$

Plugging P_{effe} = 1 – P_{loss} into Equation (6.71):

$$p_{loss} = \left(1 - p_{loss}\right) \frac{A_s E_s}{A_c E_c} \tag{6.72}$$

Now P_{loss} is determined as:

$$p_{loss} = \frac{A_s E_s}{A_c E_c + A_s E_s} \tag{6.73}$$

Equation (6.73) is the same as Equation (6.56) from the theoretical development of this study.

6.6 Influences of variables on transfer length

6.6.1 Elastic modulus and interface stiffness

It has been argued for many years that concrete strength influences transfer length. It is also believed that the bond at the interface has the greatest influence on the transfer length but nobody has yet showed either compelling test data or theoretical solution to demonstrate how the bond at the interface influences transfer length. The material parameters and geometry of FA550, the AASHTO type specimens in Russell's tests, are used to illustrate the influence of concrete elastic modulus and interface stiffness on transfer length. Those two variables are increased from zero to twice that involved in Russell's tests to demonstrate their effects on transfer length. Note that only the axial force caused by prestressing force is plotted, and that axial force due to curvature change or gravity is not included nor discussed in this section.

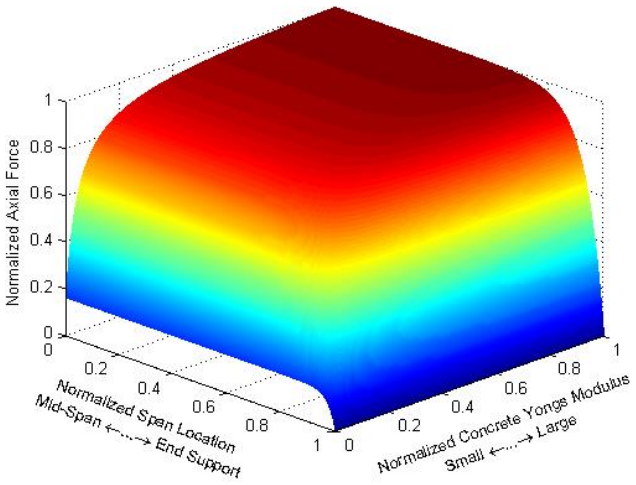

Figure 6-11: Influence of concrete elastic modulus on axial force. (L_{max}=162 in, Ec_{max}=8400.5 ksi and N_{max}=149.13 kips)

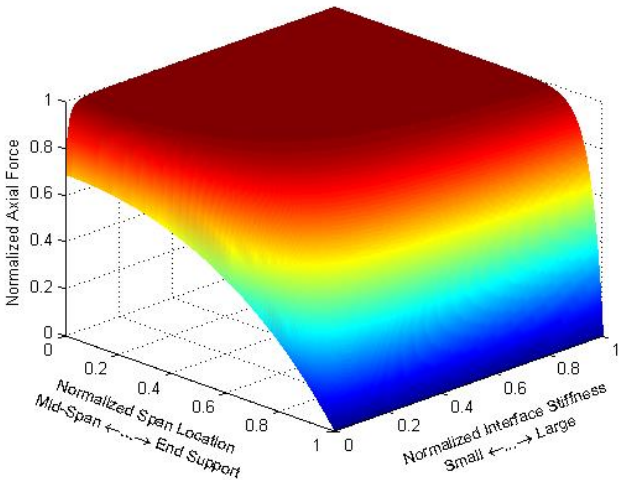

Figure 6-12: Influence of concrete interface stiffness on axial force. (L_{max}=162 in, K_{max}=364.7 kip/in and N_{max}=143.77 kips)

In Figure 6-11, the influence of elastic modulus shows interesting features. Theoretically, no matter how low the concrete elastic modulus is, there will always be an axial force plateau. The plateau indicates the end of transfer length and the beginning of effective prestress because the axial force does not change

within the plateau and consequently there is no slip or interface force between the strands and concrete. However, as shown in Figure 6-11, even if the effective prestressing force is reached, the axial force may still be small when the concrete elastic modulus is low due to elastic shortening.

In Figure 6-12, not surprisingly, it is demonstrated that the bond stiffness is very influential on the axial force, and therefore transfer length. For example, unlike in the elastic modulus variation, if the bond stiffness drops below a certain threshold, there will not be an axial force plateau. This means that, below that threshold bond stiffness, the effective prestress is not going to be reached at the mid-span and the transfer length is even longer than the entire span.

In reality, when the concrete elastic modulus, typically calculated from concrete strength for design purposes, becomes lower, the bond becomes weaker and consequently the interface stiffness drops as well. In order to compare, the plots in Figure 6-11 and Figure 6-12 are intersected with 95% of the effective prestressing force, which is given by the right hand side of Equation (6.62).

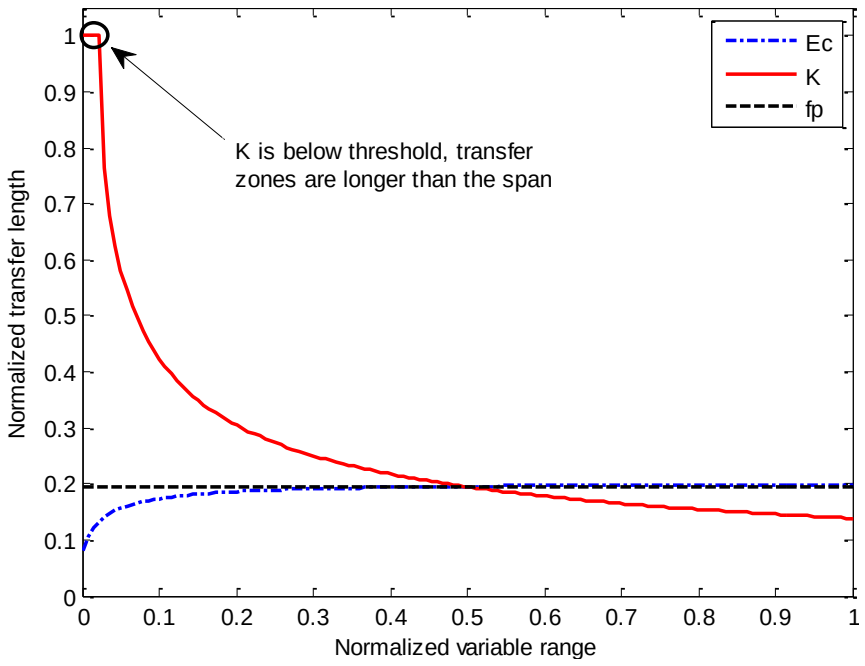

Figure 6-13: Transfer length as function of different variables. (Lt_{max}=162 in, Ec_{max}=8400.5 ksi, K_{max}=364.7 kip/in and fp_{max}/As =-405 kips).

One of the conclusions that Figure 6-13 demonstrates is that the concrete elastic modulus has little influence on the transfer length. This conclusion supports claims made by Kaar[47] and disproves claims made by Michelle[48]. However, this conclusion was determined without considering the influence of concrete strength on the interface stiffness K. Given the possibility that stronger concrete will increase the bond stiffness, this additional influence is likely the reason that Michelle claims that transfer length is related to concrete strength. Therefore the overall results of transfer length may seem to decrease when concrete strength increases. Again, Michelle failed to exclude other variables such as interface stiffness while trying to focus on concrete strength. Also, Figure 6-13 demonstrates that the transfer length is greatly related to the bond stiffness K. For example, as the bond stiffness increases from zero to the maximum value, the transfer length decreases from 162 inches to 20 inches.

6.6.2 Prestressing force

It has been reported that the prestressing force magnitude is related to the transfer length. Although this could have seemingly been observed from testing, the mechanism may not be well understood. First of all, if the bond-slip relationship is in the linear range, the prestressing force will not be related to the transfer length, as demonstrated in Equation (6.64) and Figure 6-13. However, in reality the bond-slip relationship is likely to be nonlinear near the end supports and some of the concrete surrounding the strands may be fractured by higher prestressing force. So as a result, higher levels of prestressing force could result in longer transfer lengths due to poorer bonding. For this reason, it is clear from the perspective of this theoretical development that the bond-slip condition associated with different prestressing force magnitude, which is already included in the interface stiffness K, affects the transfer length rather than the prestressing force itself.

6.6.3 Strand diameter

As demonstrated by the theoretical development and bond stiffness definition, strand diameter based on which AASHTO-LRFD[79] calculates transfer length may not be directly related to transfer length. The primary factor discovered in this dissertation is the total amount of interface area between concrete and strands, which affects the interface stiffness K first then the interface stiffness K affects transfer length. For example, consider two scenarios: (1) ten 0.6 inch strands are used but placed a certain distance apart, and (2) those ten strands are bundled and placed together. For those two cases, the total prestressing forces and strand total diameters are the same; however for the second case the interface areas would be less due to the fact that the inner strands are not in direct contact with the concrete. Consequently, for the second case, the interface stiffness K becomes smaller and transfer length becomes larger in Equation (6.65).

6.7 Conclusions

This study derives a set of governing equations and closed form solutions that rigorously define the mechanics of prestressing concrete. The key characteristic of strand-concrete interface slip is included in the development to solve the transfer length problem. Additionally, the theoretical development also resulted in mechanics-based formulas that address elastic shortening loss and prestress loss due to slip within the transfer zone. Specific conclusions include:

1. It is demonstrated analytically that the PCI Design Handbook, AASHTO-LRFD specification and ACI-318 provisions for prestress loss due to elastic shortening are only applicable to small reinforcement ratio components and will overestimate the prestress loss for large reinforcement ratio components whereas the formulation derived herein is accurate without limitation.

2. Transfer length is derived based on pure mechanical definition instead of empirical data as used by other researchers in the past investigations, and the derived formula is validated against test data.

3. The roles of concrete strength, prestressing force and strand diameter that were previously thought to directly affect transfer length however actually influence the interface stiffness, which in turn affects transfer length.

4. The rigorous strand force gain due to curvature developed in this chapter is able to consider the existence of slip and large reinforcement ratios, which could not be accounted for in the past. It is also simplified for application outside of transfer zones, for example critical sections at or near midspan.

It is concluded that the developed theory can improve prestress concrete analysis and design, and can provide a new perspective in prestressing structural analysis. Comparisons with testing data demonstrate agreement with the developed theory.

Chapter 7 Practical approaches to predict transfer length

7.1 Introduction and scope

Chapter 6 focused on the theoretical development and validation of the application of composite theory to prestressed concrete structures. However, in reality there may be many difficulties to quantify the bonding condition between tendons and concrete interface, and the transfer length formula in Chapter 6, Equation (6.64), is also lengthy.

In this chapter with the goal of simplifying the previous results under the normal design condition, the transfer length formula is firstly simplified according to the finite parameter range under normal design conditions. Then another important step forward in the theoretical system is that upon mathematical manipulation and simplification, the interface bonding stiffness can be quantified based on measured end slip data. All the theoretical developments are validated against experimental data in the literature. Additionally, comparisons on the bonding conditions among different strands configurations and discussions of correlation between strand diameter and transfer length are provided.

7.2 Simplification for engineering applications

7.2.1 Simplification of closed form transfer length solution

Equation (6.64) is the transfer length closed form solution. However, it may be too complicated to be used for ordinary engineering applications and therefore it is simplified by taking advantage of the fact that realistic prestressed concrete structures have finite parameter ranges. In other words, several expressions can be eliminated or simplified to arrive at a concise expression of transfer length without losing much accuracy. Therefore Equation (6.64) can be transformed to:

$$L_t = \frac{\beta_B}{\chi_B}\left(\ln e^{\frac{l\chi_B}{2\beta_B}} - \ln(\lambda_t + \sqrt{\lambda_t^2 - 1}) \right) \tag{7.1}$$

By plugging $\lambda_t = (1\text{-}\gamma)\ cosh(\chi_B l/(2\beta_B))$ and letting $\mu = \chi_B l\ /\ (2\beta_B)$, Equation (7.1) is further transformed to:

$$L_t = \frac{\beta_B}{\chi_B}\left(\ln e^{\mu} - \ln\left((1-\gamma)\cosh(\mu) + \sqrt{(1-\gamma)^2 \cosh^2(\mu) - 1} \right) \right) \tag{7.2}$$

Then considering $cosh(\mu) + sinh(\mu) = e^{\mu}$, Equation (7.2) becomes:

$$L_t = \frac{\beta_B}{\chi_B} \ln\left(\frac{\sinh(\mu) + \cosh(\mu)}{(1-\gamma)\cosh(\mu) + \sqrt{(1-\gamma)^2 \cosh^2(\mu) - 1}} \right) \tag{7.3}$$

It can be noted from Equation (7.3) that if the complicated bracketed term can be simplified as a constant, a concise transfer length expression would result. Fortunately, this is possible for practical design parameter ranges. For typical prestressed structures, $\mu = \chi_B l\ /\ (2\beta_B)$ is large enough to make $cosh(\mu) = sinh(\mu)$ and $(1\text{-}\gamma)^2 cosh^2(\mu) - 1 = (1\text{-}\gamma)^2 cosh^2(\mu)$. Equation (7.3) then becomes:

$$L_t = \frac{\beta_B}{\chi_B} \ln\left(\frac{1}{1-\gamma} \right) \tag{7.4}$$

7.2.2 Transfer length based on end slip

Regardless of whether Equation (6.64) or Equation (7.4) is used, the transfer length expression requires that the concrete strand interface stiffness be an input. However, it would be difficult to nondestructively quantify that parameter on a specific existing prestressed member, if possible at all. The alternative would be to use pull-out tests of very similar concrete and strand samples, and then to recalibrate the pull-out test results appropriately to accommodate the nonlinearities associated with load conditions applied on the actual members. In order to obtain the realistic interface stiffness, this

recalibration procedure, discussed in the sections 6.6.1 and 6.6.2 of Chapter 6, may involve the elimination of deformations from strands and concrete themselves and consideration of appropriate amount of plastic behaviors.

However, the end slip is easy to measure, and once the end slip is known, the interface stiffness on the specific specimen can be calculated accordingly. So the main task here is to relate Equation (6.41) to Equation (6.42) and Equation (7.4). First, by substituting $x = l / 2$ into Equation (6.41) and making $\mu = \chi_B l / (2\beta_B)$, Equation (6.41) is transformed into:

$$\frac{2\varphi_{pe}}{l\varepsilon_{is}} = \frac{\tanh \mu}{\mu} \tag{7.5}$$

where $\varphi_{pe} = \varphi_p(l/2)$ = end slip due to prestressing force. It is difficult to obtain the explicit solution of μ in Equation (7.5). However, it can be simplified since, for realistic prestressed concrete members, μ as a variable will be so large that $\tanh \mu$ becomes approximately equal to 1. For example, the specimens used for validation in the following section have μ values ranging from 3.96 to 6.58, which results in $\tanh \mu$ from 0.99927 to 0.9999961. Note, for specimen T15-H-S3 that has the lowest μ value of 3.96, the prestressing force actually cannot even be all transferred to the concrete as in Figure 7-9 since the transfer lengths are greater than the span length. In reality, this situation is rare and even with this situation the approximation of $\tanh \mu = 1$ will only result in error of 0.073%. So with this simplification μ is obtained as:

$$\mu = \frac{l\varepsilon_{is}}{2\varphi_{pe}} \tag{7.6}$$

By plugging $\mu = \chi_B l / (2\beta_B)$ into Equation (7.6), χ_B is also obtained as:

$$\chi_B = \frac{\varepsilon_{is}\beta_B}{\varphi_{pe}} \tag{7.7}$$

Span length and initial prestrain in the strands are known, and the end slip is measured. Therefore everything in Equation (7.6) and Equation (7.7) is determined. Then, after plugging Equation (7.7) into Equation (7.4), the transfer length based on measured end slip can be determined as:

$$L_t = \frac{\varphi_{pe}}{\varepsilon_{is}} \ln\left(\frac{1}{1-\gamma}\right) \tag{7.8}$$

7.2.3 Strain profile based on end slip

Similarly to the way Equation (7.8) is derived with end slip known, after plugging Equation (7.7) into Equation (6.42), Equation (6.42) becomes:

$$N_p = -\beta_B^2 \eta \varepsilon_{is} \left(1 - \frac{\cosh\left(\frac{\varepsilon_{is} x}{\varphi_{pe}}\right)}{\cosh\left(\frac{l\varepsilon_{is}}{2\varphi_{pe}}\right)}\right) \tag{7.9}$$

Consequently, the strain profile can be determined based on Equation (7.9). Note, Equation (7.9) only includes the prestressing related force (self-weight and external loads are not considered). The resultant force associated with self-weight and external loads can be considered as well under normal design conditions by the same theoretical composite theory framework developed in Chapter 6 as:

$$M_s = M_{ex}\beta_B^2 \tag{7.10}$$

$$N_s = \frac{M_{ex}\alpha_B^2}{e} \tag{7.11}$$

where M_s = resultant bending moment in concrete due to gravity load; M_{ex} = external applied bending moment including self-weight; N_s = resultant axial force due in both concrete and reinforcement or tendons due to gravity load.

Theoretically, Equations (7.10) and (7.11) are only applicable to locations that are outside of the transfer zones. Inside of transfer zones, the slip compensation terms need to be added. However, the external bending moment is usually very small within the transfer zones and the resulting compensation terms will not play a significant role. Therefore the strain at any position can be determined as:

$$\varepsilon = \frac{1}{E_c}\left(\frac{\left(N_p + N_s\right)}{A_c} + \frac{\left(eN_p + M_s\right)\times d}{I_c}\right) \tag{7.12}$$

where d = the distance from the centroid to the position of interest. Additionally, in Equation (7.10) and Equations (7.11), β_B^2 is very close to 1 and α_B^2 is very close to 0. So for prestressing structures under normal design conditions, using $M_s = M_{ex}$ and $N_s = 0$ in Equation (7.12) are acceptable. Furthermore, if the prestressed concrete structures are only subjected to gravity load as in the validation tests, using $M_s = 0$ and $N_s = 0$ in Equation (7.12) should be acceptable since the force in strand due to gravity load is negligible compared to the prestressing force. As a result, when only prestressing force is considered, the strain can be calculated as:

$$\varepsilon = \frac{N_p}{E_c}\left(\frac{1}{A_c} + \frac{de}{I_c}\right) \tag{7.13}$$

Equations (7.8), (7.9), (7.12) and (7.13) imply that knowing the end slip of a specimen will not only enable the prediction of transfer length but will also make it possible to calculate the internal forces, bending moments and the entire strain profile of the prestressed structure at any position. This is because the end slip as the indicator of bonding condition will yield the interface stiffness, which is the

only unknown parameter in the theory developed in Chapter 6. So if the transfer length of existing prestressed structures needs to be evaluated, there is no need to measure and calculate interface stiffness beforehand, and this constant can be calculated after measuring the end slip of the specific specimen of interest.

7.3 Existing theory on transfer length

As discussed in the literature review section, among the existing studies, no matter what assumptions are presumed, the formula takes the same form as:

$$L_t = \alpha \frac{\varphi_{pe}}{\varepsilon_{is}} \tag{7.14}$$

where α = the constant depending on assumed stress distribution. α = 2 for linear distribution and α = 3 for parabolic distribution. Equation (7.14) was derived theoretically based on a stress distribution assumption. Unlike most of the transfer length studies, relating end slip to transfer length is theoretically sound. The only issue is that the stress distribution must be assumed and if stress distribution can be assumed correctly, Equation (7.14) will yield correct transfer length.

The differences and arguments between those studies mainly concentrate on the values of α. It has been reported to be from 1.5 to 4.0[83] but α is believed to typically be between 2.0 and 3.0; other values are for rare cases. One very important point about this α parameter is that α is found to be heavily dependent on the criteria used to determine transfer length. For example, if the 95% AMS[49] method is to be used, α is likely to be close to 2.0. However, if the 95% Effective Prestressing Force (EPF) is used then α is likely to be close to 3.0. This is because transfer length is a concept made up for design convenience and it cannot be measured directly and depends on the measurement criteria. In the discussion in the Section 7.4.1, especially Table 7-1, it will be shown that this α is dependent on the criteria γ.

7.4 Validations and Discussions

7.4.1 Comparison with existing approaches

It could be observed that Equations (7.8) and (7.14) have very similar expression forms, and the only difference is the constant in front of $\varphi_{pe} / \varepsilon_{is}$. However, plugging $\gamma = 0.95$ into Equation (7.8) results in:

$$L_t = 3\frac{\varphi_{pe}}{\varepsilon_{is}} \tag{7.15}$$

So now it is obvious that Equation (7.8) is the same as Equation (7.14) with $\alpha = 3$ (parabolic stress distribution). Similar to Equations (7.8) and (7.15), when plugging $\gamma = 0.95$ into Equation (7.4), it becomes:

$$L_t = 3\frac{\beta_B}{\chi_B} \tag{7.16}$$

It should be recognized that the definition of transfer length depends on γ. This is because transfer length, unlike deflection or other variables, is an ambiguous concept and therefore difficult to determine either theoretically or experimentally. From its definition, it is the position where axial force no longer changes over the span. However, theoretically, the axial force changes as a hyperbolic sine function along the entire span; therefore, although the magnitude of change is very small outside of the transfer zones, the axial force will keep increasing until reaching the mid-span. It is also very difficult to experimentally measure such consistent and stable strain profiles that indicate the end of transfer length. So in reality, in order to determine it, there must be certain criterion to define it, which is defined by γ in the present study. The 95% AMS method[49] is usually employed to experimentally determine the transfer length. However, the 95% AMS method uses average measured plateau values instead of theoretically obtained effective prestressing strain in the 95% EPF, and due to the averaging procedure it tends to yield smaller α values than the 95% EPF.

For design purpose, it is difficult to decide which α value is superior. Because, in design the prestressing force is assumed to be bilinear, but the reality is that it is a smooth curve governed in form of hyperbolic *sine* function. Consequently, when the effective prestressing force is determined, longer transfer length, although accurate according to its definition, may result in underestimated prestressing force near the end of transfer zones.

Table 7-1: Variation of α as function of γ

γ	77.7%	86.5%	91.8%	95.0%	98.2%
α	1.5	2.0	2.5	3.0	4.0

7.4.2 Validations and discussions

In this section, data from Kim's dissertation[84] is used to validate the theoretical development. The specimens tested all have span length of 118.11 inches and rectangular cross sections with height of 7.874 inches and width ranging from 4.437 inches to 7.528 inches. There are two types of strands, 0.5 and 0.6 inch diameter strands, placed with various transverse eccentricities and lateral spacing in those specimens. Ten single strand specimens, M13-H-C4-1(2), M13-H-C5-1(2), M15-H-C3-1(2), M15-H-C4-1(2), and M15-H-C5-1(2) and six twin strands specimens T13-H-S3, T13-H-S4, T13-H-S5, T15-H-S3, T15-H-S4, and T15-H-S5 are used for validation. In those specimen names, M represents single strand and T represents twin strands. The number 13 represents 0.5 inch diameter strand and number 15 represents 0.6 inch diameter strand. The other letters and numbers represent different eccentricities, spacing and specimen numbers. More details can be found in Kim's and Oh's works[84][85].

In the calculation, the measured end slips are used to obtain axial forces in Equation (7.9), then bending moment is also calculated by the axial forces multiplying the eccentricity. Therefore the concrete strain profile can be determined using Equation (7.12) to compare with measured data in those specimens.

Note, in Figure 7-1 to Figure 7-11, the closed form solution refers to the transfer length calculated by Equation (6.64) with $\gamma = 0.95$ and χ_B obtained from Equation (7.7) since end slip data are available, and linear stress solution refers to Equation (7.14) with $\alpha = 2$. Again, to be clear, in the validation section below no parameter value is assumed and all of the inputs data are determined according to the reported or measured results.

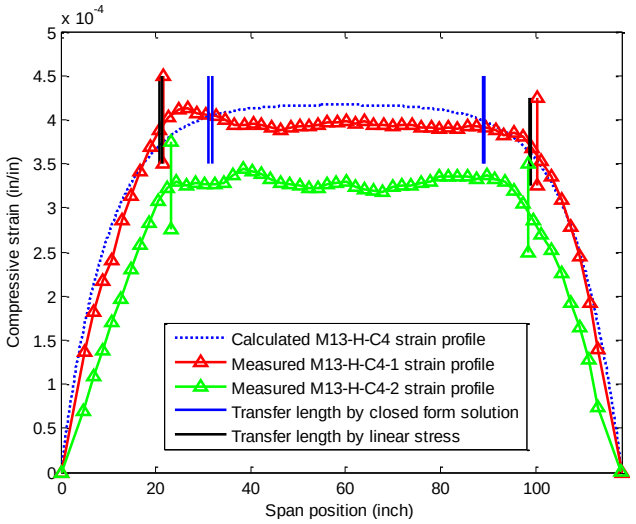

Figure 7-1: M13-H-C4 specimens strain profiles

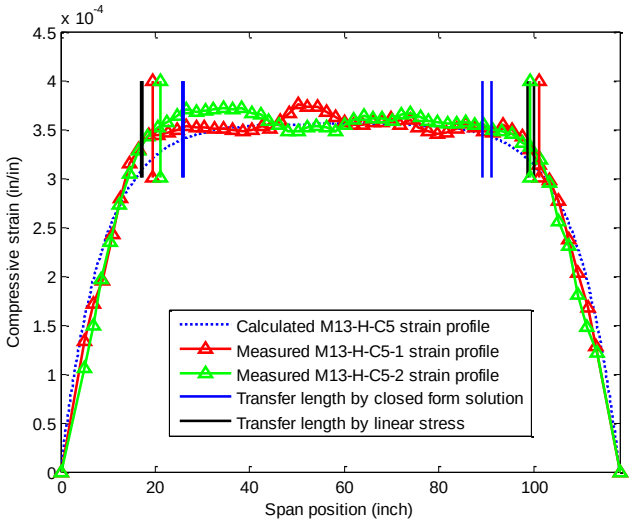

Figure 7-2: M13-H-C5 specimens strain profiles

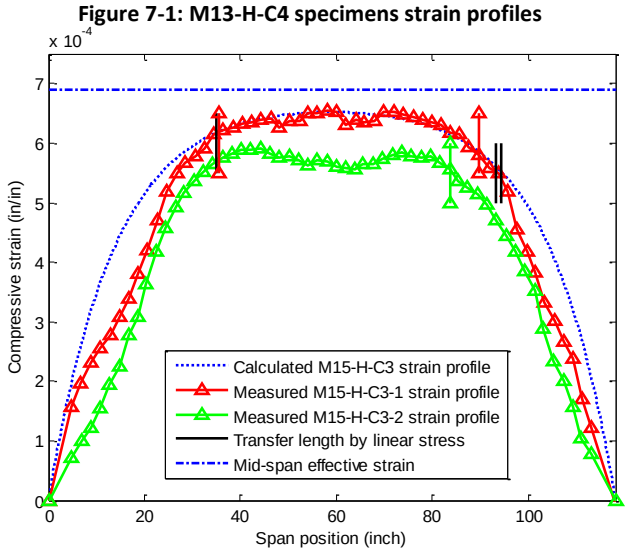

Figure 7-3: M15-H-C3 specimens strain profiles

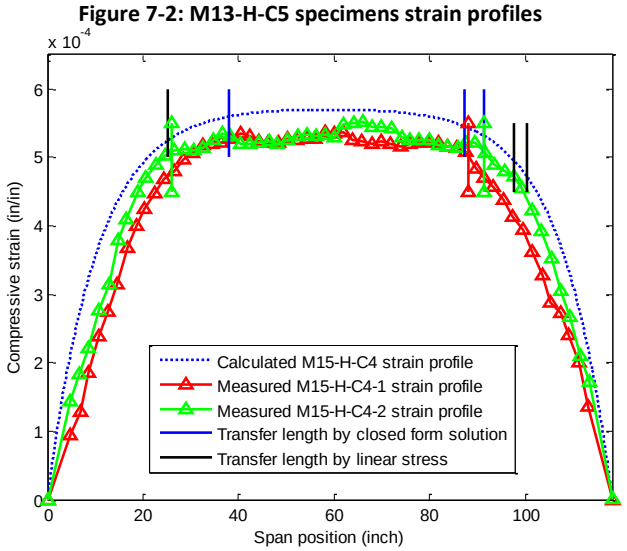

Figure 7-4: M15-H-C4 specimens strain profiles

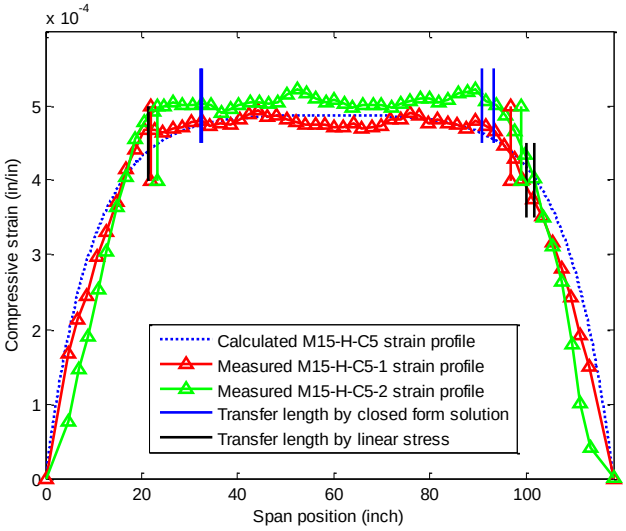

Figure 7-5: M15-H-C5 specimens strain profiles

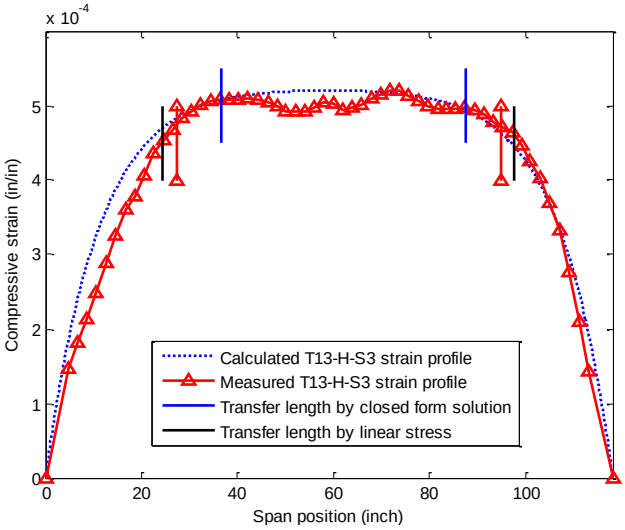

Figure 7-6: T13-H-S3 specimens strain profiles

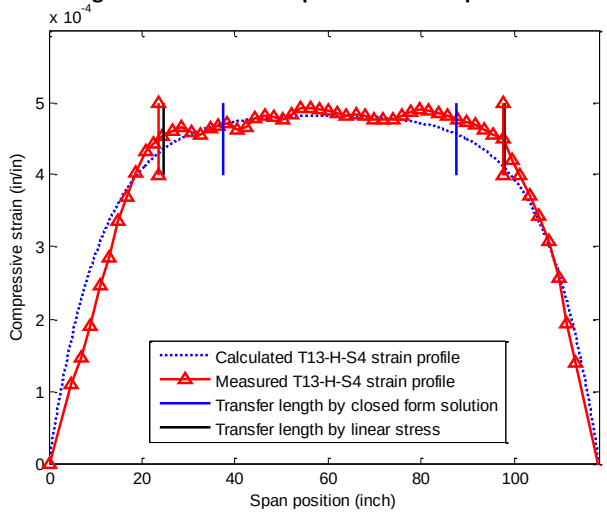

Figure 7-7: T13-H-S4 specimens strain profiles

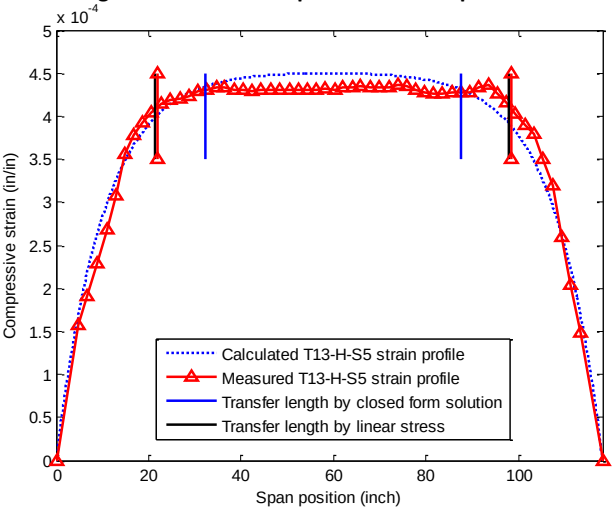

Figure 7-8: T13-H-S5 specimens strain profiles

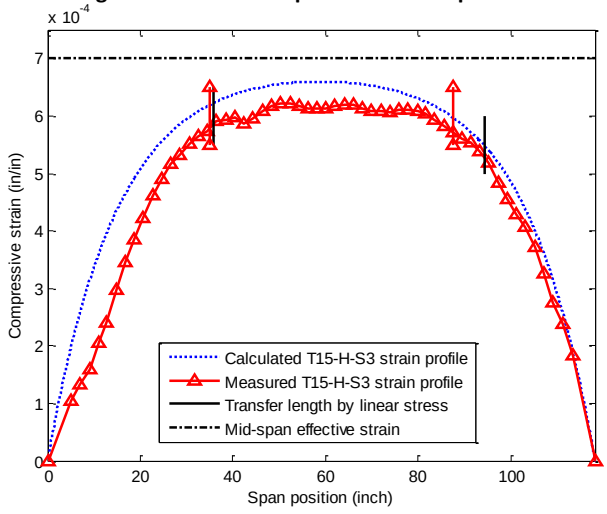

Figure 7-9: T15-H-S3 specimens strain profiles

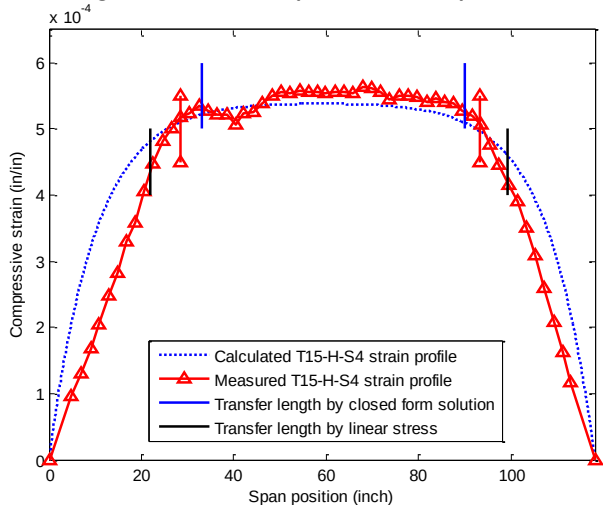

Figure 7-10: T15-H-S4 specimens strain profiles

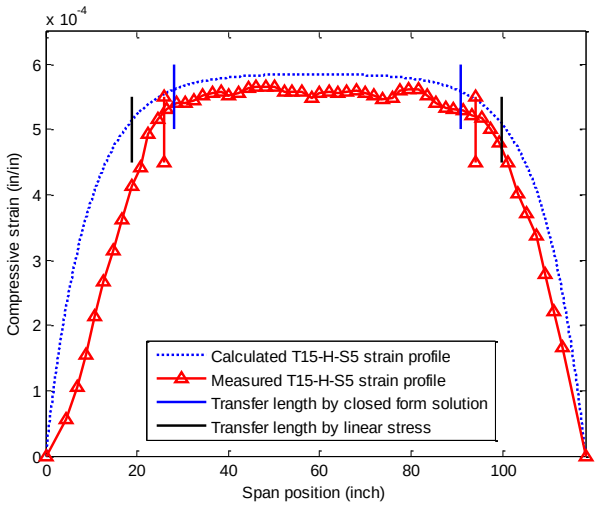

Figure 7-11: T15-H-S5 specimens strain profiles

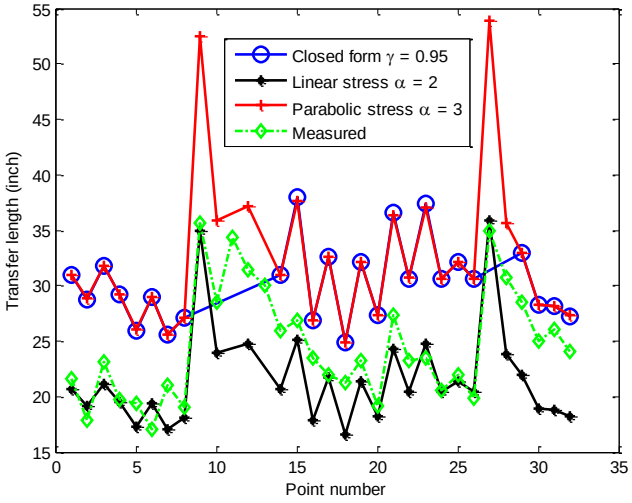

Figure 7-12: Transfer lengths of all specimens

As demonstrated through Figure 7-1 to Figure 7-11, the method developed herein for predicting the strain profiles and transfer length based on measured end slip data, results in good accuracy that has never been reported in the literature. In the Chapter 6, the interface bonding stiffness parameter was approximated based on corresponding pull-out test results. However, now it can be directly determined from end slip data and incorporated into solutions to predict strain profiles. Additionally, transfer lengths are plotted in Figure 7-12 and presented in Table 7-2 for further comparison.

There are however noticeable bonding problems with two 0.6 inch diameter strand specimens, namely, M15-HC3 in Figure 7-3, and T15-H-S3 in Figure 7-9. Strands in those two specimens cannot transfer all of the prestressing force to the concrete; instead there are considerable amount of slip loss at the mid-span and the effective prestressing force cannot be achieved.

One important issue that should be clarified before the discussion on transfer length results is that the transfer length, as discussed earlier, cannot be directly measured and the reported values may depend on the strain gauge position as well as strand position and even involve researchers' own interpolations. Therefore the transfer length data obtained from the tests may not serve as a very accurate benchmark.

Actually, from Figure 7-1 to Figure 7-11, the actual transfer lengths tend to be larger than the measured values. This is because the 95% AMS procedure can result in smaller effective strain due to the 95% factor and the plateau values averaging process.

The point numbers in Figure 7-12 are listed in Table 7-2. In Figure 7-12 and Table 7-2, the first thing noticed is the fact that Equation (7.8) with $\gamma = 0.95$ is basically equivalent to Equation (7.14) with $\alpha = 3$, which demonstrates the validities of the simplifications employed in Equations (7.4), (7.6), and (7.8). Secondly, the measured transfer lengths are close to that predicted by the formula by assuming linear interface stress distribution, $\alpha = 2$. However, looking back at the strain profiles in Figure 7-1 to Figure 7-11 and the definition of transfer length, $\alpha = 3$ is actually more reasonable to use whereas $\alpha = 2$ tends to predict shorter transfer length results. Equations (6.64), (7.4), (7.8) and (7.14) with $\alpha = 3$ will yield essentially the same transfer length results. However, Equation (6.64) cannot be used when transfer lengths are larger than the span length whereas Equations (7.8) and (7.14) still can yield results based on measured end slip, for example in M15-H-C3 and T15-H-S3.

Table 7-2: Transfer lengths comparison

	Point number		Measured (in)		Linear stress (in)		Parabolic stress (in)		Closed form w/ γ = 0.95 (in)	
	Cut end	Dead end	Cut end	Dead end	Cut end	Dead end	Cut end	Dead end	Cut end	Dead end
M13-H-C4-1	**1**	**2**	21.57	17.91	20.67	19.21	31.01	28.82	31.00	28.80
M13-H-C4-2	**3**	**4**	23.11	19.72	21.19	19.46	31.79	29.19	31.80	29.17
M13-H-C5-1	**5**	**6**	19.37	17.09	17.33	19.34	26.00	29.01	25.96	28.99
M13-H-C5-2	**7**	**8**	20.98	19.02	17.09	18.09	25.64	27.14	25.60	27.10
M15-H-C3-1	**9**	**10**	35.59	28.54	34.97	23.95	52.46	35.93	-*	-*
M15-H-C3-2	**11**	**12**	34.33	31.45	-*	24.77	-*	37.16	-*	-*
M15-H-C4-1	**13**	**14**	30.00	25.98	-*	20.66	-*	30.99	-*	30.99
M15-H-C4-2	**15**	**16**	26.85	23.46	25.10	17.92	37.65	26.88	38.03	26.85
M15-H-C5-1	**17**	**18**	21.93	21.26	21.72	16.58	32.58	24.87	32.62	24.83
M15-H-C5-2	**19**	**20**	23.27	19.13	21.43	18.23	32.15	27.35	32.17	27.31
T13-H-S3	**21**	**22**	27.36	23.27	24.26	20.45	36.39	30.68	36.63	30.67
T13-H-S4	**23**	**24**	23.43	20.55	24.72	20.39	37.08	30.59	37.40	30.58
T13-H-S5	**25**	**26**	21.97	19.80	21.41	20.39	32.12	30.59	32.14	30.58
T15-H-S3	**27**	**28**	35.00	30.71	35.91	23.78	53.87	35.67	-	-

T15-H-S4	**29**	**30**	28.54	25.00	21.94	18.86	32.91	28.29	32.96	28.27
T15-H-S5	**31**	**32**	26.06	24.09	18.78	18.21	28.17	27.32	28.15	27.28

*Missing data due to damage of instrument upon prestressing force release.

7.5 Discussion on the bond condition and demand

7.5.1 Evaluation of strand bonding condition

Kim's work[84] includes a variety of specimens, which makes it possible to compare and study the influence of some variables. For example, the single strand specimens M13-H-C4-1(2), M13-H-C5-1(2) differ from each other only by eccentricity, and M15-H-C3-1(2), M15-H-C4-1(2), and M15-H-C5-1(2) differ from M13-H-C4-1(2), M13-H-C5-1(2) by strand diameter. Similarly, specimens T13-H-S3, T13-H-S4, T13-H-S5, T15-H-S3, T15-H-S4, and T15-H-S5 make it possible to study the influence of spacing between strands. The strand bonding stiffness of specimens are tabulated in Table 7-3 for discussion.

Another very important statement about the interface stiffness is that the existence of possible nonlinear bond-slip relationship along the tendons is recognized. However, based on the comparison between comprehensive testing data and corresponding analyses, uniform and constant interface stiffness along the prestressing tendons can achieve accuracy that is adequate for engineering analysis. In addition, one of the merits of using constant interface stiffness is that the complicated nonlinear differential equations can be simplified into linear equations, which makes it possible to determine the concise closed form solutions for the sake of design and easy understanding. Again, this study aims at developing practical approaches to determine the transfer length and at not over-complicating the problem while maintaining sufficient accuracy, so it is not useful and probably insignificant to include nonlinearities in this study. Unlike studies by others that were focused on the nonlinearities that can no longer be applied to engineering practice, this study can be easily adopted and included in design guides and analysis. On the other hand, if more precise solutions are of interest, those can be obtained by

replacing the interface stiffness with a reliable bond-slip function in the governing equations and solving the governing equations numerically.

Table 7-3: Interface stiffness comparison

	End slip (in)		χ_B	K
	Cut end	Dead end		
M13-H-C4-1	0.0734	0.0683	0.0977	4.0392e+04
M13-H-C4-2	0.0753	0.0691		
M13-H-C5-1	0.0616	0.0687	0.1101	5.1250e+04
M13-H-C5-2	0.0607	0.0643		
M15-H-C3-1	0.1243	0.0851	0.0696	2.8698e+04
M15-H-C3-2	-*	0.0880		
M15-H-C4-1	-*	0.0734	0.0922	5.0345e+04
M15-H-C4-2	0.0892	0.0637		
M15-H-C5-1	0.0772	0.0589	0.1010	6.0507e+04
M15-H-C5-2	0.0761	0.0648		
T13-H-S3	0.0862	0.0726	0.0880	6.4520e+04
T13-H-S4	0.0878	0.0724	0.0873	6.3728e+04
T13-H-S5	0.0761	0.0724	0.0943	7.4611e+04
T15-H-S3	0.1276	0.0845	0.0656	5.0078e+04
T15-H-S4	0.0780	0.0670	0.0964	1.0961e+05
T15-H-S5	0.0667	0.0647	0.1062	1.3246e+05

*Missing data due to damage of instrument upon prestressing force release.

In Table 7-3, there are several important observations regarding the bonding condition of the strands. Firstly, the double strand specimens, M15-H-C3, M15-H-C4 and M15-H-C5 have approximately double the bonding stiffness of the corresponding single strand specimens, T15-H-S3, T15-H-S4 and T15-H-S5. Secondly, the 0.6 inch diameter strand specimens, M15-H-C4 and M15-H-C5 have also approximately 1.2 times the bonding stiffness than the 0.5 inch diameter strand specimens M15-H-C4 and M15-H-C5 due to the increase in interface areas. However, another observation is that the twin 0.5 inch strand specimens T13-H-S3, T13-H-S4 and T13-H-S5 exhibit lower strand bonding stiffness than expected upon the corresponding single 0.5 inch strand specimens, M13-H-C4 and M13-H-C5. It is likely that since these twin 0.5 inch strand specimens have the smallest spacing, the surrounding concrete at this small spacing is inadequate to provide the necessary support and thus results in lower interface stiffness. The same

trend can also be observed on 0.6 inch twin strands specimens T15-H-S3, T15-H-S4 and T15-H-S5, where spacing is the only variable. In those specimens, the interface bonding stiffness will increase as strand spacing increases.

7.5.2 Correlation between transfer length and strand diameter

The popular observation that transfer length is proportional to strand diameter as codified in ACI 318 may be explained from another perspective. The reason that larger strand diameter specimens tend to be associated with longer transfer length is that large diameter strand will decrease the number of strands required for a specific cross section or increase the size of cross section for a specific amount of strands. The first scenario will result in less interface area, less interface stiffness and therefore longer transfer length. The second scenario will bring in larger demand of interface stiffness and bond than current strands provide already, which therefore results in longer transfer length.

For example, specimens M13-H-C4, M13-H-C5, M15-H-C4, and M15-H-C5 are all designed to have zero tensile stress at the top fiber upon prestress release. However, M13-H-C4 and M13-H-C5 have 0.5 inch diameter strand whereas M15-H-C4 and M15-H-C5 have 0.6 inch diameter strand. These four groups of specimen well simulated the realistic situation. For example, as in Table 7-2, the transfer lengths of M13-H-C4 and M13-H-C5 are shorter than M15-H-C4 and M15-H-C5. Meanwhile, as demonstrated in Table 7-3, χ_B of M13-H-C4 and M13-H-C5 are larger than that of M15-H-C4 and M15-H-C5. χ_B essentially represents the bonding stiffness demand, which is used in Equation (7.4). This demonstrates well that larger strand diameter specimens will either have larger demand or have smaller interface bonding stiffness, and both scenarios will result in shorter transfer length.

7.6 Application and comparison

ACI 318[71] defines the transfer length as:

$$l_t = \left(\frac{f_{se}}{3000} \right) d_b \tag{7.17}$$

AASHTO LRFD[79] defines transfer length as:

$$l_t = 60 d_b \tag{7.18}$$

where f_{se} = effective prestressing force in psi and d_b = strand nominal diameter in inch. For the ACI 318 approach in Equation (7.17), the effective prestressing force is the force remaining after immediate prestress losses. For grade 270 prestressing strand prestressed to 75% of its tensile strength, and assuming 10% of immediate prestress losses, Equation (7.17) becomes l_t = 60.75 d_b, which is very close to AASHTO LRFD provision of transfer length in Equation (7.18). However, those two equations do not consider the bonding condition at the strand-concrete interface or the cross section properties of the prestressed concrete structures, which may be inappropriate. This study derives transfer length as Equation (7.4), or Equation (7.8) if measured end slip data is available. Equation (7.4) and Equation (7.8) account for the cross section properties and strand interface bonding stiffness and consider the transfer length as the consequence of the interaction between those mechanical properties. Equation (7.4) however takes all of those influences into consideration along with all of the immediate prestress losses, but interface bonding must be assumed. Equation (7.8) on the other hand takes advantage of measured end slip data to determine the interface bonding condition and precisely yield the desired results. Therefore, in order to demonstrate impact of those two equations, the transfer length expressions from ACI 318 and AASHTO LRFD along with actual tested beams are compared.

All of the strands were pretensioned to 75% of their tensile strength, so the initial prestresses are 202500 psi for all specimens (1 psi = 6.89 kPa). The immediate prestress losses are calculated in accordance to Equations (6.47) and (6.55), which include curvature gain due to self-weight and elastic shortening loss. Note that both of the two approaches need a criteria γ to define when transfer length is

achieved from strain profile data, and that γ = 0.865 is used to comply with testing data measured by the 95% AMS approach. The strands are reported to be in fresh and new condition and neither rust nor oil exists on the surface. Therefore the interface stiffness, according to Chapter 6, is again taken as 40000 (lbf/in) for each 0.5 inch diameter strand and 48000 (lbf/in) for each 0.6 inch diameter strand (1 inch = 25.4 mm, 1 lbf = 4.45 N). If more than one strand is placed, the interface bonding stiffness should be multiplied by the amount of strand.

Table 7-4: Transfer length calculation according to ACI 318

	Gain due to self-weight (%)	Elastic shortening loss (%)	Total immediate losses (%)	Effective prestress (psi)	Transfer length (in)
M13-H-C4-1	0.2	6.13	5.90	190553	31.76
M13-H-C4-2					
M13-H-C5-1	0.19	5.21	5.02	192335	32.06
M13-H-C5-2					
M15-H-C3-1	0.26	9.72	9.46	183344	36.67
M15-H-C3-2					
M15-H-C4-1	0.22	8.31	8.09	186118	37.22
M15-H-C4-2					
M15-H-C5-1	0.19	7.09	6.90	188528	37.71
M15-H-C5-2					
T13-H-S3	0.19	7.59	7.40	187515	31.25
T13-H-S4	0.19	7.04	6.85	188629	31.44
T13-H-S5	0.19	6.57	6.38	189581	31.60
T15-H-S3	0.18	9.85	9.67	182918	36.58
T15-H-S4	0.16	7.78	7.62	187070	37.41
T15-H-S5	0.16	8.42	8.26	185774	37.15

Table 7-5: Transfer lengths comparison

	Measured by 95% AMS (in)		Measured average of both ends (in)	ACI 318 (in)	AASHTO LRFD (in)	Eq.(7.4) w/ γ = 86.5% (in)	Eq.(7.8) w/ γ = 86.5% (in)	
	Cut end	Dead end					Cut end	Dead end
M13-H-C4-1	21.57	17.91	19.74	31.76	30	20.23	20.67	19.21
M13-H-C4-2	23.11	19.72	21.42				21.19	19.46
M13-H-C5-1	19.37	17.09	18.23	32.06	30	20.33	17.33	19.34
M13-H-C5-2	20.98	19.02	20				17.09	18.09
M15-H-C3-1	35.59	28.54	32.07	36.67	36	21.57	34.97	23.95
M15-H-C3-2	34.33	31.45	32.89				-*	24.77
M15-H-C4-1	30.00	25.98	27.99	37.22	36	21.74	-*	20.66
M15-H-C4-2	26.85	23.46	25.16				25.10	17.92
M15-H-C5-1	21.93	21.26	21.60	37.71	36	21.88	21.72	16.58
M15-H-C5-2	23.27	19.13	21.20				21.43	18.23
T13-H-S3	27.36	23.27	25.32	31.25	30	20.07	24.26	20.45
T13-H-S4	23.43	20.55	21.99	31.44	30	20.13	24.72	20.39
T13-H-S5	21.97	19.80	20.89	31.60	30	20.18	21.41	20.39
T15-H-S3	35.00	30.71	32.86	36.58	36	21.55	35.91	23.78
T15-H-S4	28.54	25.00	26.77	37.41	36	21.80	21.94	18.86
T15-H-S5	26.06	24.09	25.08	37.15	36	21.73	18.78	18.21

*Missing data due to damage of instrument upon prestressing force release.

Table 7-4 summarizes the ACI 318 transfer length results calculation. Table 7-5 compares the transfer length data between ACI 318, AASHTO LRFD and approach developed herein and demonstrates that the ACI 318 and AASHTO LRFD transfer length predictions would yield roughly the same results on transfer length for grade 270 strand pretensioned to 75% of their tensile strength, but the results have obvious discrepancy with testing data that is obtained in accordance to the 95% AMS approach. On the other hand, the results from Equation (7.4) would result in better agreement with the same set of test data than ACI 318 and AASHTO LRFD methods. Based upon the transfer length prediction comparisons presented in Table 7-5, not surprisingly, the most ideal way to predict transfer length is to use Equation (7.8) when end slip data is available since the end slip data clearly represent the bonding condition between strands and concrete and other influences such as surface condition, strand diameter, strand spacing and concrete strength are all accounted for. Even if the end slip data is not available, Equation

(7.4) would yield more reasonable results than the transfer length formulas in ACI 318 and AASHTO LRFD.

7.7 Conclusions

This chapter develops practical and accurate approaches to evaluate transfer length in prestressed concrete beams. The derivations are validated against comprehensive sets of testing data and show very satisfactory accuracy. Firstly, it demonstrates that the application of composite theory to the prestress transfer problem is valid. Secondly, this study further simplified the closed form solutions developed in Chapter 6 and established a solid foundation for its practical application to prestressed concrete design. For example, by measuring the end slips of specific specimens, its strain profile in addition to transfer length can be determined. Thirdly, by taking advantage of test data presented in the literature, the strand bonding conditions are evaluated. It confirms the conclusions presented in Chapter 6 that 0.6 inch diameter strand would have a 20% greater bonding stiffness than the 0.5 inch diameter strand if all other conditions are kept the constant. It also demonstrates that the strand bonding stiffness is also proportional to the total number of strands.

Chapter 8 Summary and future work

This dissertation develops a general form of composite theory in linear and elastic range, and applies it to a number of applications such as sandwich structures and prestressed concrete. All those applications are validated against comprehensive testing data in the literature, and the validations show very satisfactory results. This dissertation provides a new perspective from interactive composite theory and improves some existing analyses and design approaches in each application area, such as immediate prestress losses and transfer length. Specifically, for unsymmetrical and symmetrical sandwich structures that are discussed in Chapters 4 and 5, it is concluded that:

1. The analysis approach in Chapter 4 captures transverse interaction and results in more reasonable results than Newmark's approach, especially in terms of bending moment. The resultant stresses also show apparent difference between the two approaches. The model developed through the present research balances the complexity and accuracy by supplementing important transverse interaction as a decoupled load case.

2. Another important aspect of the theory and analysis procedure in Chapters 4 and 5 is that the governing equations are all solved with closed form solutions, which lends convenience to future application to practical design and analysis. Also the upper and lower bounds of those solutions are derived and provided in closed forms, and in that way the estimation of internal forces in any partially composite structures is made possible.

3. The Discrete Model presented in Chapter 5 can improve the stress calculation accuracy near shear connectors and capture the key characteristic of ICSP structures.

4. Sandwich structures deflection is decomposed and classified as flexural and shear components. Furthermore, the upper and lower bounds of deflection, end slip and internal forces are derived and verified against full-scale test data.

5. The deflection associated with shear deformation can be so large that it can dominate the deflection when the middle layer stiffness is relatively small (demonstrated in Figure 5-9).

On the other hand, for the transfer length and immediate prestress losses in prestressed concrete structures, conclusions from this study are drawn as:

6. Developed theory in Chapters 6 and 7 can improve prestress concrete analysis and design, and can provide a new perspective for prestressing structural analysis. Comparisons with testing data demonstrate agreement with the developed theory.

7. It is demonstrated analytically in Chapter 6 that the PCI Design Handbook, AASHTO-LRFD specification and ACI-318 provisions for prestress loss due to elastic shortening are only applicable to small reinforcement ratio components and will overestimate the prestress loss for large reinforcement ratio components whereas the formulation derived herein is accurate without limitation.

8. Transfer length solution in Chapters 6 and 7 is derived based on pure mechanical definition instead of empirical data as used by other researchers in the past investigations, and the derived formula is validated against test data.

9. In Chapters 6 and 7, the roles of concrete strength, prestressing force and strand diameter that were previously thought to directly affect transfer length, however, are shown actually to influence the interface stiffness, which in turn affects transfer length.

10. The rigorous strand force gain due to curvature developed in Chapter 6 is able to consider the existence of slip and large reinforcement ratios, which could not be accounted for in the past. It is also simplified for application outside of transfer zones, for example critical sections at or near midspan.

11. A practical approach to evaluate and quantify the strand-cocnrete interface bonding of existing prestressed concrete structures is presented in Chapter 7 and validated against test data. By taking advantage of this approach, it is confirmed that 0.6 inch diameter strand would have a 20% greater bonding stiffness than the 0.5 inch diameter strand if all other conditions are kept the constant. It also demonstrates that the strand bonding stiffness is also proportional to the total number of strands.

For sandwich structures, this study decouples the longitudinal land transverse interactions and investigates them separately. However, the longitudinal and transverse effects are actually coupled. It is recommended that future work could include the discussion and evaluation on the mechanics of coupling. Additionally, transforming the theory presented here into design methodology and additional discussions of nonlinear properties associated with sandwich structures are also recommended for the future studies.

For transfer length and prestress losses, future work could include the investigations in large displacement and nonlinear ranges, and also the investigation of time dependent behavior of concrete.

The publications associated with sandwich structures in this dissertation are:

1. Bai, Fengtao, Davidson, James. “Analysis of partially composite foam insulated concrete sandwich structures.” *Engineering Structures*, 91 (2015) 197–209.

2. Bai, Fengtao, Davidson, James. “Partially composite sandwich structures with unsymmetrical wythes and transverse interaction.” *Engineering Structures*, 116 (2016): 178-191.

The publications associated with transfer length and immediate prestress losses in this dissertation are:

3. Bai, Fengtao, Davidson, James. “Composite theory for transfer length and immediate prestress losses in prestressed concrete structures.” Under review, 2015.

4. Bai, Fengtao, Davidson, James. “Practical approaches for predicting transfer length and strain profile.” Under review, 2015.

5. Bai, Fengtao, Davidson, James. “Composite theory for prestressed concrete girders draped tendon and bond-slip relationship.” Under review, 2016.

References

[1] Granholm, H. “Om sammansatta balkar och pelare med särskild hänsyn till spikade träkonstruktioner.” (On composite beams and columns with particular regard to nailed timber structures). *Transaction of Chalmer University of Technical*, No. 88. Gothenburg 1949.

[2] Holmberg, Ake, and Erik Plem. “Behaviour of load-bearing sandwich-type structures.” *Handlingar nr 49 Transactions*, Statens institut för byggnadsforskning, 1965.

[3] Newmark, Nathan M., Chester P. Siess, and IvanM Viest. "Tests and analysis of composite beams with incomplete interaction." *Proc. Soc. Exp. Stress Anal* 9.1 (1951): 75-92.

[4] Goodman, James Richard. “Layered wood systems with interlayer slip.” *PhD thesis*, University of California, Berkeley, Calif 1967.

[5] Chapman, J. C., and S. Balakrishnan. "Experiments on composite beams." *The Structural Engineer* 42.11 (1964): 369-383.

[6] Ranzi, G., F. Gara, and P. Ansourian. "General method of analysis for composite beams with longitudinal and transverse partial interaction." *Computers & structures* 84.31 (2006): 2373-2384.

[7] Adekola, A. O. "Partial interaction between elastically connected elements of a composite beam." *International Journal of Solids and Structures* 4.11 (1968): 1125-1135.

[8] Allen, Howard G. "Analysis and design of structural sandwich panels." Vol. 51. Oxford: Pergamon press, 1969.

[9] Hartsock, John A. "Design of foam-filled structures." Technomic Publishing Company, CT 1969.

[10] Ha, K. H. "Exact analysis of bending and overall buckling of sandwich beam systems." *Computers & Structures* 45.1 (1992): 31-40.

[11] Ha, K. H. "Finite element analysis of sandwich plates: an overview." *Computers & Structures* 37.4 (1990): 397-403.

[12] Davies, J. Michael. "The analysis of sandwich panels with profiled faces." *Eighth international*

specialty conference on cold-formed steel structures. (1986: November 11-12; Missouri S&T (formerly the University of Missouri-Rolla), St. Louis, Missouri).

[13] Gordaninejad, Faramarz, and Charles W. Bert. "A new theory for bending of thick sandwich beams." *International Journal of Mechanical Sciences* 31.11 (1989): 925-934.

[14] Goyal, Vijay K., and Rakesh K. Kapania. "A shear-deformable beam element for the analysis of laminated composites." *Finite Elements in Analysis and Design* 43.6 (2007): 463-477.

[15] Noor, Ahmed K., W. Scott Burton, and Charles W. Bert. "Computational models for sandwich panels and shells." *Applied Mechanics Reviews* 49.3 (1996): 155-199.

[16] Girhammar, Ulf Arne, and Vijaya KA Gopu. "Composite beam-columns with interlayer slip - exact analysis." *Journal of Structural Engineering* 119.4 (1993): 1265-1282.

[17] Ranzi, G., M. A. Bradford, and B. Uy. "A direct stiffness analysis of a composite beam with partial interaction." *International Journal for Numerical Methods in Engineering* 61.5 (2004): 657-672.

[18] Ranzi, Gianluca. "Locking problems in the partial interaction analysis of multi-layered composite beams." *Engineering Structures* 30.10 (2008): 2900-2911.

[19] Salari, M. R., Spacone, E., Shing, P. B., & Frangopol, D. M. "Nonlinear analysis of composite beams with deformable shear connectors." *Journal of Structural Engineering* 124.10 (1998): 1148-1158.

[20] Sousa Jr, João Batista M., and Amilton R. da Silva. "Analytical and numerical analysis of multilayered beams with interlayer slip." *Engineering Structures* 32.6 (2010): 1671-1680.

[21] Fabbrocino, G., G. Manfredi, and E. Cosenza. "Analysis of continuous composite beams including partial interaction and bond." *Journal of Structural Engineering* 126.11 (2000): 1288-1294.

[22] Xu, Rongqiao, and Yu-Fei Wu. "Two-dimensional analytical solutions of simply supported composite beams with interlayer slips." *International Journal of Solids and Structures* 44.1 (2007): 165-175.

[23] Xu, Rongqiao, and Haojiang Ding. "Two-dimensional solutions for orthotropic materials by the state space method." *Composite Structures* 78.3 (2007): 325-336.

[24] Hassan, Tarek K. and Rizkalla, Sami H.. “Analysis and design guidelines of precast, prestressed concrete, composite load-bearing sandwich wall panels reinforced with CFRP grid.” *PCI Journal* 55.2 (2010): 147-162.

[25] Naito, C., Hoemann, J., Beacraft, M., and Bewick, B.. ”Performance and Characterization of Shear

Ties for Use in Insulated Precast Concrete Sandwich Wall Panels." *Journal of Structural Engineering* 138.1(2012): 52–61.

[26] Pessiki, Stephen, and Alexandar Mlynarczyk. "Experimental Evaluation of the Composite Behavior of Precast Concrete Sandwich Wall Panels." *PCI Journal* 48.2 (2003): 54-71.

[27] Salmon, David C., Amin Einea, Maher K. Tadros, and Todd D. Culp. "Full scale testing of precast concrete sandwich panels." *ACI Structural Journal* 94, no. 4 (1997).

[28] Bush, Thomas D., and Wu Zhiqi. "Flexural analysis of prestressed concrete sandwich panels with truss connectors." *PCI Journal* 43.5 (1998): 76-86.

[29] Salmon, David C., and Amin Einea. "Partially composite sandwich panel deflections." *Journal of Structural Engineering* 121.4 (1995): 778-783.

[30] Frankl, Bernard A., Gregory W. Lucier, Tarek K. Hassan, and Sami H. Rizkalla. "Behavior of precast, prestressed concrete sandwich wall panels reinforced with CFRP shear grid." *PCI journal* 56, no. 2 (2011): 42-54.

[31] Naito, Clay, Robert Dinan, and Bryan Bewick. "Use of Precast Concrete Walls for Blast Protection of Steel Stud Construction." *Journal of Performance of Constructed Facilities* 25.5 (2011): 454-463.

[32] Naito, Clay J., John M. Hoemann, Jonathon S. Shull, Aaron Saucier, Hani A. Salim, Bryan T. Bewick, and Michael I. Hammons. ‘‘Precast/Prestressed Concrete Experiments Performance on Non-Load Bearing Sandwich Wall Panels.” *Air Force Research Laboratory Report*, *AFRL-RX-TY-TR-2011–0021*, Tyndall Air Force Base, Panama City, FL 2011.

[33] Naito, Clay, Mark Beacraft, John Hoemann, Jonathan Shull, Hani Salim, and Bryan Bewick. “Blast Performance of Single-Span Precast Concrete Sandwich Wall Panels.” *Journal of Structural Engineering* (2014) 140(12), 04014096.

[34] Naito, Clay J., John M. Hoemann, Bryan T. Bewick, and Michael I. Hammons. ‘‘Evaluation of shear tie connectors for use in insulated concrete sandwich panels.” *Interim report. AFRL-Rx-TY-TR-2009-4600*, 2009.

[35] Pfeifer, Donald Wayne, and J. A. Hanson. "Precast Concrete Wall Panels: Flexural Stiffness of Sandwich Panels." *ACI Special Publication* 11 (1965).

[36] Woltman, Greg, Douglas Tomlinson, and Amir Fam. "Investigation of Various GFRP Shear

Connectors for Insulated Precast Concrete Sandwich Wall Panels." *Journal of Composites for Construction* 17.5 (2013): 711-721.

[37] Tomlinson, Douglas, and Amir Fam. "Experimental Investigation of Precast Concrete Insulated Sandwich Panels with Glass Fiber-Reinforced Polymer Shear Connectors." *ACI Structural Journal* 111.1-6 (2014).

[38] Benayoune, A., A. Aziz A. Samad, D. N. Trikha, A. Abdullah Abang Ali, and A. A. Ashrabov. "Structural behavior of eccentrically loaded precast sandwich panels." *Construction and Building Materials* 20.9 (2006): 713-724.

[39] Gara, Fabrizio, Laura Ragni, Davide Roia, and Luigino Dezi. "Experimental tests and numerical modelling of wall sandwich panels." *Engineering Structures* 37 (2012): 193-204.

[40] Benayoune, A., AA Abdul Samad, A. A. Abang Ali, and D. N. Trikha. "Response of pre-cast reinforced composite sandwich panels to axial loading." *Construction and Building Materials* 21.3 (2007): 677-685.

[41] Benayoune, A., A. A. Samad, D. N. Trikha, A. A. Ali, and S. H. M. Ellinna. "Flexural behaviour of pre-cast concrete sandwich composite panel–Experimental and theoretical investigations." *Construction and Building Materials* 22.4 (2008): 580-592.

[42] Bush, Thomas D., and Gregory L. Stine. "Flexural behavior of composite precast concrete sandwich panels with continuous truss connectors." *PCI Journal* 39.2 (1994).

[43] Einea, Amin. "Structural and thermal efficiency of precast concrete sandwich panel systems." (January 1, 1992). *ETD collection for University of Nebraska - Lincoln.* Paper AAI9308172.

[44] Einea, Amin, David C. Salmon, Maher K. Tadros, and Todd Culp. "A new structurally and thermally efficient precast sandwich panel system." *PCI Journal* 39.4 (1994): 90-101.

[45] Bai, Fengtao, Davidson, James. “Analysis of partially composite foam insulated concrete sandwich structures.” *Engineering Structures*. 91 (2015) 197–209.

[46] Bai, Fengtao, Davidson, James. “Theory for composite sandwich structures with unsymmetrical wythes and transverse interaction.” *Engineering Structures*. 116 (2016) 178–191.

[47] Kaar, Paul H., Robert W. La Fraugh, and M. A. Maas. *Influence of concrete strength on strand transfer length*. *PCI Journal*, V. 8, No. 5, (October 1963), pp. 47-67.

[48] Mitchell, Denis, et al. "Influence of high strength concrete on transfer and development length of pretensioning strand." *Precast/Prestressed Concrete Institute Journal,* 38.3 (1993).

[49] Russell, Bruce W., and Ned Hamilton Burns. *Design Guidelines for Transfer, Development and Debonding of Large Diameter Seven Wire Strands in Pretensioned Concrete Girders. Final Report*. No. FHWA/TX-93+ 1210-5F. (1993).

[50] Zia, P., Preston, H. K., Scott, N. L., & Workman, E. B. Estimating prestress losses. *Concrete International*, *1*(6), 32-38. (1979).

[51] Tadros, M. K. "Prestress losses in pretensioned high-strength concrete bridge girders. NCHRP Report 496, National Cooperative Highway Research Program." *Transportation Research Board, National Research Council* (2003).

[52] Tadros, Maher K., Amin Ghali, and Arthur W. Meyer. "Prestressed Loss and Deflection of Precast Concrete Members." *Journal Prestressed Concrete Institute* 30.1 (1985): 114-141.

[53] Carroll, J. Chris, Thomas E. Cousins, and Carin L. Roberts-Wollmann. "A practical approach for finite-element modeling of transfer length in pretensioned, prestressed concrete members using end-slip methodology." *PCI Journal* 59.3 (2014).

[54] Balazs, Gyorgy L. "Transfer length of prestressing strand as a function of draw-in and initial prestress." *PCI Journal* 38.2 (1993): 86-93.

[55] Barnes, Robert W., Ned Hamilton Burns, and Michael Eugene Kreger. *Development length of 0.6-inch prestressing strand in standard I-shaped pretensioned concrete beams*. No. FHWA/TX-02/1388-1,. (1999).

[56] Boehm, Kurtis McKinley, Robert W. Barnes, and Anton K. Schindler. *Performance of Self-Consolidating Concrete In Prestressed Girders*. No. FHWA/ALDOT 930-602. Highway Research Center, Harbert Engineering Center, (2010).

[57] Janney, Jack R. "Nature of bond in pre-tensioned prestressed concrete." *ACI Journal Proceedings*. Vol. 50. No. 5. ACI, (1954).

[58] Marti-Vargas, J. R., Arbelaez, C. A., Serna-Ros, P., & Castro-Bugallo, C. Reliability of transfer length estimation from strand end slip. *ACI Structural Journal*, *104*(4). (2007).

[59] Kose, Mehmet M. "Prediction of transfer length of prestressing strands using neural networks." *ACI*

Structural Journal 104.2 (2007).

[60] Marti-Vargas, Jose R., Francesc J. Ferri, and Victor Yepes. "Prediction of the transfer length of prestressing strands with neural networks." *Computers and Concrete* 12.2 (2013): 187-209.

[61] Kose, Mehmet M., and Cafer Kayadelen. "Modeling of transfer length of prestressing strands using genetic programming and neuro-fuzzy." *Advances in Engineering Software* 41.2 (2010): 315-322.

[62] Abdelatif, Amged O., John S. Owen, and Mohammed FM Hussein. "Modelling the prestress transfer in pre-tensioned concrete elements." *Finite Elements in Analysis and Design* 94 (2015): 47-63.

[63] Arab, Amir A., Sameh S. Badie, and Majid T. Manzari. "A methodological approach for finite element modeling of pretensioned concrete members at the release of pretensioning." *Engineering Structures* 33.6 (2011): 1918-1929.

[64] Buckner, C. Dale. "A review of strand development length for pretensioned concrete members." *PCI journal* 40.2 (1995): 84-99.

[65] Tabatabai, Habib, and Timothy J. Dickson. "The history of the prestressing strand development length equation." *Precast/Prestressed Concrete Institute Journal* 38.6 (1993).

[66] Martí-Vargas, José R., and W. Micah Hale. "Predicting strand transfer length in pretensioned concrete: Eurocode versus North American practice." *Journal of Bridge Engineering* 18.12 (2013): 1270-1280.

[67] Kahn, Lawrence F., Jason C. Dill, and Chris G. Reutlinger. "Transfer and development length of 15-mm strand in high performance concrete girders."*Journal of Structural Engineering* 128.7 (2002): 913-921.

[68] Martí-Vargas, J. R., Serna, P., Navarro-Gregori, J., & Bonet, J. L. Effects of concrete composition on transmission length of prestressing strands. *Construction and Building Materials*, *27*(1), 350-356. (2012).

[69] Zia, Paul, and Talat Mostafa. "Development length of prestressing strands." *Precast/Prestressed Concrete Institute Journal* 22.5 (1977).

[70] PCI Industry Handbook Committee. "PCI Design Handbook: Precast and Prestressed Concrete, 7th edition.", Precast/Prestressed Concrete Institute. (2010).

[71] ACI Committee. Building code requirements for structural concrete (ACI 318-05) and commentary

(ACI 318R-05). American Concrete Institute. (2005).

[72] Dang, C. N., Murray, C. D., Floyd, R. W., Hale, W. M., & Martí-Vargas, J. R. Analysis of bond stress distribution for prestressing strand by Standard Test for Strand Bond. *Engineering Structures*, *72*, 152-159. (2014).

[73] *fib* 2010. *fib* Model code for concrete structures 2010. Ernst & Sohn, Wiley, (2013).

[74] Chao, S. H., A. E. Naaman, and G. J. Parra-Montesinos. Local Bond Stress-Slip Models for Reinforcing Bars and Prestressing Strands in High-Performance Fiber- Reinforced Cement Composites. *Special Publication* 272 (2010): 151-172.

[75] Tadros, M.K., Al-Omaishi, N., Seguirant, S.J., and Gallt, J.G. “Prestress Losses in Pretensioned High-Strength Concrete Bridge Girders,” Transportation Research Board, National Cooperative Highway Research Program (NCHRP) Report 496, Washington, D.C., (2003), 73 pp.

[76] Russell, B, and Ramirez, J., “Transfer, Development, and Splice Length for Strand/Reinforcement in High-Strength Concrete,” National Cooperative Highway Research Program (NCHRP) Report 603, Transportation Research Board, (2008).

[77] PCI Committee on Prestress Losses, “Recommendations for Estimating Prestress Losses,” Journal of the Prestressed Concrete Institute, V. 20 No. 4, July-Aug. (1975), pp. 43-75.

[78] Floyd, Royce W., W. Micah Hale, and Michael B. Howland. "Measured transfer length of 0.6 in. prestressing strands cast in lightweight self-consolidating concrete." *PCI Journal* 60.3 (2015): 84-98.

[79] AASHTO, LRFD Bridge Design Specifications. *Washington, DC: American Association of State Highway and Transportation Officials*. (2012).

[80] ASTM A1081/A1081M. Standard test method for evaluating bond of sevenwire steel prestressing strand. West Conshohocken, PA: ASTM International; (2012).

[81] Rose, Dallas R., and Bruce W. Russell. "Investigation of standardized tests to measure the bond performance of prestressing strand." *PCI journal* 42, no. 4 (1997): 56-80.

[82] Guyon, Y. “*Prestressed Concrete*.” Vol. 1. New York, NY: John Wiley and Sons Inc. (1960).

[83] Marti-Vargas, J. R., Arbelaez, C. A., Serna-Ros, P., & Castro-Bugallo, C.. “Reliability of transfer length estimation from strand end slip.” *ACI Structural Journal*, *104*(4). (2007).

[84] Kim, E. S., “Analysis of Prestress Transfer Zone and Prediction of Transfer Length in Pretensioned

Prestressed Concrete Member," *PhD thesis*, Department of Civil Engineering, Seoul National University, Seoul, South Korea, (2000), 232 pp.

[85] Oh, Byung Hwan, and Eui Sung Kim. "Realistic evaluation of transfer lengths in pretensioned, prestressed concrete members." *ACI Structural Journal* 97, no. 6 (2000).

[86] Barnes, R. W., Grove, J. W., & Burns, N. H. Experimental assessment of factors affecting transfer length. *ACI Structural Journal*,*100*(6), 740-748. (2003).

[87] Russell, Bruce W., and Ned H. Burns. "Measurement of transfer lengths on pretensioned concrete elements." *Journal of Structural Engineering* 123.5 (1997): 541-549.

[88] Hanson, Norman W., and Paul H. Kaar. "Flexural Bond Tests." *Journal of the American Concrete Institute* (1959). ACI JOURNAL, *Proceedings* V. 55, No. 7, Jan. (1959)

[89] Peterman, Robert J., Julio A. Ramirez, and Jan Olek. Evaluation of strand transfer and development lengths in pretensioned girders with semi-lightweight concrete. No. FHWA/IN/JTRP-99/3,1999.

[90] Peterman, Robert J., and Kyle H. Larson. Evaluating the Bond Performance of Self-Consolidating Concrete in Prestressing Applications. No. KS-10-3. 2011.

[91] Peterman, Robert J. "A simple quality assurance test for strand bond." *PCI journal* 54.2 (2009): 143-161.

[92] Osborn, Andrew EN, John S. Lawler, and James D. Connolly. *Acceptance tests for surface characteristics of steel strands in prestressed concrete*. Vol. 621. Transportation Research Board, 2008.